I. TEMPERATURE GRADIENTS IN TURBULENT AIR STREAMS

II. THERMODYNAMIC PROPERTIES OF METHANE AT LOW TEMPERATURE

Thesis by

William Harrison Corcoran

In Partial Fulfillment of the Requirements

For the Degree of

Doctor of Philosophy

California Institute of Technology

Pasadena, California

1948

ACKNOWLEDGMENT

The construction of the apparatus would not have been possible without the untiring efforts of Glenn W. Billman. He and David M. Mason contributed greatly to the experimental work.

Bruce H. Sage is responsible for the initiation of the heat transfer investigations in the Department of Chemical Engineering. It is only through his effort that major impetus has been given to the program. The work reported here is merely a beginning, and it is hoped that Professor Sage meets with every success in the future because his interest in careful measurement of physical quantities to improve engineering techniques, particularly in heat and mass transfer, deserves much commendation. The assistance and advice of Professor William N. Lacey is also acknowledged.

The work of the staff of the laboratory in various mechanical problems and in particular in the construction of a central temperature-measuring bench is appreciated. The efforts of Willard De Witt, George Griffith, Robert C. Beacham, and Hollis H. Reamer in many overtime hours have contributed significantly to the progress of the program.

ABSTRACT

I.

Equipment is described that was used in making velocity and temperature measurements at various points within an air stream flowing in a smooth, rectangular channel 0.675 inch in height, 12 3/8 inches in width, and 162 inches in length. The aspect ratio of the channel was such that flow along the center line was essentially two-dimensional. In addition to equipment for velocity and temperature measurements, means were provided for establishing the thermal flux from the upper wall of the channel into the flowing air stream.

The apparatus was applied to a research problem concerned with the analogy between momentum transfer and heat transfer. Steady state, two-dimensional flow of air was attained at the downstream portion of the channel. Observations were made in the Reynolds number range of 18,000 to 48,000. The experimental data were examined on the basis of heat and momentum transfer equations whose basic forms were first suggested by Osborne Reynolds. It was found that in the turbulent core the coefficient of eddy conductivity for heat was practically constant and approximately 1.3 times the coefficient of eddy viscosity.

II.

Thermodynamic properties of methane were computed using values of $(\frac{\partial H}{\partial P})_T$ and the compressibility factor Z obtained from experimental measurements, and theoretical information for heat capacities at zero pressure. Data are tabulated for the temperature range from 70 to -230° F and the pressure range from zero to 1400 pounds per square inch. A temperature-entropy diagram of methane in this low temperature region is presented.

TABLE OF CONTENTS

I. TEMPERATURE GRADIENTS IN TURBULENT AIR STREAMS

INTRODUCTION

Osborne Reynolds (1) first suggested that heat and momentum transfer are accomplished in an analagous manner. His theory, however, was applicable only to the turbulent core of fluid streams. L. Prandtl (2) and G. I. Taylor (3) extended Reynolds work to include the laminar layer at the channel wall. Further refinement was made by Th. von Kármán (4) who introduced the concept of the buffer layer* between the laminar layer and the main turbulent core. A consideration of the evolved theory shows that the nature of the two equations**

$$\frac{\tau g}{\sigma} = (\nu + \epsilon_m) \frac{du}{dy} \qquad (1)$$

$$\frac{\dot{Q}}{c_p \sigma} = -(K + \epsilon_c) \frac{dt}{dy} \qquad (2)$$

allows an analogy to be drawn between heat and momentum transfer. The analogy is that ϵ_m from the shear equation is essentially identical with ϵ_c in the heat transfer equation. It is thus implied that if the shear distribution is known in the channel together with the velocity gradient and fluid properties, then the heat transfer may be established if the temperature gradient is known.

---

* See Appendix

** The equations are dimensionally correct with respect to the nomenclature. Conversion factors for differences in units are not included.

The latter procedure is based on the assumption that ϵ_m as computed from Equation 1 may be directly substituted for ϵ_c in Equation 2. Recent literature (5) states that instead of an equality existing between ϵ_c and ϵ_m, the ratio ϵ_c / ϵ_m may be between 1 and 1.7. Hence there is still uncertainty as to how the eddy viscosity, ϵ_m, may be properly transformed to the eddy conductivity.

To investigate more fully the apparent analogy between momentum and heat transfer, an apparatus was constructed by the Department of Chemical Engineering and used for a study of heat transfer in steady, two-dimensional air streams. The work accomplished with this equipment is described in the Appendix. The results were not capable of satisfactory analysis since means were not available for establishing the rate of change in temperature along the axis of flow, and it was not known as to whether or not fully developed velocity and temperature profiles were obtained at the downstream end. To mitigate the difficulties encountered, a new apparatus was designed and constructed. It is the intent of this discussion to present the details of the new equipment design and review experimental results obtained in its application to a study of the analogy between momentum and heat transfer. It is to be noted that the work involved was necessarily concerned mainly with the design and instrumentation of the apparatus. Experimental investigations were at a minimum because of the time required to construct equipment that would allow all the necessary quantities in Equations 1 and 2 to be accurately measured.

DESIGN OF EQUIPMENT

The main features of the new apparatus were intended to eliminate the experimental difficulties encountered previously. First, the channel length was increased from 63 to 162 inches. The greater length allowed more certainty in establishing fully developed velocity and temperature profiles at the downstream end of the channel. The second main feature was the inclusion of traversing equipment such that velocity and temperature measurements could be made to within a foot of the entrance or the exit of the channel. Besides the two main changes in the equipment design, provisions were made for more rapid circulation of oil used in maintaining the upper and lower walls of the channel at fixed temperatures. The oil circulation of the earlier equipment was at the rate of 0.2 feet per second while the new rate was designed to be 3 feet per second. By providing more rapid circulation of the oil more satisfactory temperature control was expected.

Air System

The original equipment was planned for measurements in air streams at Reynolds numbers up to 100,000. Because of space limitations no changes were proposed in the approximate size of the channel or in the size of the blower used to drive the air. An isometric view of the new equipment is shown in Figure 1 and a schematic layout in Figure 2. Also photographs giving more detail of the general nature of the apparatus are presented as Figures 3 and 4. Figure 5 gives a view of the channel cross section, and it

is noted that it resembles in general Figure 4 of the Appendix. The height of the channel was a nominal 3/4 inch and the width 12 3/8 inches. It is believed that two-dimensional flow was attained along the lateral median line since the aspect ratio was approximately 16.

The air system was operated as a closed circuit, and a detailed schematic elevation is shown in Figure 6. The center line of the channel was 46.83 inches above floor level, and the working length was 162 inches as determined by the lengths of the copper plates forming the upper and lower walls, as noted in Figure 5. In operation, the air passed from the blower to a heating section where two 500-watt on-off heaters and one 500-watt variable heater were located. These heaters provided the necessary fixed heat in controlling the temperature of the air stream during a run. After leaving the heating section, the air then moved into a long straight run before entering a venturi meter whose reading was used to maintain constancy of flow. The straight pipe leading to the venturi meter had a length compatible with recommendations given by Sprenkle (6). After leaving the venturi meter the air then moved into a channel entrance box where it was turned 180 degrees to enter the working channel. The channel entrance box was provided with turning vanes as shown in Figure 7 and also in Figure 2. The vanes were designed with radii of 3.14 inches and back to back spacing of 2 inches. Details on the optimum contour of the vanes were obtained from information presented by Patterson (7). The cross section of the channel entrance box at the exit from the venturi meter was 10

inches by 14 inches.

As the air made its second 90 degree turn in the entrance box, it passed into a commercial air filter packed with copper turnings and next into a straightening section whose honeycombs had lengths equal to six times their hydraulic radii. At the exit of the straightening section, the air channel had a height of 8 inches and a width of 12 inches. The air then moved into a contraction section which brought the cross section to that of the working channel in a length of 10 inches. It is thus seen that care was exercised in an attempt to provide a uniform velocity distribution at the entrance to the working section.

The air ran horizontally in the working section between two copper plates as noted in Figures 1 and 4. In operation the upper copper plate was maintained at a higher temperature than the lower plate. As the air approached the downstream end of the working channel it was felt that steady state conditions were attained wherein the heat transfer through the air stream was constant from point to point normal to the stream, and no rate of change of temperature of the air occurred along the axis of flow. In addition it was believed that the velocity and temperature profiles here were fully developed for the given type of channel.

As the air left the working section it entered the channel exit box shown in Figure 8 and also included as point 1 in the schematic sketch, Figure 6. After leaving the channel exit box the air passed into a connecting section leading to the blower. At this point the circuit was completed.

The blower as shown in Figure 9 is a Utility Fan Company No. 2 exhauster and was powered by a Sterling Speedtrol Unit having a 3 horsepower rating. The Speedtrol unit in combination with different pulley systems to the blower allowed a continuous variation in the blower speed from 640 to 5700 rpm. Reynolds numbers of interest were covered by this speed range. Lower air speeds could have been attained by inserting chokes in the air lines.

During operation, the air was maintained at a predetermined temperature by means of a 200-watt control heater located at point 14 in Figure 6. Input to the heater was controlled by an electronic circuit so that the energy added was proportional to the displacement from the zero point of a mirror of a galvanometer connected to a bridge circuit. The bridge was essentially as shown in Figure 10, one arm being located in the air stream. The location of the control point was at point n in Figure 2. The temperature of the air stream was measured with a platinum resistance thermometer mounted at m adjacent to the control element.

Perhaps the most noteworthy feature of the channel was the provision for the movable side walls. End views of the side walls are shown in Figure 5. They were made of bakelite with steel backing plates to facilitate movement by hand. The bakelite pieces were 3/4 inch thick, 1 5/16 inches in width, and 11 inches in length. Sealing between the copper walls and the bakelite blocks was achieved by means of felt strips mounted in grooves milled in the blocks. Figure 11 shows a side view of a typical side wall installation.

Figure 12 gives a view of a group of the side blocks. Figure 13 shows the side view of the air channel with the side walls removed.

Although in the present work only a 6-inch venturi meter was used in controlling the air flow, three other units were also designed. They had nominal sizes of 1 1/2, 3, and 8 inches. The purpose of four units was to provide the proper size for the different flow rates under consideration so that minimum differentials of two centimeters of kerosene and maximum differentials of 20 centimeters could be realized. Design of the meters was made according to specifications described in the manual "Fluid Meters, Their Theory and Application" (8). Instead of providing several holes in the walls of the meters for connection to piezometer rings, the meters were constructed so that continuous openings existed at the entrance pressure connection and at the throat pressure connection. Figure 14 gives a schematic cross section of the venturi meter showing the slotted pressure openings. The meters were first prepared as aluminum castings, and then the castings were machined to precise dimensions. The procedure is recommended since very satisfactory meters were obtained at a relatively low cost. Figure 15 shows the 6-inch venturi meter mounted in the air line.

Oil System

In order to maintain the copper walls of the working channel at fixed temperatures, countercurrent oil circulation was provided. The direction of flow for both the upper and lower

oil baths is indicated in Figure 1. No checks were made on the flow rate that was attained in the equipment. The original plan was, however, to have the oil flow at approximately 3 feet per second with a maximum temperature drop of 0.2° F as it passed from the entrance to the exit end. In order to attain the desired circulation, two low-head, high-capacity pumps were obtained from the Economy Pump Company. The pumps were propeller type with axial flow and had ratings of 500 gallons per minute at heads corresponding to 5 feet of water. Temperature control with the allowed oil circulation rates was satisfactory.

The upper oil bath was suspended from two 4-inch I-beams as shown in Figure 3. A close up view of the support system is shown in Figure 11. The copper plate that formed the upper wall of the air channel in turn formed the lower wall of the upper oil bath. The copper plate was mounted on the oil bath by fastenings shown in Figure 5. Garlock gasketing was used for sealing. For all practical purposes the lower oil bath was a mirror image of the upper bath.

The cross sections of the oil baths normal to the direction of flow were 36 square inches which was slightly greater than the cross section of the 6-inch iron pipe used in the return lines. The oil flowed to the risers shown in Figure 1 as it passed to the return systems. Figure 16 shows the upper and lower oil lines as they left the working section of the equipment. Figure 17 shows the upper and lower oil lines as they entered the temperature

control baths on the right hand side of the photograph. The discharge lines of the axial flow pumps formed the right angle turns just ahead of the entrance to the control baths.

In the design of the heat transfer equipment it was considered that investigations were to be made under conditions such that heat was to be transferred from the lower to the upper plate through the air stream as well as from the upper to the lower plate. Also it was expected that runs were to be made where heat was to be transferred from both plates to the air stream. Thus to allow for flexibility, the heating and cooling elements in the upper and lower baths were designed to be identical. For heating there were two 2000-watt, one 1000-watt, and one 500-watt fixed heaters thus giving a total capacity of 5500 watts in each oil bath. Control heating was accomplished by means of a 250-watt heater connected to an electronic droop control circuit. In addition there was also a 500-watt heater mounted with a variac control on its input. Figure 18 shows the control panel for all the heaters in the oil and air streams. All the fixed heaters plus the variac controlled units were mounted on the exterior of the oil pipes forming the return lines. In addition to the heating facilities each oil system was also provided with refrigeration, both internal and external coils being used. Figure 16 shows the external coils on the left center of the picture. On the right hand side of the photograph are shown the electrical connections for heating elements.

The temperatures of the oil baths were measured approximately 6 feet from the control heaters at the points k and l

indicated in Figure 2. Figure 19 shows the brass cases enclosing the control thermometers along with the resistance thermometers. The resistance thermometers were standard platinum units. The control thermometers used in conjunction with the droop control circuits had copper resistance elements with resistances of about 20 ohms.

It was anticipated that the oil baths were to be operated at a maximum temperature of 160° F and a minimum of 70° F. Operation in even as small a temperature range as this required provision for thermal expansion of the various metal parts in the oil system. It was planned that the main expansion and contraction would be relieved by the Magnalastic expansion bellows located just upstream from the pumps as noted in Figure 1. Also to prevent bulging of the copper plates from stresses in thermal expansion, the plates were provided with floating connections to the steel flanges of the oil baths. The shanks of the fasteners mounted in the copper plates passed through clearance holes in the steel flanges and through copper clamping bars mounted on the other face of the flanges as shown schematically in Figure 5. This method was not satisfactory since bowing of the copper plates occurred to such an extent that the central part of the channel had a height of 0.675 inch as compared to the desired figure of 0.75 inch. Thus in practice the channel was not truly rectangular. Instead the outer edges were 0.75 inch apart with a taper to the center as noted above. It is not believed, however, that the two-dimensional character of the flow along the center line of the channel was

appreciably affected. Before proceeding to heat transfer studies requiring temperature and velocity measurements other than along the center line it will be necessary to correct the bowing by means of clamps and supporting spacers between the upper and lower plates.

Each oil bath held approximately 80 gallons of oil. For safety reasons the oil was kept in the baths only during operation and was drained to an underground tank during layoff periods. When another run was started, the oil was pumped back into the system. Brown neutral oil obtained from the Union Oil Company was used for the fluid.

Copper Plates

Special copper plates were procured for the working channel. They were 162 inches in length and 15 inches in width with a thickness of 0.361 inch. The copper was cold rolled and of high conductivity, oxygen-free stock. Since the plates were rolled on a special order and were run through the mill as single units, their edges were slightly warped from the rolling operation. In general, however, their surfaces were very nearly plane. Prior to installation they were rubbed with emery paper and polished so that they had surface finishes on the standard aircraft scale of approximately 25. During operation slight oxidation occurred, but it was not sufficient to impair the polish characteristics of the surface. Any flow investigation made in the channel must be described as pertaining to flow in smooth channels.

Instruments

The quantities of main interest in making a study of the analogy between momentum transfer and heat transfer are indicated in Equations 1 and 2. To obtain values of τ and point velocities, pressure measurements were required. Also in obtaining velocities by means of a hot wire anemometer, voltage measurements had to be made. Temperature measurements were necessary for establishing dt/dy in the flowing stream and in addition for control of the air stream and the oil baths at specified temperatures. For the establishment of the thermal flux, $\dot{Q}$, from the upper plate when considering heat transfer normal to the flowing stream calorimetric measurements were desirable. The instrumentation of the apparatus was considered from the standpoint of obtaining precise and accurate values of all the aforementioned quantities.

Of main importance in the instrumentation was the pitot tube which was mounted on the lateral center line of the channel and at the downstream end as shown in Figure 20 and point j in Figure 2. The tube was moved in a vertical plane by means of a micrometer head that mounted in the upper part of the post shown in Figure 21. Figure 22 shows the pitot tube in position immediately under the upper copper plate and between the two copper plates. The reflection of the tube is shown in the upper copper plate, and it was possible by means of this reflection to locate accurately the position of the tube with respect to the plate. An optical system allowed measurements to be made of the distance between the tube and its image. The location of the tube in the stream with respect

to the wall was then one half the distance between the object and image.

The vertical cross section of the pitot tube mounting was effectively the same as that shown in Figure 6 of the Appendix. The vertical post mounting the tube in the later apparatus was reduced in diameter so as to give less interference with the air flow. The actual pitot tube was 3/4 inch in length as extended from the vertical support tube. Its outside diameter was 0.026 inch and its inside diameter was 0.015 inch. The nose was rounded to a hemispherical shape. Figure 23 gives a detail of the tube dimensions. These dimensions are in agreement with optimum pitot tube design as described by Goldstein (9). The pitot tube had a two-fold application: 1, it was the basic standard in calibrating the hot wire anemometer and 2, it was used for vertical velocity traverses at its fixed position.

A second instrument of use in establishing the flow characteristics was a series of piezometer bars for measuring the pressure drop along the channel. They were located at points a, b, and c in Figure 2. A detail of the design is given in Figure 24. The pressure holes in the copper plates were eleven in number at each piezometer position and were spaced one inch apart. Their diameter was 1/32 inch. The streamside of the holes after drilling had all burrs removed so that in considering the diameter of the holes in relation to the size of the working channel and the care exercised in their machining it is believed that accurate static pressure measurements were possible.

Pressure leads from the pitot tube and the piezometer bars were taken to a gang manometer shown in Figure 25. The manometer was of conventional design, and by having all the tubes connected to a common atmospheric leg the number of tubes required for a given number of pressure measurements was practically halved. Kerosene was used as a manometer fluid, and the deflections were measured by means of a vertical component cathetometer also shown in Figure 25. In addition to the piezometer and pitot tube heads, the venturi meter differential was also read on the gang manometer.

The micromanometer shown in the upper right hand portion of Figure 25 was designed for use in reading pitot pressures at stream velocities of 30 feet per second or less. A closer view of the instrument is given in Figure 26. It consisted of a dial gauge in connection with a moving tilted arm mounted on a block and screw mechanism. The tilt of the arm was approximately 10 degrees and thus allowed small changes in pressure to be observed readily. The interesting feature of the micromanometer design was that the dial gauge could be moved in its gross position by one inch steps so that if necessary a total deflection of three inches could have been accurately measured.

After measurements of velocity with the fixed pitot tube and of the pressure drop along the channel by means of piezometer bars, the next measurement of interest was the one allowed by the hot wire anemometer. As noted previously, the equipment was designed to allow temperature and velocity measurements to be made along the full length of the working channel.

To attain this end, the upper and lower walls of the channel were mounted independently from each other as may be noted in Figures 11 and 13. To provide for the measurements at different points along the channel a traverse gear was designed for mounting the temperature and velocity measuring instruments. A view of the working side of the equipment is shown in Figure 27. It mounted a hot wire anemometer on two 0.020-inch steel wires that ran laterally through the channel and may be seen in Figure 27 entering the side walls of the channel. The traverse gear ran on rails as noted in Figures 28 and 29. A sectional view of the rails is given in Figure 30. They were planed to close tolerances in the Astrophysics shop of the California Institute of Technology. The task was difficult as the rails were 15 feet in length which was 2 1/2 feet longer than the total travel of the planer bed, and so two separate cuts were required in the machining.

The axial movement of the traverse gear mounting the hot wire anemometer was achieved by means of the hand wheel system shown on the left hand side of Figure 15. Vertical movement of the anemometer was accomplished by means of the lower right hand wheel in Figure 27. The counter shown indicated 0.0001 inch for each integer in the last figure so that the relative position of the anemometer in a vertical plane was very accurately fixed. For moving the hot wire laterally the upper left hand wheel in Figure 27 was used. The right hand integer in the counter corresponded to 0.001 inch so that the lateral position of the hot wire was accurately determined. In order to allow the hot wire to be moved

close to the upper or lower plates a tilting mechanism was included in the design of the traverse gear. The lower left wheel in Figure 27 operated the tilting arm shown as a horizontal bar in the center of the figure. For absolute determination of the position of the hot wire anemometer with respect to the upper and lower walls of the channel, an optical system was used which is also shown in Figure 27. The anemometer was moved close to the wall and the distance between the object and image was determined by viewing through a glass side wall shown in Figures 27 and 28. The distance of the instrument from the plate of interest was taken as half the distance between the object and image. A Starrett dial gauge with a total travel of one inch and 1/1000 inch divisions was used for locating the vertical position of the telescope. After the hot wire anemometer had been located with respect to the walls of the system, it was moved in the stream by means of the hand wheels previously described. The location of the anemometer in the stream was probably accurate within $\pm$ 0.001 inch.

A sketch of the hot wire anemometer is given in Figure 31. Its mounting in the working channel was as presented in Figure 32. The pitot tube shown in Figure 32 was an addition made for work not described in this paper. The hot wire element of the anemometer was prepared with 1 mil platinum wire in a length of 1 centimeter. One mil wire was used because it was felt that a larger size was not required for greater sensitivity since the air speeds of interest were relatively low and that a smaller size was not necessary for use in the 0.675-inch channel. The wire was

mounted on two steel needles 2 1/2 inches from the leading steel support wire so that the support wires should not have affected the velocity measurement at the position of the hot wire. For convenience the hot wire anemometer was also used as a resistance thermometer. Thus after making a velocity measurement it was possible to turn off the current to the hot wire and measure the wire resistance at the surrounding stream temperature. The size of the platinum resistance wire as compared to thermocouples that would have been used alternatively for temperature measurement was very advantageous since it was possible to move the temperature measuring instrument in this case to within a few thousandths of an inch of the channel walls, thus furnishing more detailed information on the existing temperature gradients in the fluid stream.

Electrical leads for the hot wire anemometer were run to the platinum wire in slots milled on the inner surfaces of the support needles shown in Figure 32. Because of space limitations it was necessary to use No. 36 B. & S., double silk-covered copper wire. The two potential method was used in determining the resistance of the hot wire when it was used as a resistance thermometer. Consequently two No. 36 wires were run to each side of the resistance wire. They were led out through the bakelite support case and along the rear steel support wires. When in use as an anemometer, one set of leads provided current, and the second set of copper leads was used for measuring the potential drop across the wire.

The constant resistance method was applied in the anemometry work. A diagram of the operating circuit is shown

in Figure 33. The anemometer was calibrated against the fixed pitot tube. In operation the current was measured by determining the voltage drop across a standard resistance having a nominal value of 0.05 ohm. The emf across the hot wire was obtained as previously described. Currents less than 200 milliamperes were used in the work, the wire being held at a temperature of approximately 158° F when the stream temperatures were 100 to 120° F. The purpose of operating the hot wire at a relatively low temperature was to minimize possible changes in the resistance characteristics of the wire through aging so that after the calibration had been obtained as a resistance thermometer, it would be possible for it to remain constant within the limits of the desired experimental accuracy.

In the work described here, heat transfer measurements were made from the upper plate to the flowing air stream. As in the earlier work described in the Appendix, the thermal flux was to be determined by means of a copper block calorimeter mounted in the upper copper plate. In the new apparatus it was decided that rather than to bore the copper plate to allow the calorimeter to be set into position and form part of the upper wall of the channel it would be mechanically more simple to mount the copper block on the oil stream side of the upper copper plate. Electrical analogy measurements showed that the design was feasible from the standpoint of producing an isothermal surface at the position of the calorimeter and on the air stream side of the copper plate. Therefore the calorimeter was prepared as shown in Figure 34. The

effective diameter of the calorimeter was 3.125 inches. Two calorimeters were installed on the equipment, one at the downstream end and the other at the middle. Figure 2 designates the positions of the two calorimeters as points h and j. Figure 35 shows the inside view of the calorimeter. The copper block with its milled groove for the resistance wire used in the energy input is shown inside the steel cylinder. The ring around the steel cylinder was part of the oil seal ring preventing leakage from the upper oil bath. The seal ring system was of the type shown in Figure 36 which was used for sealing the pitot tube post as it emerged from the upper oil bath.

In the operation of the calorimeters the energy input was controlled by means of thermocouples. The method was essentially the same as that used in the preliminary work. In Figure 34 the central hole in the copper block of the calorimeter was for a thermocouple mounted in the copper plate immediately underneath the calorimeter. In heat transfer operations the temperature of this thermocouple was kept the same as that of one immediately upstream from the calorimeter. Under such conditions it was assumed that the energy input from the calorimeter to the air stream was the same as that from the surrounding copper plate to the air stream. The positions of the thermocouples upstream from each calorimeter are shown in Figure 2 at points e and g. Additional control for operating the calorimeter was provided in the form of a differential thermocouple mounted in the groove at the base of

the copper block. By maintaining a zero temperature difference across the annulus a secondary control on temperature equilibrium was achieved. In order to eliminate energy losses by conduction, the steel jacket of the calorimeter was evacuated. The two calorimeters operated from the same vacuum system. A Cenco Hyvac fore-pump was used along with metal oil diffusion pumps as may be observed in Figure 4 and in detail in Figure 32.

The operation of the calorimeters was not entirely successful. In using the system whereby no temperature discontinuity was provided between the calorimeter block and the surrounding copper plates as in the preliminary work and as shown in Figure 10 of the Appendix, it was found that before energy addition was made to the calorimeter the temperature reading of the central thermocouple beneath the calorimeter was not much different from that of the thermocouple located immediately upstream from the calorimeter. Thus in adding energy to bring the calorimeter into equilibrium with the surrounding copper plate there was insufficient temperature difference to allow precise control of the energy input. Consequently inconsistent values for the different runs were obtained.

The calorimeter electrical circuit is presented in Figure 38. The resistance wire mounted in the upper surface of the copper block noted in Figure 35 was No. 26 Advance wire and had a resistance of 12 ohms. The current input was determined by measuring the emf across a standard resistance having a nominal

value of 0.005 ohm. The voltage applied to the heating element was obtained by measuring the emf across the 75 ohm portion of the divided resistance indicated in Figure 38. Both calorimeters were energized from the same voltage source, namely four 6-volt storage batteries in series.

In the establishment of the temperature profile between the copper plates it was necessary to know the temperatures of the plates. The temperatures were obtained from thermocouples mounted in the plates in the same manner as demonstrated in Figure 10 of the Appendix where the thermocouple is located just ahead of the calorimeter shield. Holes were bored so that the thermocouples were within 1/32 inch of the air side of the copper plates. The couples were located as shown in Figure 2 at points d, e, f, and g and at distances noted in Figure 20. The main temperature and velocity traverses along the vertical section of the stream were made at point g in Figure 2. Thermocouples were located in both plates, the ones in the lower plate being mirror images of those in the upper plate. As also mentioned previously, thermocouples were used in controlling the energy input to the calorimeters. In all instances the couples were copper-constantan and prepared with No. 30 wire. The junctions were butt-joined with silver solder in a hydrogen flame. A 32° F junction was used for reference. A schematic layout of the thermocouple circuits is given in Figure 39.

Gross temperatures of the air stream and of the control oil baths were measured by means of resistance thermometers of the

type commercially available from the Leeds and Northrup Company. The location of the thermometers has been described in sections concerned with the oil and air streams.

CALIBRATIONS

Resistance Thermometers

The resistance thermometers were calibrated against a Leeds and Northrup standard thermometer. Only three calibration points were considered, 32, 100, and 160° F. Since the data showed only a small deviation from a straight line drawn between the points at 32 and 160° F, the interpolation for intermediate temperatures was performed using the straight line as a basis for a residual method. A plot of $R_{meas} - R_{calc} / R_{32}$ was prepared versus temperature. All the thermometers including the standard had practically the same residual curve. Values of the calibrations of the three thermometers used in experimental work are given in Table I.

Standard Resistances

Standard resistances were used in both the hot wire anemometer and calorimeter circuits. Their values were obtained by placing them in series with certain standard resistances available in the laboratory and making emf measurements across both the basic standard and the standard at the same time. The measurements were made using nominal current values of 15 milliamperes. The standard resistances were made of manganin, and the calibrations were corrected to 25° C. As the temperature coefficient of

resistivity of manganin is zero at 25° C and since the resistances were established with accuracy of better than one part in 40,000, no corrections for temperature variation were applied to the resistances when used in the experimental runs, because the accuracy of calibration exceeded the accuracy of the application of the circuits containing the resistances. Table II gives the values of the standard resistances used in the different circuits.

Thermocouples

For the experiments of interest the thermocouples were calibrated at temperatures of 100, 110, and 120° F. In calibrating the thermocouples at a given temperature, oil was circulated in the oil baths while the air stream between the copper plates was stagnant. After equilibrium was attained wherein it was believed that the air sides of the copper plates were at the same temperatures as the oil baths, voltage readings on the thermocouples were taken. The measurements were made on a White potentiometer and were precise to within 0.2 microvolt. The main limitation on the accuracy of the calibrations was the effect of any miscellaneous thermocouple influences in the thermocouple circuits. Also the calibrations depended directly on the correctness of the resistance thermometers used in measuring the temperatures of the oil baths. The thermocouples at the upstream end of the working channel which was at the exit end of the oil streams probably had the largest errors since the control points for the oil baths were at the downstream end of the channel, and heat losses to the room may have caused unaccounted for temperature variations in the oil baths at positions away from

the control points. Table III gives the thermocouple calibrations at 100, 110, and 120° F. The data were applied only at 100 and 120° F so that for small variations from these temperatures, linear interpolations or extrapolations were used.

Hot Wire Anemometer Calibrated as a Resistance Thermometer

The hot wire instrument was calibrated as a resistance thermometer at temperatures of 100, 110, and 120° F at air speeds from zero to 90 feet per second. In the calibration the oil baths were operated at exactly the desired temperature. At the point where the resistance thermometer was calibrated an effort was made to have the free stream temperature of the air correspond to that of the oil baths. In order to accomplish the latter situation it was necessary to take into account the fact that as the air passed from the channel entrance box into the contraction section and then into the working channel, it underwent what was essentially an adiabatic expansion. For the different air speeds involved, the temperature at the entrance to the contraction section, which was also the point at which the air control thermometer was located, was held at a value such that as the air expanded into the working channel it attained the temperature of the oil baths. During the calibration of the hot wire as a resistance thermometer it was located at the downstream end of the working channel, and it is believed that by the time the air reached that point the desired free stream temperature was actually obtained. Any small variations from the desired value of this temperature at the channel

entrance should have been eliminated in the 12-foot run between the copper plates held at the correct temperatures. Figure 40 gives a plot of the resistance values versus air velocity at constant temperatures. Between zero and 60 feet per second the adiabatic recovery factor for the resistance thermometer appears to be approximately zero and then slowly rises above 60 feet per second. It may be that at the higher speeds the recovery factor was still approximately zero but slight strains in the resistance wire caused changes in its resistance values. Tabulated values of the resistances as a function of air velocity are given in Table IV.

Calibration of Hot Wire Anemometer

The hot wire anemometer was operated using the constant resistance method. A diagram of the circuit has been given in Figure 33. A resistance of 2.3625 ohms was used as the fixed value. This resistance corresponds to a temperature of approximately 158° F so that in measurements in the air channel with the upper wall at 120° F and the lower wall at 100° F the minimum temperature differential between the hot wire and air stream was 38° F. It is apparent that the temperature of the air stream had an effect of considerable consequence on the heat transfer from the hot wire. As suggested for such cases the calibration equation taking into account the temperature difference between the wire and the air stream was used. The theoretical equation is of the form

$$i^2R = (a + b\sqrt{u})(R - R_a) \qquad (3)$$

where i is the current, R is the constant resistance, R_a is the resistance of the hot wire corresponding to the point temperature, and a and b are calibration constants. In calibrating the hot wire the data were considered on the basis of Equation 3. The variation of density in the air stream was not taken into account because it was slight for a temperature change of 20° F. In the calibration, a measurement of the stream velocity was obtained by means of the fixed pitot tube, and the current required to maintain the hot wire at the selected resistance value was measured for the same stream line. Also the temperature at the point was obtained using the hot wire as a resistance thermometer. From the data, values of $i^2 / R - R_a$ were computed and plotted versus the square root of the air velocity. The calibrations were made before the beginning of an experimental run, and check points were obtained at the end of the run. The runs required approximately 24 hours for completion, and it was found that the calibration of the wire would change during that time so that the current required for a given velocity and stream temperature would drop by one half to one per cent. The variation of the calibration probably was caused by accumulation of dust on the wire during the run. As a consequence of the percentage change in current the measured air velocity would change on the order of two to four per cent. In all, the anemometry techniques as applied here were not entirely satisfactory. In future work it will be necessary to be more precise in measurement of currents and also

to insure a minimum of external influences such as dust which may change the wire calibration.

In operating the circuit shown in Figure 33 the bridge could not be balanced when the galvanometer was at maximum sensitivity because of large fluctuations of current that resulted from fluctuations in the heat transfer at the hot wire. All measurements were thus made using the circuit with the galvanometer at low sensitivity.

Three experimental runs were completed in which calibrations of the hot wire were made concurrently. It was possible to obtain calibrations at temperatures between approximately 105 and 115° F. In plotting the data and taking into account the air temperature it was found that rather than having the term $R - R_a$ to the first power the data followed more closely a plot using $(R - R_a)^{0.8}$ so that the general equation assumed a form

$$\frac{i^2}{(R - R_a)^{0.8}} = (a + b\sqrt{u}) \qquad (4)$$

with the proper units being applied. In other words the calibrations showed less dependence on the temperature than indicated in the theoretical Equation 3. Velocities between the points of calibration obtained in each run and zero feet per second were interpolated by extending the calibration curve to the $i^2 / (R - R_a)^{0.8}$ value obtained for still air. The calibration curves for three experimental runs are presented in Figure 41. The points for the different

runs do not lie on the same curve because the calibration of the wire changed appreciably between Tests 5 and 6.

Because of the uncertainties introduced by the changing calibration of the hot wire, the data obtained with this instrument were used only for measurement of velocity near the channel walls and for comparing the velocity profiles in a relative manner from point to point within the channel. The experimental data for the main channel velocities were procured from pitot tube measurements. This procedure was possible since the main temperature and velocity traverses were made at a position just upstream from the pitot tube.

Pitot Tube

Since the pitot tube was designed in accordance with accepted procedures it was not calibrated against a basic standard. Its coefficient of discharge was taken as one, and the velocity as measured by it was then obtained by evaluating $\sqrt{2gH}$, in which H is the height of fluid in feet corresponding to the pressure at the point of measurement, and g is the acceleration due to gravity.

PRECISION AND ACCURACY OF MEASUREMENTS

Pressure

The gang manometer was used in measuring the total head recorded by the pitot tube and the static pressures at the upstream, central, and downstream piezometer bars. With the cathetometer shown in Figure 25, the pressure differentials could be read within 0.01 centimeter of kerosene. Use was not made of the micromanometer in the work reported here since it was not felt that the precision

allowed by it was necessary. The micromanometer could be read to 0.001 inch of kerosene where the corresponding limiting value for the vertical component cathetometer was 0.004 inch. Density measurements on the kerosene used in the manometers were obtained by means of pycnometer readings at 17, 25, and 32° C so that in this temperature range the density values were known within two parts in eight thousand.

Temperature

Temperature measurements were made at a central point. Considerable effort was spent on the temperature measuring installation since it was an integral part of the laboratory. Figure 42 shows the temperature bench. The two instruments on the left hand side are the Mueller bridges used in the precision measurement of resistances. The central instrument is the K-2 potentiometer and the instrument on the right is the White potentiometer, the latter two instruments being used for voltage measurements. Figures 43 and 44 show the galvanometers and wiring in the internal part of the temperature bench.

The temperatures at the control points in the oil baths and the air stream were measured on the Mueller bridges. It was possible to measure the resistances of the thermometers to within one figure in the fourth decimal place. Considering the values of the resistances as recorded in Table I it is seen that the precision corresponded to 0.003° F. The absolute values of the temperatures, however, were not obtained within such small limits. Uncertainties

in the calibration of the bridge coils and of the resistance thermometers gave indication that the temperatures at the control points in the three streams were known to within $\pm 0.01^{\circ}$ F.

In making measurements with the hot wire anemometer used as a resistance thermometer, the Mueller bridge was also used. The resistance that was measured in this instance was of the order of 2.2 ohms. At the stream velocities of interest, fluctuations in temperature probably resulting from slight movement of the wire made it somewhat difficult to measure the resistance within $\pm$ 0.0002 ohm. This uncertainty in a platinum resistance of 2.2 ohms corresponds to a temperature uncertainty of $\pm 0.05^{\circ}$ F. It is probable that most of the measurements made with the hot wire as a resistance wire were more accurate than indicated by the last figure. The consistency of the temperature measurements made in a vertical traverse in the flowing stream showed that the relative values of temperatures were probably precise within $\pm 0.02^{\circ}$ F.

The plate temperatures and temperatures within the calorimeter blocks were obtained by means of copper-constantan thermocouples. Their calibrations were obtained within $\pm$ 0.2 microvolt as the degree of precision which corresponds to approximately $\pm 0.01^{\circ}$ F. Considering the possible errors in the calibration values used for the resistance thermometers it is believed that the calibration of the thermocouples was probably accurate within $\pm 0.02^{\circ}$ F. In the experimental runs it is probable that

the error in the thermocouple measurements was not greater than $\pm 0.03^{\circ}$ F. Miscellaneous thermocouple effects accounted for some of the uncertainty.

Electrical Energy

As noted in previous discussion the energy input to the calorimeters was found to be inconsistent. It is difficult to estimate the accuracy of the results. The errors did not result, however, from any difficulties in measuring the current and voltage existing at the heater elements in the calorimeters. The upstream calorimeter was used in the work as there was oil leakage into the downstream calorimeter. Emf measurements across the standard 0.005 ohm resistance were obtained to within $\pm$ 0.2 microvolt, and the emf across the 75 ohm resistance of the voltage divider shown in Figure 38 was measured to within $\pm$ 0.00002 volt. Voltages across the standard 0.005 ohm resistance were read on the White potentiometer and those across the 75 ohm resistance on the K-2 potentiometer.

Precision of measurement of the energy input to the hot wire anemometer was limited by difficulties in balancing the bridge circuit noted in Figure 33. It was not possible to reproduce the current to within $\pm$ 0.3 per cent. When considering the fact that the velocity is proportional to the fourth power of the current, the precision difficulties involved here resulted in an added velocity uncertainty of approximately $\pm$ 1 per cent. Changes in the calibration of the hot wire were probably more significant than the precision difficulties concerned. A variation of 1 per cent in the calibration current corresponded to a resulting

uncertainty in the velocity of about 4 per cent. In summing all the errors involved in the hot wire anemometry it is believed that at a speed of 90 feet per second an uncertainty of ± 5 feet per second in the measurement of the air velocity existed, and at a speed of 30 feet per second the inaccuracy was ± 1 1/2 feet per second. Further Departmental studies of experimental techniques in the application of the hot wire to velocity measurements in flowing streams having temperature gradients will certainly allow improved accuracy in the use of the instrument.

Pitot Tube Velocity

The total pressure at the pitot tube was corrected to the total dynamic head by means of a static pressure obtained from the interpolation of readings of the piezometer bars at the center part of the channel and at the downstream end. Errors involved in this operation plus the fact that the pressure readings were obtained within 0.01 centimeter indicate that the dynamic head was known within ± 0.01 centimeter of kerosene. Including these errors and the uncertainty in the discharge coefficient of the pitot tube, it is believed that at 35 feet per second the velocity was known within ± 0.6 foot per second and at 90 feet per second within ± 1 foot per second.

EXPERIMENTAL RESULTS

It was the intent of the present work to make measurements on all quantities other than fluid properties in Equations 1 and 2 for steady state, two-dimensional flow of turbulent air streams.

Thus the item of main importance was to insure that steady state conditions had been attained. It was decided that the detailed temperature and velocity measurements should be made at the downstream end of the channel at point g in Figure 2. It was felt that after a travel of approximately 11 feet in the working section the temperature and velocity profiles at this downstream section would be fully developed. To check on the fully developed character of the flow, the work was planned to allow for rapid temperature and velocity profile measurements at points e and f of Figure 2 upstream from the section of main interest.

Three experimental runs were made. The experimental data were analyzed assuming two-dimensional flow so that the Reynolds numbers characterizing the flow were computed for integrated temperature and velocity measurements made at the downstream end of the channel. The measurements were all made on the lateral center line. Thermocouple No. 18 marked the point of the main traverse, and the distance of the couple from the end of the channel is shown in Figure 20.

Runs were made at Reynolds numbers of 18,446 , 33,981 , and 47,719. In all cases the temperature at the control point in the upper oil bath was held at a nominal 120° F. Also the temperature at the control point of the lower oil bath was held at a nominal 100° F. Since steady state conditions were being considered and heat was being transferred from the upper plate through the air stream and to the lower plate, it was decided to

control the entering air at 110° F. The point for air control is indicated as m in Figure 2. It was expected that the air would come to the bulk equilibrium temperature prior to measurement at the downstream end of the channel.

Before proceeding with a discussion of the results it is apropos to review the terms in Equations 1 and 2 with particular regard to what quantities had to be measured to allow an analysis of the relation between heat and momentum transfer. First, in Equation 1, τ was obtained from a measurement of the pressure drop along the channel. After τ there was only one other term in the momentum equation that had to be established. This term was the velocity gradient, du/dy. In the experimental work considered here du/dy was obtained by making a velocity traverse from the upper wall to the lower wall of the channel and graphically determining the slope from the velocity-distance plot. The other terms in Equation 1 were established from data available in the literature. Values of μ were obtained from data collected by Keenan and Kaye (10). Values for σ were calculated considering air as a perfect gas and using the experimental value at 32° F and 14.7 pounds per square inch absolute.

Equation 2 also had two quantities to be determined experimentally. First there was $\dot{Q}$ which was to be determined from calorimetric measurements. The results, however, were not satisfactory, and so heat transfer quantities were obtained by considering the temperature gradient in the laminar layer at the

upper plate and using the equation

$$\dot{Q} = -k\frac{dt}{dy} \qquad (5)$$

The quantity dt/dy to be used in this equation and also in Equation 2 was determined graphically from a plot of temperature versus distance as obtained in a traverse from the upper to the lower plate. Data for the specific heat capacity, C_p, and k, the thermal conductivity, again were obtained from Keenan and Kaye (10). Specific weights were calculated as described above.

Velocities for the steady state conditions in the turbulent core at the downstream traverse point were derived from data obtained in a traverse with the fixed position pitot tube. The velocities near the walls were developed using the calibrations shown in Figure 41. Temperature data were obtained using the hot wire anemometer as a resistance thermometer. To check as to whether or not the velocity and temperature profiles were fully developed at the main working section, temperature and velocity measurements were made at upstream points as previously described. The velocity data for the different test sections in a given run were considered only on a relative basis since variations in the calibration of the hot wire over a single run which required as long as 24 hours resulted in uncertainty in the absolute velocity values. Consequently the comparative velocity data in the three tests which may be designated as 5, 6, and 7 in order of increasing Reynolds numbers were analyzed on the basis

of the velocity deficiency which may be written as follows

$$\frac{u_{max} - u}{u_*} \equiv u_d \qquad (6)$$

This procedure allowed the shape of the velocity curves to be compared, and even though there was uncertainty in the absolute value of the velocity it was possible to determine if the flow was fully developed. Figures 45, 46, and 47 show the velocity deficiency curves for Tests 5, 6, and 7 respectively. It is observed that the velocity profiles appear to be of the same shape from the middle of the working channel to the downstream end. Pertinent flow data for the tests are given in Table V.

There was considerably less difficulty in ascertaining if the temperature profiles represented the steady state. Figures 48, 49, and 50 show the temperature distributions for the three different tests. Smooth curves are drawn through points representing the measurements at the downstream or main test section which differ only slightly from those at the upstream stations.

In addition to the indications given by the temperature and velocity traverses as to the steady state character of the flow, Figure 51 shows the temperatures at the control points in the upper and lower oil baths as a function of time during the tests. It is observed that the temperatures at these points did not vary more than $\pm$ 0.02° F and that the mean variations were of the order of $\pm$ 0.005° F.

Velocity profiles for the main traverse point at g in Figure 2 are presented in Figures 52, 53, and 54. It is to be observed that non-symmetrical patterns were obtained, the higher velocities being found in the portion of the channel near the lower plate, which was at the lower temperature. In addition to the asymmetrical features of the velocity curves it should also be noted that the maximum velocities occurred progressively closer to the lower plate as the Reynolds number was increased. Several factors must be considered in reviewing the import of the data. One of these is that some secondary flow in a lateral direction might have been possible because of leaks in the movable side wall sections. During the runs, however, care was taken to see that leaks of consequence were eliminated. It is not believed that the leaks were a determining factor in establishing the velocity profiles that were obtained. In an effort to uncover further information on the flow patterns the data were analyzed in terms of generalized velocity parameters. Values of u^+ and y^+ were computed*, and the results are shown in Figures 55, 56, and 57. The superimposed curves indicated in these plots are those obtained empirically (11) for flow in smooth channels from numerous data of other investigators. It is seen that the experimental values in Tests 5, 6, and 7 for the upper portion of the

---

* Computations of u^+ and y^+ were based on τ_{om}. Probably τ_{oU} should have been used for the data at the upper plate and τ_{oL} for those at the lower.

channel fall reasonably close to the generalized velocity curves. Data for the lower half of the channel, however, appear to represent a different type of flow. It is within the realm of possibility that the temperature gradient in the stream and particularly in the laminar layers may have brought about variations from normal flow patterns by causing less friction and turbulence losses. The effect seemed to be one located near the lower or cooler plate. Figure 58 shows the velocity distribution obtained under isothermal conditions at the main downstream traverse point but at a relatively low speed. The existing temperature was 100° F. It is noted here that the velocity profile was more symmetrical with respect to the center of the channel. Two operations were performed, however, before this isothermal profile was taken. The channel side walls were made slightly more tight, and a very fine layer of dust was removed from the lower copper plate. It is not believed that these operations had any major effect on the type of velocity profile that would exist under isothermal or non-isothermal conditions. The asymmetry noted in the present work for the non-isothermal cases was only slightly suggested in the preliminary work as may be observed in Figure 11 of the Appendix. Here the temperature difference was only 10° F across the stream.

Experimental velocity data for Tests 5, 6, and 7 are presented in Table VI. Corresponding temperature values are given in Table VII. In reviewing the data it will be noted that traverses were made to within 0.004 inch of the upper plate and no closer than 0.013 inch of the lower plate. It was possible to make a better

approach to the upper plate because of the shape of the needles supporting the hot wire, and because the wire itself projected towards the upper plate. In future work it is planned that the needles will be made more flat at the tip and that smaller diameter platinum wire will be used. Much more satisfactory velocity and temperature measurements near the wall will be possible.

ANALYSIS OF RESULTS

The experimental data were treated with the main aim of determining values of the eddy viscosity from the momentum equation and the eddy conductivity from the heat transfer equation. The initial steps in the treatment of the data were the computations of the mean velocities and the weighted mean temperatures to be used in calculating Reynolds numbers. The mean velocity was obtained by making the following integration.

$$U = \frac{\int u \, d\left(\frac{y}{y_o}\right)}{\Delta\left(\frac{y}{y_o}\right)} \tag{7}$$

The mean temperature was taken to be a weighted mean obtained as follows:

$$t_m = \frac{\int u t \, d\left(\frac{y}{y_o}\right)}{U \, \Delta\left(\frac{y}{y_o}\right)} \tag{8}$$

In using the weighted mean a temperature was obtained that represented the thermodynamic temperature of the fluid if it were brought to rest and completely mixed in a reservoir. After obtaining the mean temperatures and velocities, Reynolds numbers were computed

from the equation

$$Re = \frac{4mU}{\nu} \tag{9}$$

The Reynolds numbers and mean values of the temperature and velocity are recorded in Table V.

The shear distributions for the different tests were computed from the change of pressure along the axis of flow. Because of the asymmetry existing in the velocity curves asymmetrical shear distributions for the different tests were obtained as shown in Figures 59, 60, and 61. In symmetrical flow the idealized shear distribution would show equal values of the shear at the upper and lower walls with zero shear at $y_o/2$. This idealized distribution is given as

$$\tau = -\frac{dp}{dx}\left(y_o/2 - y\right) \tag{10}$$

For no pressure gradients in the y direction, dp/dx is a constant for all values of y, and so the differential equation for the idealized shear becomes

$$\frac{d\tau}{dy} = \frac{dp}{dx} \tag{11}$$

Hence the slope of the shear distribution line is constant, and with zero shear at the off center point where the velocity gradient is zero, asymmetrical wall values for τ result. Values of the mean shear at the wall along with mean values pertaining specifically to the upper and lower plates are presented in Table V.

The rate of thermal transfer of energy from the upper copper plate to the air stream was ascertained from the slope of the temperature traverse at the wall since the calorimetric data were inconsistent. An enlarged representation of the temperature fields at the upper plate is given in Figure 62. It was assumed that the temperatures measured 0.004 inch from the upper plate were in the laminar layer where the temperature gradient was constant. The assumption was fairly sound for Test 5 conducted at a Reynolds number of 18,446. In this test a y^+ value of 3 based on τ_{o_m} was achieved at the upper plate. A value of 5 is normally taken as the maximum for the laminar layer. In Test 6 the assumption was not quite as satisfactory since the minimum y^+ value was 6.5 which is in the buffer layer which corresponds to y^+ values in the range 5 to 30. Similarly in Test 7 the minimum y^+ value was 6.8 which was again just outside the laminar layer. After graphically determining dt/dy, values of $\dot{Q}$ were computed. Then the Nusselt numbers for the channel under the given conditions of heat transfer were evaluated for the three tests. A plot of the results is given in Figure 63 where the Nusselt numbers are given as functions of the Reynolds number. In preparing the curve, the Nusselt number for Test 5 was taken as being most representative. The slope of the curve was determined by plotting an empirical equation recommended by McAdams (12) and making the experimental plot parallel to that of the empirical equation. Table VIII presents the data used and the results

obtained in the computation of the rate of thermal transfer, $\dot{Q}$.

Equations 1 and 2 were rearranged for relating the quantities used in solving for the eddy terms. The eddy viscosity was determined as a point function in the stream by means of the equation

$$\epsilon_m = \frac{\tau g}{\frac{du}{dy}\sigma} - \nu \qquad (12)$$

Similarly the eddy conductivity was calculated from the relationship

$$\epsilon_c = \frac{-\dot{Q}}{C_p \sigma \frac{dt}{dy}} - K \qquad (13)$$

The eddy viscosities and eddy conductivities are plotted in Figures 64, 65, and 66 for Tests 5, 6, and 7, respectively. The computed values of ϵ_m for the different runs are given in Table IX and those for ϵ_c in Table X.

It is noted that the portion of the channel toward the upper copper plate gave values capable of analysis. It is this same region that presented velocity distributions closer to those expected in smooth conduits. The portion of the channel near the lower copper plate was found to give larger eddy terms having greater uncertainty because of the difficulty in reading the relatively smaller values of du/dy and dt/dy. The eddy viscosity was more greatly affected. The difference in flow between the upper and lower portions in a vertical traverse of the channel is emphasized by the observed differences in the eddy conductivities. If the temperature distribution plots of Figures 48, 49, and 50 are

examined, it is seen that at small values of y/y_o corresponding to the lower portion of the channel, the temperature curve has a smaller slope as indicated by the dip in the essentially straight line portion in the turbulent core. This dipping accounts for the humps in the eddy conductivity curves and appears to be related to the increased eddy viscosity in this zone of flow. The seemingly more consistent results obtained for y/y_o greater than 0.5 indicate that the data in this section may be used in comparing values of the eddy conductivities and the eddy viscosities in the turbulent core. The relation appears to be a simple linear one. The data for y/y_o less than 0.5 should not, however, be discarded. They do serve to show the sensitive relationship between the eddy terms and the first derivatives of the temperature and velocity with respect to distance for small values of these latter quantities in the center of the channel.

Selected values of the eddy conductivities and the eddy viscosities for the turbulent core in the region $y/y_o > 0.5$ are recorded in Table XI. The ratios for ϵ_c and ϵ_m are included. They are within the range of ratios noted by Martinelli (5) who states that the more recent work on heat transfer gives ratios of ϵ_c / ϵ_m in the range of 1.0 to 1.7. The earlier preliminary work in the Department of Chemical Engineering showed that the two quantities were nearly equal, but these earlier data were not as capable of analysis as were those presented here.

Figure 67 is a logarithmic plot of the eddy conductivities and eddy viscosities given in Table XI. The quantities are given

as functions of the Reynolds number. Selection of the Reynolds number as the independent parameter was made on the basis that the slopes of the temperature-distance graphs were practically constant in the turbulent core for a Reynolds number range from 18,000 to 48,000. Since dt/dy was a constant, Equation 2 shows that ϵ_c would depend directly upon $\dot{Q}$ in the turbulent core where $\dot{Q}$ in turn would be related logarithmically to the Reynolds number as is implied in Figure 63. Also the eddy viscosity has been noted to be a function of the Reynolds number (13). It thus appears that with the eddy viscosity and eddy conductivity being dependent upon the Reynolds number in the same manner they should be simply related. Thus the data for the channel positions $y/y_o > 0.5$ appear to be more representative than those for $y/y_o < 0.5$.

The eddy terms may be prepared as dimensionless quantities for correlation purposes (14). Following such a procedure the selected eddy quantities in the turbulent core were divided by $4mu_*$ and presented in Table XI. It appears that from the work completed here constant values of $\frac{\epsilon_c}{4mu_*}$ may be expected. The treatment using u_* has merit since ϵ_c will increase in much the same manner as u_*, as the Reynolds number is increased.

CONCLUSIONS

The eddy conductivity as determined from experimental data recorded herein has a value in the turbulent core approximately 1.3 times that of the eddy viscosity. Further work is necessary to clarify the relationship since here the stream

showed an unexpected velocity distribution. It will be necessary to perform further work to determine whether this distribution is particularly characteristic of flow in the given channel when temperature gradients exist.

A consideration of the temperature distributions in the flowing air stream shows that the eddy conductivity is directly related to the Reynolds number since the temperature gradient in the turbulent core was found to be constant within the range of Reynolds numbers considered. The gradient decreased slightly as expected for increasing Reynolds numbers. The effect, however, was not great.

Figures 64, 65, and 66 show that the eddy conductivity had essentially a constant value in each case in the central core of the fluid stream. It seems logical that these results may be extended to the situation where $\dot{Q}$ is not a constant from point to point in a plane normal to the direction of flow. In other words ϵ_c for the turbulent core in all instances is taken as a function of the bulk flow conditions and not of the imposed temperature gradients in much the same manner that the thermal conductivity of a homogeneous substance is a function only of the temperature and pressure. Thus the equation for heat transfer in turbulent streams

$$\dot{Q} = - \epsilon_c \frac{dt}{dy} \qquad (14)$$

where ϵ_c is large compared to K, becomes the counterpart of Equation 5 for molecular heat transfer. When ϵ_c is a constant in the turbulent core, variations in $\dot{Q}$ are accounted for by changes in dt/dy.

An analysis of the heat transfer data in the turbulent core showed that practically a constant value of $\frac{\epsilon_c}{4mu_*}$ existed for the temperature fields and Reynolds numbers that were investigated. Therefore it may be possible to prepare generalized heat transfer equations for turbulent streams using this quantity. It is merely another expression relating momentum transfer and heat transfer, but it may be more satisfactory than correlating methods heretofore used.

Nomenclature

a = dimensional constant

b = dimensional constant

C_p = isobaric heat capacity, $\frac{\text{Btu}}{\text{lb } ^\circ\text{F}}$

$\frac{dt}{dy}$ = temperature gradient at y with sign determined by that of $\dot{Q}$, $^\circ\text{F/ft}$

$\frac{du}{dy}$ = velocity gradient at y taken with sign always positive, sec^{-1}

g = acceleration due to gravity, ft/sec^2

h = heat transfer coefficient, $\frac{\text{Btu}}{\text{hr.ft}^2\ ^\circ\text{F}} = \frac{\dot{Q}}{\Delta t}$

H = head of fluid at point of measurement, $\frac{\text{ft lb}}{\text{lb}}$

i = current strength, amperes

k = thermal conductivity of fluid, $\frac{\text{Btu ft}}{\text{hr ft}^2\ ^\circ\text{F}}$

K = thermometric conductivity, $\frac{\text{ft}^2}{\text{hr}} = \frac{k}{C_p \sigma}$

log = logarithm to the base 10

m = hydraulic radius, ft

Nu = Nusselt number, dimensionless, $= \frac{4mh}{k}$

p = pressure, lb/ft^2

Pr = Prandtl number, dimensionless, $= \frac{\mu C_p g}{k}$

$\dot{Q}$ = rate of thermal transfer of energy per unit area normal to direction of fluid flow, $\frac{\text{Btu}}{\text{hr ft}^2}$

R = fixed resistance of hot wire, ohm

R_a = resistance of hot wire corresponding to t, ohm

R_{meas} = measured resistance, ohm

R_{calc} = calculated resistance, ohm

R_{32} = resistance at the ice point, ohm

Re = Reynolds number, dimensionless, $= \frac{4mU}{\nu}$

Nomenclature (cont.)

t = time average temperature at any point $\frac{y}{y_o}$, ^oF

t_m = weighted bulk temperature based on velocity and temperature traverse at main working section, ^oF

u = time average velocity at any point $\frac{y}{y_o}$, ft/sec

u_d = velocity deficiency, dimensionless, $= \frac{u_{max} - u}{u_*}$

u_* = friction velocity, ft/sec $= \sqrt{\frac{\tau_{o_m} g}{\sigma}}$

u^+ = velocity to friction velocity ratio, dimensionless, $= u/u_*$

U = bulk velocity based on integrated velocity traverse at main traverse point, ft/sec

x = distance in direction of flow, ft

y, y_L = distance from lower wall, in. or ft as units require

y_U = distance from upper wall, in. or ft as units require

y_o = channel height, in. or ft as units require

$\frac{y}{y_o}$ = fractional distance from lower wall

y_L^+ = friction distance parameter, dimensionless, $= \frac{y_L u_*}{\nu}$

y_U^+ = friction distance parameter, dimensionless, $= \frac{y_U u_*}{\nu}$

Δ = difference notation

ϵ_c = eddy conductivity, ft^2/sec

ϵ_m = eddy viscosity, ft^2/sec

μ = absolute viscosity of fluid, lb sec/ft^2

ν = kinematic viscosity of fluid, ft^2/sec

σ = specific weight, lb/ft^3

τ = shear stress at any point y/y_o, lb/ft^2

τ_{o_L} = shear stress at lower wall, lb/ft^2

τ_{o_m} = mean of τ_{o_L} and τ_{o_U}, lb/ft^2

τ_{o_U} = shear stress at upper wall, lb/ft^2

REFERENCES

1. O. Reynolds, "On the Extent and Action of the Heating Surface for Steam Boilers", Proceedings of the Manchester Literary and Philosophical Society, 14, 7, (1874). Also: O. Reynolds, "Papers on Mechanical and Physical Subjects", Cambridge, 1, 81-85 (1890)

2. L. Prandtl, "Bemerkung über den Wärmeüberträgung im Rohr", Physikalische Zeitshrift, 29, 487-489 (1928)

3. G. I. Taylor, "Conditions at the Surface of a Hot Body Exposed to the Wind", Great Britain Advisory Committee for Aeronautics, Reports and Memoranda No. 272, 2, 423-429 (1916-1917)

4. Th. von Kármán, "The Analogy between Fluid Friction and Heat Transfer", Trans. A.S.M.E., 61, 705-710 (1939)

5. R. C. Martinelli, "Further Remarks on the Analogy between Heat and Momentum Transfer", Paper presented at Sixth International Congress for Applied Mechanics; Paris, France; September, 1946

6. R. E. Sprenkle, "Piping Arrangements for Acceptable Flow Meter Accuracy", Paper presented at the Annual Meeting, New York, New York, November 27 - December 1, 1944, of the American Society of Mechanical Engineers

7. G. N. Patterson, "Corner Losses in Ducts", Aircraft Engineering (1937)

8. "Fluid Meters, Their Theory and Application", A.S.M.E. Research Publication, 4th ed (1937)

9. S. Goldstein, ed, "Modern Developments in Fluid Dynamics", Oxford University Press, I, 248-250 (1938)

10. J. H. Keenan and J. Kaye, "Thermodynamic Properties of Air", John Wiley and Sons (1945)

11. L. M. K. Boelter, R. C. Martinelli, and F. Johassen, "Remarks on the Analogy Between Heat Transfer and Momentum Transfer", Trans. A.S.M.E. 63, 447 (1941)

12. W. H. McAdams, "Heat Transmission", McGraw-Hill, 168 (1942)

13. Hunter Rouse, "Elementary Mechanics of Fluids", John Wiley and Sons, 179 (1946)

14. Vito Vanoni, "Transportation of Suspended Sediment by Water", Trans. A.S.C.E., III, 67-133 (1946)

Tables

Titles for Figures

Titles for Figures (cont.)

Table I. Calibration of Resistance Thermometers

t (°F)	Thermometer No. 1 Air Stream R (ohms)	Thermometer No. 2 Upper Oil Bath R (ohms)	Thermometer No. 11 Lower Oil Bath R (ohms)
32	19.4953	18.7402	13.5625
60	20.6641	19.8643	14.3988
70	21.0803	20.2645	14.6965
80	21.4956	20.6640	14.9938
90	21.9104	21.0631	15.2906
100	22.3245	21.4617	15.5871
110	22.7374	21.8589	15.8826
120	23.1495	22.2556	16.1777
130	23.5609	22.6518	16.4725
140	23.9718	23.0477	16.7669
150	24.3818	23.4426	17.0608
160	24.7910	23.8366	17.3539

Table II. Calibrated Resistances

Circuit	Nominal Value (ohms)	Actual Value at 25° C (ohms)
Upstream calorimeter	0.005	0.0046653
	75	75.874
	1500	1500.75
Downstream calorimeter	0.005	0.0046619
	75	75.087
	1500	1500.75
Hot wire anemometer	0.05	0.051177
	0.5	0.49624

Table III. Thermocouple Calibrations

(microvolts)

Couple No.	Position	100°F	110°F	120°F
15	upper plate, d in Figure 2	1512.0	1745.0	1979.8
16	do. e in Figure 2	1517.2	1751.5	1986.8
17	do. f in Figure 2	1514.3	1748.0	1983.0
18	do. g in Figure 2	1516.7	1750.4	1986.0
19	lower plate, mirror image of 15	1511.4	1745.4	1981.6
20	do. mirror image of 16	1514.3	1747.0	1983.5
21	do. mirror image of 17	1514.5	1747.2	1984.8
22	do. mirror image of 18	1515.8	1748.7	1985.6
23	differential couple, upstream calorimeter	2.1	2.1	2.8
24	do. downstream calorimeter	1.8	0.8	1.8
26	central couple, downstream calorimeter	1513.8	1745.7	1983.4
27	north peripheral, upstream calorimeter	1515.3	1747.0	1983.6
28	east peripheral, do.	1517.3	1750.5	1986.5
29	south peripheral, do.	1515.1	1747.0	1983.4
30	west peripheral, do.	1515.4	1747.5	1984.9
31	north peripheral, downstream calorimeter	1518.9	1750.5	1989.0
32	east peripheral, do.	1518.4	1750.4	1989.3
33	south peripheral, do.	1514.5	1746.0	1984.0
34	west peripheral, do.	1518.9	1751.0	1989.4

Table IV. Calibration of Hot Wire Anemometer as a Resistance Thermometer

(Smoothed Values)

Air Velocity (ft/sec)	Resistance Values (ohms) 100° F	110° F	120° F
0	2.1371	2.1758	2.2144
10	2.1371	2.1758	2.2144
20	2.1371	2.1758	2.2144
30	2.1371	2.1758	2.2144
40	2.1371	2.1758	2.2144
50	2.1371	2.1758	2.2144
60	2.1371	2.1758	2.2144
70	2.1372	2.1759	2.2145
80	2.1374	2.1762	2.2146
90	2.1376	2.1765	2.2148

Table V. Flow Data

Test	Re	t_m (^oF)	u_{max} (ft/sec)	$(\frac{y}{y_o})_{u_{max}}$	U (ft/sec)	τ_{o_m} x10^3 (lb/ft^2)	τ_{o_U} x10^3 (lb/ft^2)	τ_{o_L} x10^3 (lb/ft^2)	u_* (ft/sec)
5	18,446	109.75	35.12	0.44	31.50	6.73	7.54	5.92	1.794
6	33,981	110.00	63.68	0.42	57.88	19.43	22.56	16.32	3.048
7	47,719	109.69	90.8	0.40	82.21	34.97	27.98	41.96	4.089

Table VI. Experimental Velocity Data

(Traverse at point g, Figure 2)

$\frac{y}{y_o}$	y_L (in.)	y_U (in.)	u (ft/sec)	ν x10^5 (ft^2/sec)	u^+	y_L^+	y_U^+
Test 5: y_o = 0.674 in., u_* = 1.794 ft/sec							
0.022a	0.015		20.65	18.87	11.51	11.89	
0.045a	0.030		27.25	18.92	15.19	23.71	
0.054	0.036		28.88	18.97	16.10	28.37	
0.058	0.039		29.16	18.97	16.25	30.47	
0.074	0.050		30.30	18.98	16.89	39.42	
0.089	0.060		31.47	19.01	17.54	47.19	
0.105	0.071		32.52	19.03	18.13	55.81	
0.120	0.081		32.79	19.03	18.28	63.64	
0.150	0.101		33.06	19.03	18.43	79.37	
0.180	0.121		33.57	19.07	18.71	94.83	
0.210	0.142		33.80	19.07	18.84	111.29	
0.239	0.161		34.35	19.07	19.15	126.25	
0.298	0.201		34.87	19.11	19.44	157.25	
0.356	0.240		34.87	19.13	19.44	187.56	
0.414	0.279		35.37	19.17	19.72	217.58	
0.472		0.356	35.14	19.18	19.59		277.52
0.528		0.318	34.88	19.23	19.44		247.22
0.585		0.280	33.93	19.27	18.91		217.30
0.643		0.241	33.70	19.29	18.78		186.75
0.701		0.202	32.13	19.31	17.91		156.36
0.759		0.162	31.04	19.33	17.30		125.29
0.789		0.142	30.20	19.37	16.83		109.57
0.819		0.122	29.65	19.37	16.53		94.19
0.848		0.102	29.09	19.37	16.22		78.27
0.880		0.082	28.48	19.42	15.88		63.09
0.919		0.055	27.35	19.43	15.25		53.88
0.926		0.050	26.63	19.43	14.84		38.50
0.942		0.039	25.63	19.48	14.29		29.93
0.956a		0.030	24.64	19.49	13.73		23.01
0.969a		0.021	20.93	19.54	11.67		16.05
0.985a		0.010	13.72	19.62	7.65		7.59
0.992a		0.005	10.19	19.68	5.68		3.80

a Velocity from hot wire anemometer measurement

Table VI. (cont.)

$\frac{y}{y_o}$	y_L (in.)	y_U (in.)	u (ft/sec)	$\nu \times 10^5$ (ft^2/sec)	u^+	y_L^+	y_U^+
Test 6: y_o = 0.676 in., u_* = 3.048 ft/sec							
0.019a	0.013		43.99	18.91	14.26	17.41	
0.029a	0.020		46.75	18.92	15.16	26.90	
0.048	0.032		51.98	18.97	16.85	42.90	
0.058	0.039		53.62	18.98	17.39	52.19	
0.074	0.050		55.22	18.98	17.91	66.97	
0.089	0.060		57.02	19.03	18.49	80.08	
0.105	0.071		58.63	19.03	19.01	94.82	
0.120	0.081		60.20	19.03	19.52	108.11	
0.150	0.101		60.65	19.07	19.67	134.58	
0.180	0.122		61.20	19.07	19.84	162.55	
0.210	0.142		61.87	19.07	20.06	189.08	
0.239	0.162		62.74	19.08	20.34	215.66	
0.297	0.201		63.70	19.13	20.65	266.88	
0.356	0.241		64.14	19.13	20.80	319.94	
0.414	0.280		64.17	19.17	20.81	370.88	
0.472		0.357	63.48	19.21	20.58		472.04
0.528		0.319	63.00	19.23	20.43		421.30
0.595		0.274	62.09	19.27	20.13		361.11
0.643		0.241	60.83	19.29	19.72		317.28
0.701		0.202	59.31	19.31	19.23		265.66
0.759		0.163	56.39	19.33	18.28		214.13
0.789		0.143	55.64	19.36	18.04		187.67
0.819		0.122	55.00	19.37	17.83		160.03
0.848		0.103	53.92	19.37	17.48		135.01
0.880		0.081	52.33	19.42	16.97		105.94
0.911		0.060	50.01	19.43	16.22		78.44
0.926		0.050	48.62	19.43	15.77		65.41
0.942		0.039	47.02	19.46	15.25		50.90
0.950		0.034	46.81	19.48	15.18		44.28
0.956a		0.030	44.94	19.48	14.57		39.12
0.970a		0.030	41.85	19.52	13.57		26.08
0.985a		0.010	32.93	19.58	10.68		12.92
0.993a		0.005	27.06	19.64	8.77		6.52
Test 7: y_o = 0.668 in., u_* = 4.089 ft/sec							
0.048	0.032		66.73	18.97	16.32	57.55	
0.058	0.039		68.78	18.98	16.82	70.02	
0.074	0.049		72.75	19.01	17.99	87.76	
0.089	0.059		75.80	19.03	18.54	105.72	
0.105	0.070		78.86	19.03	19.29	125.27	

a Velocity from hot wire anemometer measurement

Table VI. (cont.)

$\frac{y}{y_o}$	y_L (in.)	y_U (in.)	u (ft/sec)	$\nu \times 10^5$ (ft^2/sec)	u^+	y_L^+	y_U^+
0.120	0.080		81.27	19.03	19.88	143.32	
0.150	0.100		84.43	19.05	20.65	178.80	
0.180	0.120		86.77	19.07	21.22	214.42	
0.210	0.140		87.99	19.07	21.52	250.33	
0.239	0.160		89.01	19.08	21.77	285.67	
0.297	0.198		90.29	19.11	22.08	353.06	
0.356	0.238		91.09	19.13	22.28	423.86	
0.414		0.391	91.06	19.17	22.27		694.94
0.472		0.353	90.45	19.21	22.12		626.23
0.529		0.315	89.23	19.23	21.82		558.17
0.585		0.277	87.59	19.27	21.42		489.75
0.643		0.238	84.87	19.29	20.76		420.35
0.701		0.200	83.60	19.31	20.45		353.00
0.759		0.161	79.09	19.33	19.34		283.88
0.789		0.141	78.22	19.36	19.13		248.17
0.819		0.121	77.67	19.37	18.99		217.05
0.848		0.102	76.89	19.37	18.80		179.44
0.880		0.080	74.82	19.42	18.30		140.44
0.911		0.059	71.58	19.43	17.51		103.54
0.926		0.049	69.60	19.43	17.02		85.86
0.942		0.039	67.31	19.48	16.46		68.22
0.950		0.033	66.14	19.48	16.18		57.73
0.993a		0.005	43.23	19.64	10.57		8.74

a Velocity from hot wire anemometer measurement

Table VII. Experimental Temperature Data

Traverse at point g, Figure 2)

Test 5 y_o = 0.674 in.		Test 6 y_o = 0.676 in.		Test 7 y_o = 0.668 in.	
$\frac{y}{y_o}$	t (°F)	$\frac{y}{y_o}$	t (°F)	$\frac{y}{y_o}$	t (°F)
0	100.58	0	100.82	0	101.07
0.022	103.78	0.019	104.68	0.021	105.19
0.030	104.42	0.029	105.16	0.030	105.67
0.045	105.35	0.044	105.77	0.045	105.99
0.059	105.74	0.059	106.00	0.060	106.24
0.074	106.05	0.074	106.26	0.075	106.41
0.093	106.40	0.092	106.52	0.090	106.63
0.140	106.86	0.120	106.86	0.132	107.05
0.169	107.11	0.171	107.27	0.162	107.15
0.199	107.30	0.201	107.48	0.192	107.14
0.229	107.53	0.231	107.68	0.222	107.65
0.288	108.02	0.290	108.10	0.281	107.90
0.347	108.47	0.349	108.60	0.341	108.40
0.407	108.99	0.408	109.04	0.401	108.81
0.466	109.47	0.469	109.55	0.461	109.35
0.525	109.99	0.528	110.08	0.521	109.90
0.582	110.52	0.586	110.62	0.581	110.37
0.642	111.11	0.645	111.06	0.641	110.85
0.703	111.55	0.704	111.58	0.699	111.48
0.763	112.04	0.763	112.04	0.760	111.85
0.792	112.25	0.793	112.33	0.790	112.08
0.821	112.50	0.822	112.53	0.820	112.40
0.852	112.76	0.852	112.79	0.850	112.59
0.881	113.11	0.882	113.08	0.880	112.83
0.911	113.49	0.911	113.41	0.910	113.05
0.926	113.72	0.926	113.57	0.925	113.39
0.941	114.04	0.941	113.85	0.940	113.60
0.956	114.48	0.956	114.17	0.955	113.93
0.969	115.10	0.970	114.56	0.970	114.35
0.985	116.56	0.985	115.71	0.985	115.08
0.992	117.55	0.993	117.01	0.993	115.76
0.994	118.15	0.993	117.27	0.994	116.97
1	119.52	1	119.31	1	119.00

Table VIII. Thermal Transfer Data - Upper Plate to Air Stream

(as measured at point g, Figure 2)

	Test 5	Test 6	Test 7
Re	18,446	33,981	47,719
Upper plate temperature (^{o}F)	119.52	119.31	119.00
Bulk temperature, t_m (^{o}F)	109.75	110.00	109.69
Δt (^{o}F)	9.76	9.31	9.31
$-\frac{dt}{dy} \times 10^{-3}$ at upper wall ($^{o}F/ft$)	4.261	5.787	9.871
k (Btu/hr ft ^{o}F)	0.0163	0.0163	0.0163
$\dot{Q} = -k\left(\frac{dt}{dy}\right)$, (Btu/ft^{2}hr)	69.4	94.3	160.8
$h = \frac{\dot{Q}}{\Delta t}$, (Btu/ft^{2}hr ^{o}F)	7.1	10.1	17.3
4m (ft)	0.1125	0.1129	0.1115
$Nu = \frac{4mh}{k}$ (experimental)	49.7	70.9	119.5
Nu, smoothed (from Figure 63)	49.7	80.1	105.5
Selected h* (Btu/ft^{2}hr ^{o}F)	7.2	11.6	15.4
Selected $\dot{Q}$* (Btu/hr ft^2)	70.3	107.8	143.7

* As based on smoothed Nusselt number

Table IX. Values of the Eddy Viscosity, ϵ_m as Defined by Equation 12

$\frac{y}{y_o}$	t (^oF)	$\frac{du}{dy}$ x10^{-3} (sec^{-1})	σ (lb/ft^3)	τ x10^3 (lb/ft^2)	ν x10^4 (ft^2/sec)	ϵ_m x10^3 (ft^2/sec)
			Test 5: y_o = 0.674 in.			
0.01	102.64	28.430	0.0682	5.83	1.878	--
0.02	103.85	6.080	0.0680	5.70	1.881	0.26
0.04	105.09	2.208	0.0679	5.42	1.900	0.97
0.06	105.77	1.300	0.0678	5.15	1.900	1.69
0.08	106.18	0.902	0.0678	4.88	1.900	2.37
0.10	106.47	0.649	0.0677	4.62	1.903	3.19
0.15	106.98	0.388	0.0677	3.94	1.903	4.63
0.20	107.35	0.242	0.0676	3.52	1.907	6.73
0.25	107.76	0.165	0.0676	2.59	1.907	7.44
0.30	108.18	0.101	0.0675	1.92	1.910	8.83
0.35	108.59	0.054	0.0675	1.23	1.910	10.78
0.40	109.01	0.027	0.0674	0.55	1.914	9.64
0.45	109.42	0.011	0.0674	0.15	1.914	6.24
0.50	109.84	0.079	0.0673	0.83	1.918	4.83
0.55	110.23	0.136	0.0673	1.50	1.918	5.08
0.60	110.68	0.191	0.0672	2.17	1.919	5.24
0.65	111.09	0.249	0.0672	2.84	1.933	5.26
0.70	111.50	0.300	0.0671	3.52	1.938	5.42
0.75	111.92	0.369	0.0671	4.18	1.938	5.23
0.80	112.33	0.431	0.0671	4.85	1.938	5.20
0.85	112.78	0.531	0.0670	5.53	1.940	4.78
0.90	113.31	0.710	0.0669	6.18	1.943	3.98
0.92	113.62	0.840	0.0669	6.47	1.943	3.51
0.94	114.03	1.157	0.0668	6.73	1.945	2.61
0.96	114.66	1.911	0.0667	7.01	1.948	1.56
0.98	115.86	6.980	0.0666	7.28	1.951	0.31
0.99	117.19	21.81	0.0664	7.43	1.958	--
			Test 6: y_o = 0.676 in.			
0.01	104.01	16.350	0.0680	15.93	1.881	0.27
0.02	104.73	7.910	0.0679	15.54	1.883	0.74
0.04	105.53	3.455	0.0678	14.71	1.900	1.83
0.06	106.03	2.143	0.0678	14.00	1.900	2.90
0.08	106.36	1.561	0.0677	13.20	1.903	3.82

Table IX. (cont.)

$\frac{y}{y_o}$	t (^oF)	$\frac{du}{dy}$ x10^{-3} (sec^{-1})	σ (lb/ft^3)	τ x10^3 (lb/ft^2)	ν x10^4 (ft^2/sec)	ϵ_m x10^3 (ft^2/sec)
0.10	106.68	1.177	0.0677	12.44	1.903	4.83
0.15	107.13	0.665	0.0676	10.51	1.907	7.31
0.20	107.63	0.397	0.0676	8.60	1.907	10.12
0.25	107.87	0.230	0.0675	6.64	1.910	13.50
0.30	108.23	0.124	0.0675	4.68	1.910	17.71
0.35	108.62	0.063	0.0675	2.69	1.910	20.03
0.40	109.03	0.015	0.0674	0.70	1.914	9.99
0.50	109.86	0.138	0.0673	3.11	1.918	10.53
0.55	110.28	0.227	0.0673	5.07	1.918	10.49
0.60	110.68	0.328	0.0672	6.98	1.933	10.01
0.65	111.09	0.424	0.0672	8.94	1.933	9.88
0.70	111.50	0.521	0.0671	10.88	1.938	9.79
0.75	111.92	0.593	0.0671	12.81	1.938	10.15
0.80	112.33	0.736	0.0670	14.61	1.938	9.35
0.85	112.74	0.929	0.0670	16.70	1.940	9.44
0.90	113.28	1.283	0.0669	18.60	1.943	6.77
0.92	113.51	1.522	0.0669	19.40	1.943	5.93
0.94	113.82	1.920	0.0668	20.20	1.945	4.87
0.96	114.32	2.788	0.0668	20.98	1.945	3.43
0.98	115.21	5.910	0.0667	21.78	1.948	1.58
0.99	116.25	29.40	0.0666	22.14	1.951	0.17
		Test 7: y_o = 0.668 in.				
0.01	104.32	19.98	0.0680	27.20	1.881	0.46
0.02	105.14	10.54	0.0679	26.50	1.900	1.00
0.04	105.89	6.530	0.0678	25.08	1.900	1.63
0.06	106.33	4.690	0.0677	23.70	1.903	2.21
0.08	106.58	3.545	0.0677	22.30	1.903	2.81
0.10	106.76	2.770	0.0677	20.95	1.903	3.40
0.15	107.15	1.432	0.0676	17.42	1.907	5.59
0.20	107.50	0.785	0.0676	14.00	1.907	8.29
0.25	107.85	0.448	0.0676	10.45	1.907	10.91
0.30	108.19	0.248	0.0675	7.03	1.910	13.34
0.35	108.58	0.101	0.0675	3.50	1.910	16.32
0.45	109.35	0.098	0.0674	3.52	1.914	16.99
0.50	109.75	0.229	0.0673	7.01	1.918	14.43
0.55	110.10	0.389	0.0673	10.57	1.918	12.76
0.60	110.50	0.502	0.0672	14.05	1.933	13.19

Table IX. (cont.)

$\frac{y}{y_o}$	t (^oF)	$\frac{du}{dy}$ x10^{-3} (sec^{-1})	σ (lb/ft^3)	τ x10^3 (lb/ft^2)	ν x10^4 (ft^2/sec)	ϵ_m x10^3 (ft^2/sec)
0.65	110.92	0.643	0.0672	17.57	1.933	12.86
0.70	111.34	0.724	0.0671	21.04	1.938	13.74
0.75	111.71	0.855	0.0671	24.57	1.938	13.54
0.80	112.12	1.012	0.0670	28.04	1.938	13.11
0.85	112.52	1.239	0.0670	31.55	1.940	12.03
0.90	113.04	1.725	0.0669	35.02	1.943	9.57
0.92	113.27	2.130	0.0669	36.45	1.943	8.04
0.94	113.60	2.687	0.0669	37.90	1.943	6.58
0.96	114.06	4.090	0.0668	39.30	1.945	4.53
0.98	114.77	8.900	0.0667	40.65	1.948	2.01
0.99	115.44	26.03	0.0666	41.35	1.951	0.57

Table X. Values of the Eddy Conductivity, ϵ_c as Defined by Equation 13

$\frac{y}{y_o}$	t (^oF)	$-\frac{dt}{dy}$ x10^{-3} (^oF/ft)	c_p (Btu/lb^oF)	σ (lb/ft^3)	K (ft^2/hr)	$\dot{Q}$ (Btu/hr ft^2)	ϵ_c x10^3 (ft^2/ sec)
			Test 5: y_o = 0.674 in.				
0.01	102.64	2.910	0.2403	0.0682	0.970	70.3	0.14
0.02	103.85	1.630	0.2403	0.0680	0.972	70.3	0.46
0.04	105.09	0.755	0.2403	0.0679	0.979	70.3	1.31
0.06	105.77	0.459	0.2403	0.0678	0.979	70.3	2.33
0.08	106.18	0.308	0.2403	0.0678	0.979	70.3	3.60
0.10	106.47	0.231	0.2403	0.0677	0.981	70.3	4.93
0.15	106.98	0.154	0.2403	0.0677	0.981	70.3	9.65
0.20	107.35	0.141	0.2403	0.0676	0.983	70.3	8.20
0.25	107.76	0.140	0.2403	0.0676	0.983	70.3	8.27
0.30	108.18	0.145	0.2403	0.0675	0.985	70.3	8.02
0.35	108.59	0.148	0.2403	0.0675	0.985	70.3	7.87
0.40	109.01	0.148	0.2403	0.0674	0.987	70.3	7.87
0.45	109.42	0.148	0.2403	0.0674	0.994	70.3	7.87
0.50	109.84	0.148	0.2403	0.0673	0.996	70.3	7.87
0.55	110.23	0.148	0.2403	0.0673	0.996	70.3	7.87
0.60	110.68	0.148	0.2403	0.0672	0.996	70.3	7.87
0.65	111.09	0.148	0.2403	0.0672	0.996	70.3	7.87
0.70	111.50	0.148	0.2403	0.0671	0.998	70.3	7.89
0.75	111.92	0.151	0.2403	0.0671	0.998	70.3	7.71
0.80	112.33	0.152	0.2404	0.0671	0.998	70.3	7.65
0.85	112.78	0.165	0.2404	0.0670	1.003	70.3	7.04
0.90	113.31	0.230	0.2404	0.0669	1.005	70.3	4.97
0.92	113.62	0.321	0.2404	0.0669	1.005	70.3	3.49
0.94	114.03	0.466	0.2404	0.0668	1.008	70.3	2.32
0.96	114.66	0.726	0.2404	0.0667	1.009	70.3	1.39
0.98	115.86	1.500	0.2404	0.0666	1.010	70.3	0.53
0.99	117.19	3.550	0.2404	0.0664	1.012	70.3	0.06
			Test 6: y_o = 0.676 in.				
0.01	104.01	1.933	0.2403	0.0680	0.972	107.8	0.68
0.02	104.73	1.028	0.2403	0.0679	0.979	107.8	1.51
0.04	105.53	0.527	0.2403	0.0678	0.979	107.8	3.20
0.06	106.03	0.350	0.2403	0.0678	0.979	107.8	4.95
0.08	106.36	0.261	0.2403	0.0677	0.981	107.8	6.73

Table X. (cont.)

$\frac{y}{y_o}$	t (^oF)	$-\frac{dt}{dy}$ x10^{-3} (^oF/ft)	C_p (Btu/lb^oF)	σ (lb/ft^3)	K (ft^2/hr)	$\dot{Q}$ (Btu/hr ft^2)	ϵ_c x10^3 (ft^2/sec)
0.10	106.68	0.210	0.2403	0.0677	0.981	107.8	8.42
0.15	107.13	0.151	0.2403	0.0676	0.983	107.8	11.87
0.20	107.63	0.129	0.2403	0.0676	0.983	107.8	13.87
0.25	107.87	0.129	0.2403	0.0675	0.985	107.8	13.92
0.30	108.23	0.137	0.2403	0.0675	0.985	107.8	13.12
0.35	108.62	0.145	0.2403	0.0675	0.985	107.8	12.42
0.40	109.03	0.145	0.2403	0.0674	0.994	107.8	12.44
0.45	109.45	0.145	0.2403	0.0674	0.994	107.8	12.44
0.50	109.86	0.145	0.2403	0.0673	0.996	107.8	12.48
0.55	110.28	0.145	0.2403	0.0673	0.996	107.8	12.48
0.60	110.68	0.145	0.2403	0.0672	0.996	107.8	12.48
0.65	111.09	0.145	0.2403	0.0672	0.996	107.8	12.48
0.70	111.50	0.145	0.2403	0.0671	0.998	107.8	12.48
0.75	111.92	0.145	0.2403	0.0671	0.998	107.8	12.48
0.80	112.33	0.146	0.2404	0.0670	0.998	107.8	12.37
0.85	112.74	0.163	0.2404	0.0670	0.998	107.8	11.09
0.90	113.28	0.199	0.2404	0.0669	1.005	107.8	9.02
0.92	113.51	0.249	0.2404	0.0669	1.005	107.8	6.86
0.94	113.82	0.347	0.2404	0.0668	1.005	107.8	5.04
0.96	114.32	0.544	0.2404	0.0668	1.005	107.8	3.12
0.98	115.21	1.283	0.2404	0.0667	1.006	107.8	1.16
0.99	116.25	2.922	0.2404	0.0666	1.006	107.8	0.35
			Test 7: y_o = 0.668 in.				
0.01	104.32	2.198	0.2403	0.0680	0.972	143.7	0.84
0.02	105.14	1.001	0.2403	0.0679	0.979	143.7	2.16
0.04	105.89	0.441	0.2403	0.0678	0.979	143.7	5.26
0.06	106.33	0.278	0.2403	0.0677	0.981	143.7	8.52
0.08	106.58	0.196	0.2403	0.0677	0.981	143.7	12.18
0.10	106.76	0.159	0.2403	0.0677	0.981	143.7	15.11
0.15	107.15	0.123	0.2403	0.0676	0.983	143.7	19.61
0.20	107.50	0.125	0.2403	0.0676	0.983	143.7	19.23
0.25	107.85	0.133	0.2403	0.0676	0.983	143.7	18.00
0.30	108.19	0.130	0.2403	0.0675	0.985	143.7	18.43
0.35	108.58	0.135	0.2403	0.0675	0.985	143.7	17.82
0.40	108.96	0.141	0.2403	0.0674	0.994	143.7	17.14
0.45	109.35	0.141	0.2403	0.0674	0.994	143.7	17.14
0.50	109.75	0.141	0.2403	0.0673	0.996	143.7	17.19
0.55	110.10	0.141	0.2403	0.0673	0.996	143.7	17.19

Table X. (cont.)

$\frac{y}{y_o}$	t (^oF)	$-\frac{dt}{dy} \times 10^{-3}$ ($^oF/ft$)	C_p (Btu/lb^oF)	σ (lb/ft^3)	K (ft^2/hr)	$\dot{Q}$ (Btu/hr ft^2)	$\epsilon_c \times 10^3$ (ft^2/sec)
0.60	110.50	0.141	0.2403	0.0672	0.996	143.7	17.19
0.65	110.92	0.141	0.2403	0.0672	0.996	143.7	17.19
0.70	111.34	0.141	0.2403	0.0671	0.998	143.7	17.19
0.75	111.71	0.141	0.2403	0.0671	0.998	143.7	17.21
0.80	112.12	0.141	0.2404	0.0670	0.998	143.7	17.21
0.85	112.52	0.157	0.2404	0.0670	0.998	143.7	15.40
0.90	113.04	0.213	0.2404	0.0669	1.005	143.7	11.30
0.92	113.27	0.258	0.2404	0.0669	1.005	143.7	9.29
0.94	113.60	0.328	0.2404	0.0669	1.005	143.7	7.24
0.96	114.06	0.474	0.2404	0.0668	1.005	143.7	4.93
0.98	114.77	0.843	0.2404	0.0667	1.006	143.7	2.65
0.99	115.44	1.688	0.2404	0.0666	1.006	143.7	1.18

Table XI. Selected Values of ϵ_m and ϵ_c for the Turbulent Core

Data from region $y/y_o > 0.5$

Test	Re	$\epsilon_c \times 10^3$ (ft^2/sec)	$\epsilon_m \times 10^3$ (ft^2/sec)	ϵ_c / ϵ_m	$\frac{\epsilon_c}{4mu_*} \times 10^3$	$\frac{\epsilon_m}{4mu_*} \times 10^3$
5	18,446	7.9	5.3	1.50	39.0	25.6
6	33,981	12.5	10.2	1.22	36.3	29.7
7	47,719	17.2	13.4	1.28	37.7	29.4

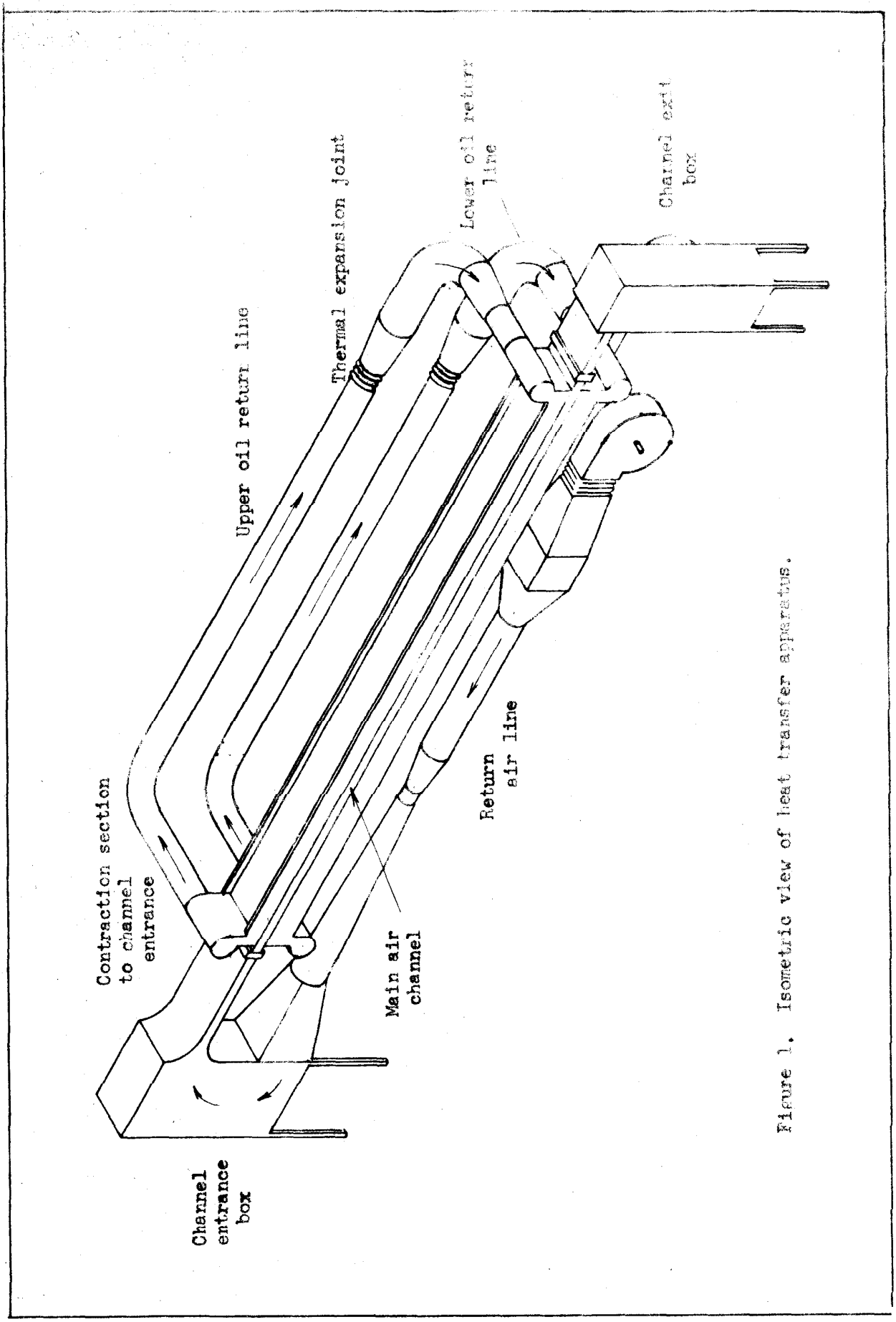

Figure 1. Isometric view of heat transfer apparatus.

Legend for Figure 2

a upstream piezometer bar

b central piezometer bar

c downstream piezometer bar

d plate thermocouple, No. 15

e plate thermocouple, No. 16

f plate thermocouple, No. 17

g plate thermocouple, No. 18

h upstream calorimeter

i downstream calorimeter

j fixed pitot tube

k temperature control and measurement, upper oil bath

l temperature control and measurement, lower oil bath

m gross temperature measurement, air stream

n temperature control point, air stream

p control heater, air stream

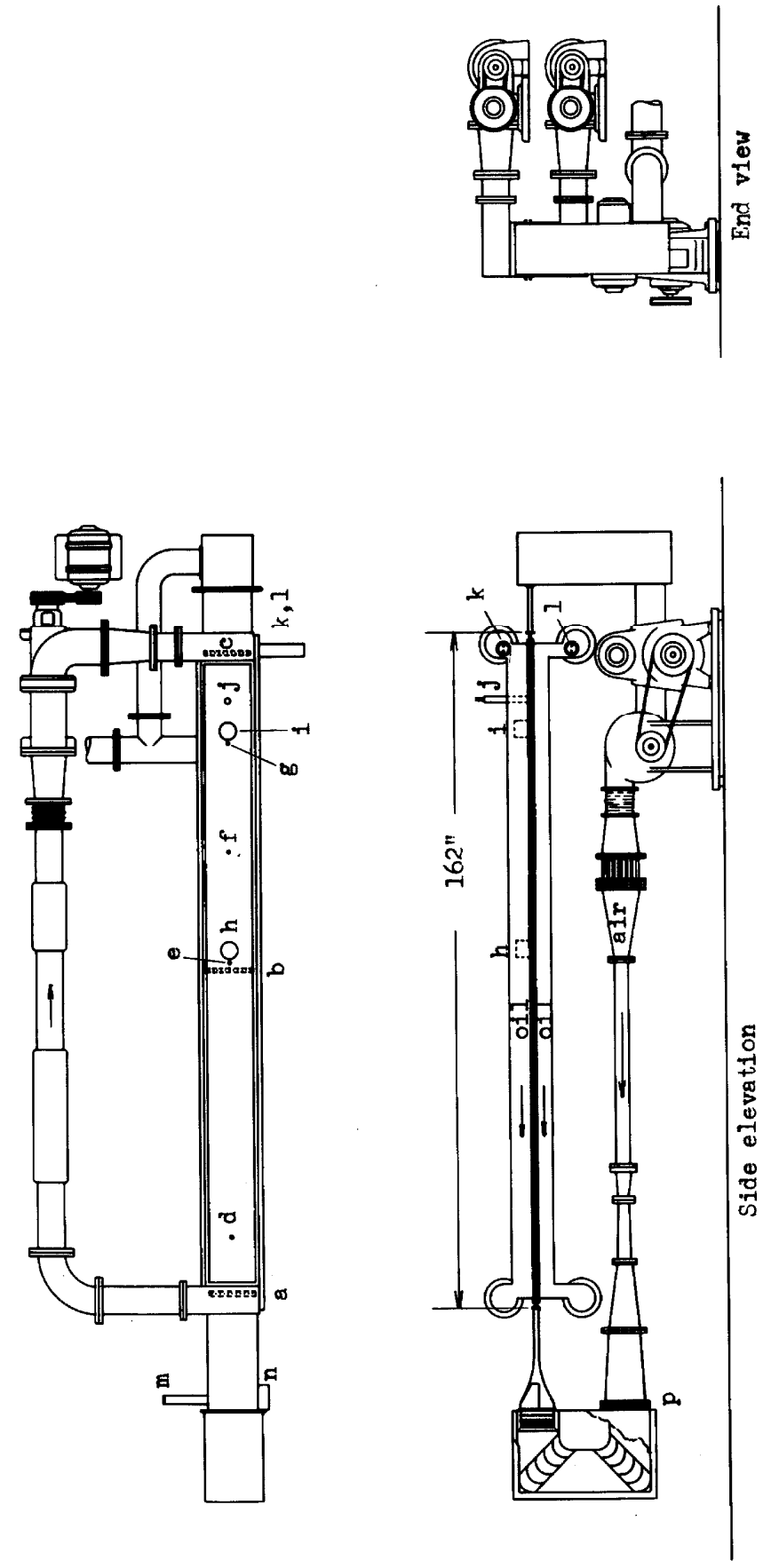

Figure 2. Schematic view of heat transfer apparatus.

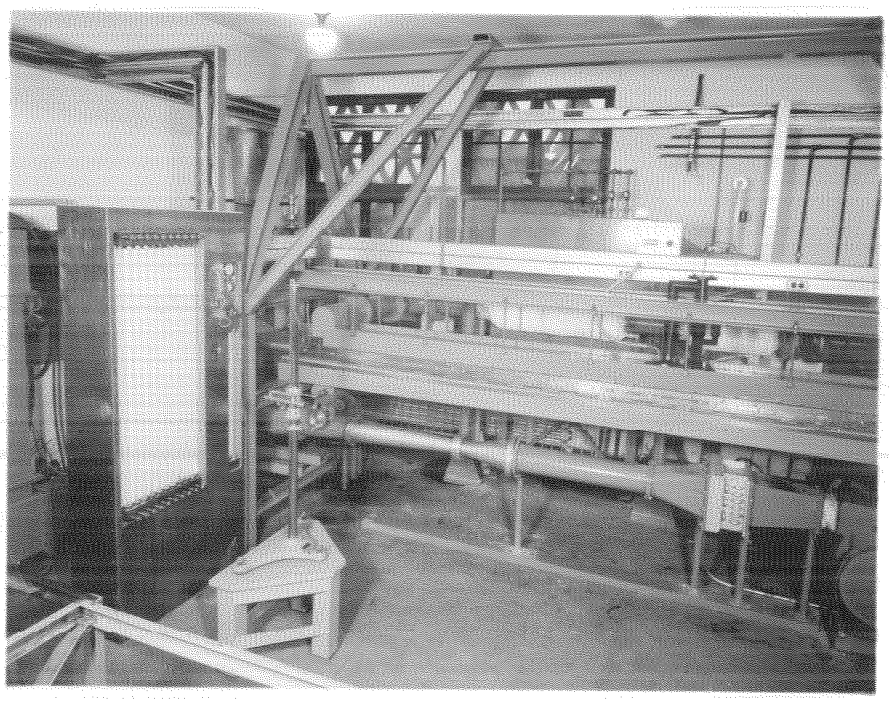

Figure 3. General view of heat transfer apparatus upstream end.

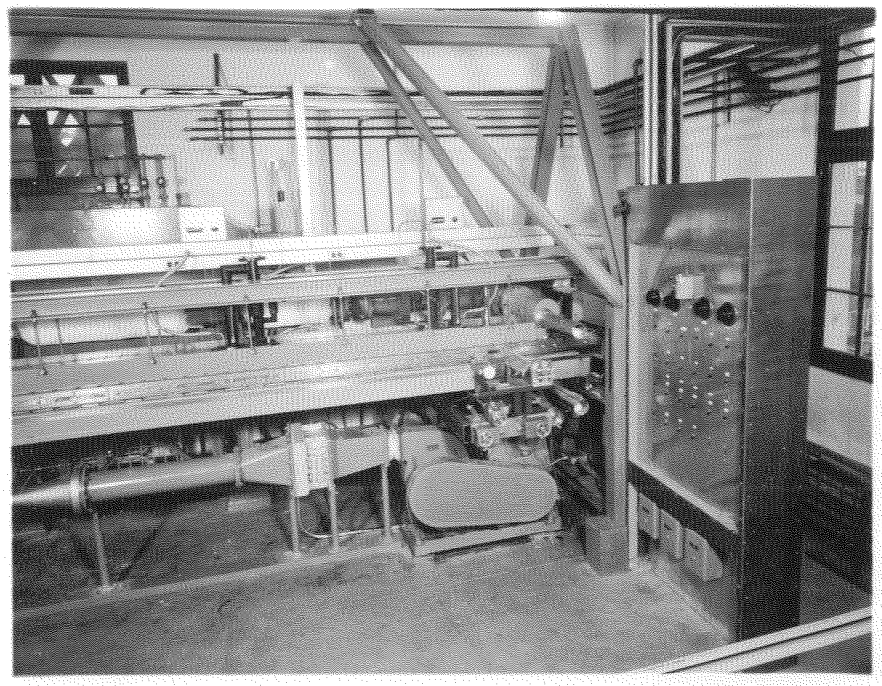

Figure 4. General view of heat transfer apparatus downstream end.

Figure 7. Channel Entrance Box.

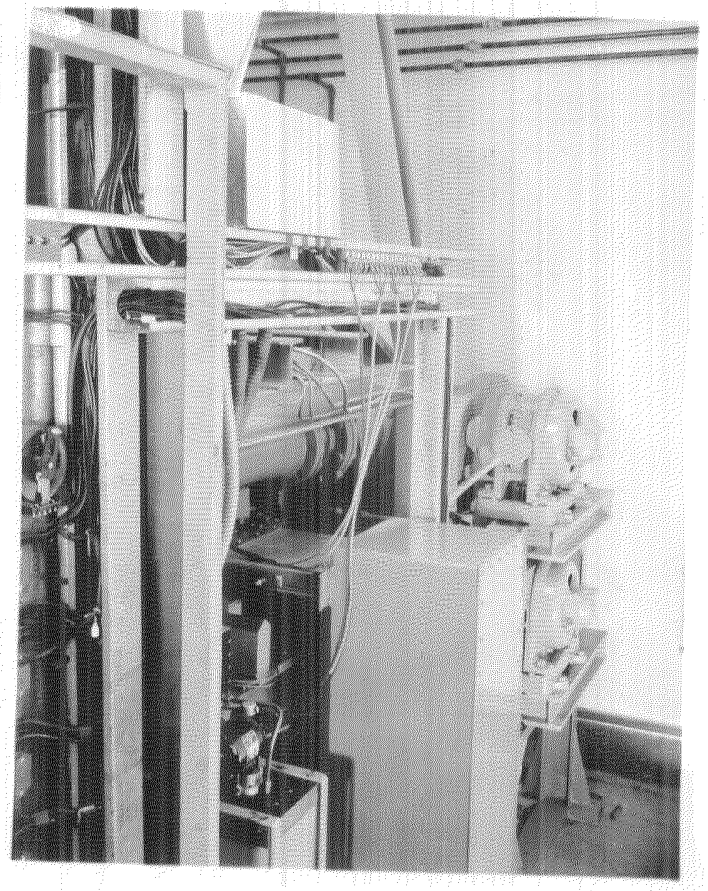

Figure 8. Channel Exit Box.

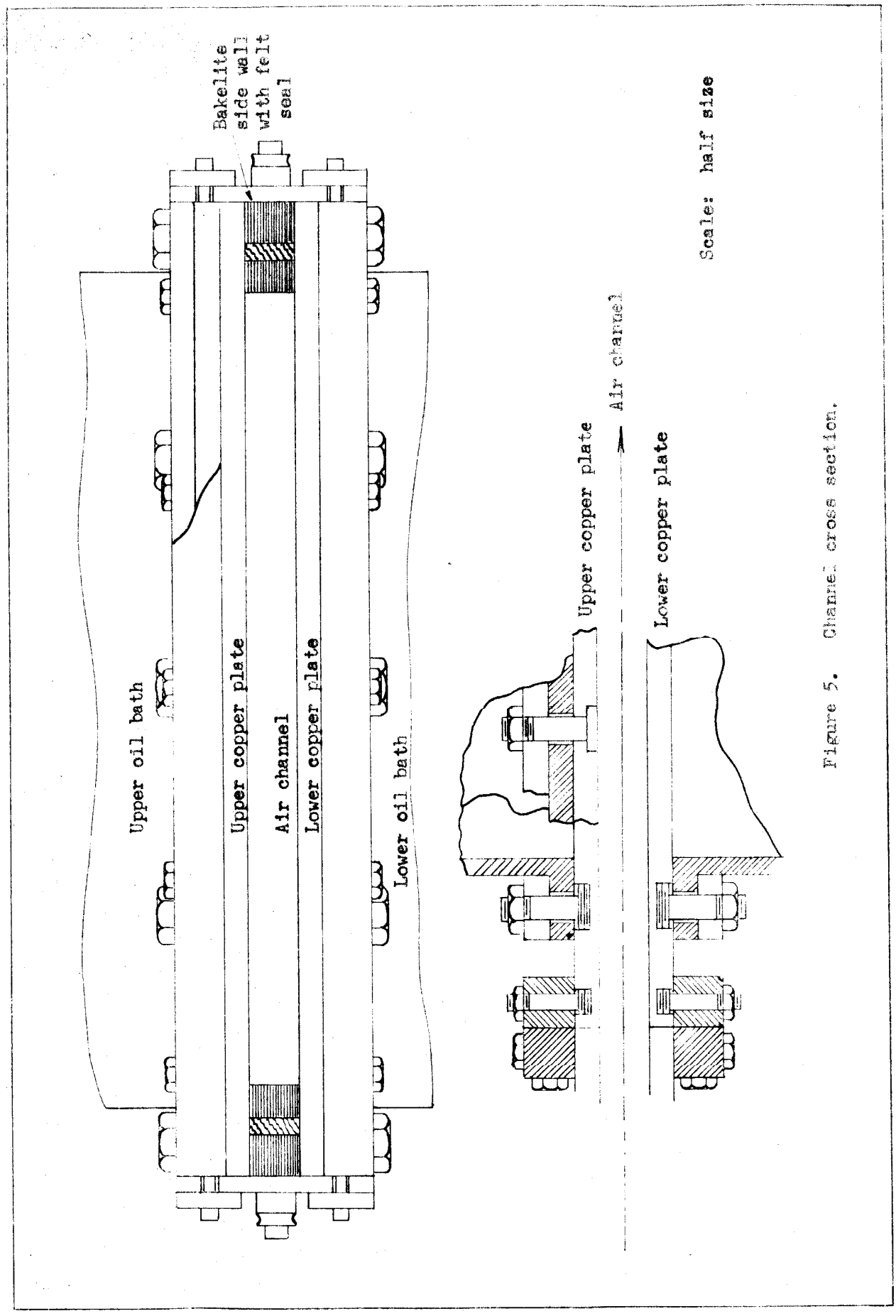

Figure 5. Channel cross section.

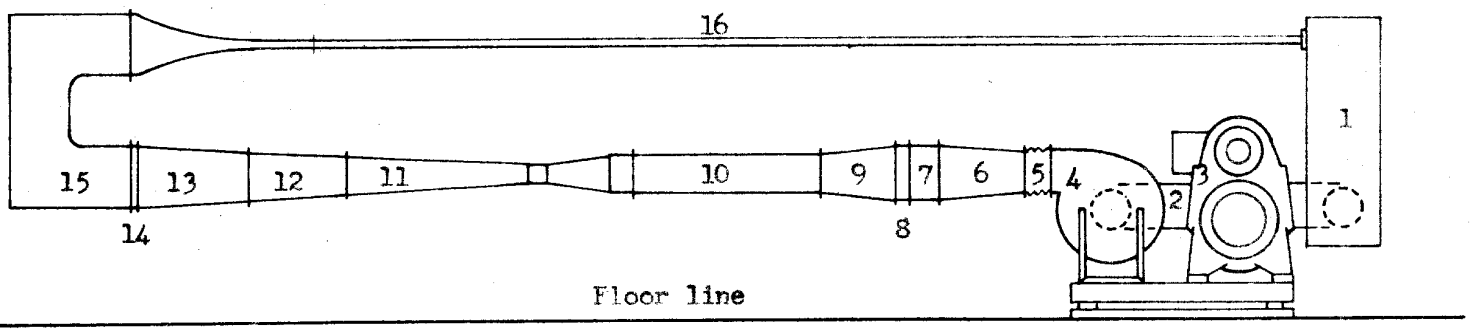

1 Channel exit box

2 Ell and tee sections

3 Variable speed motor

4 Blower

5 Canvas connector

6 Transition section, blower to cooler

7 Cooler

8 Heater, 1500 watt

9 Transition section, upstream

10 Approach section

11 Venturi meter

12 Transition section, downstream

13 Transition section, 10 in. x 14 in.

14 Heater, 200 watt

15 Channel entrance box

16 Working channel

Figure 6. Side elevation of air system.

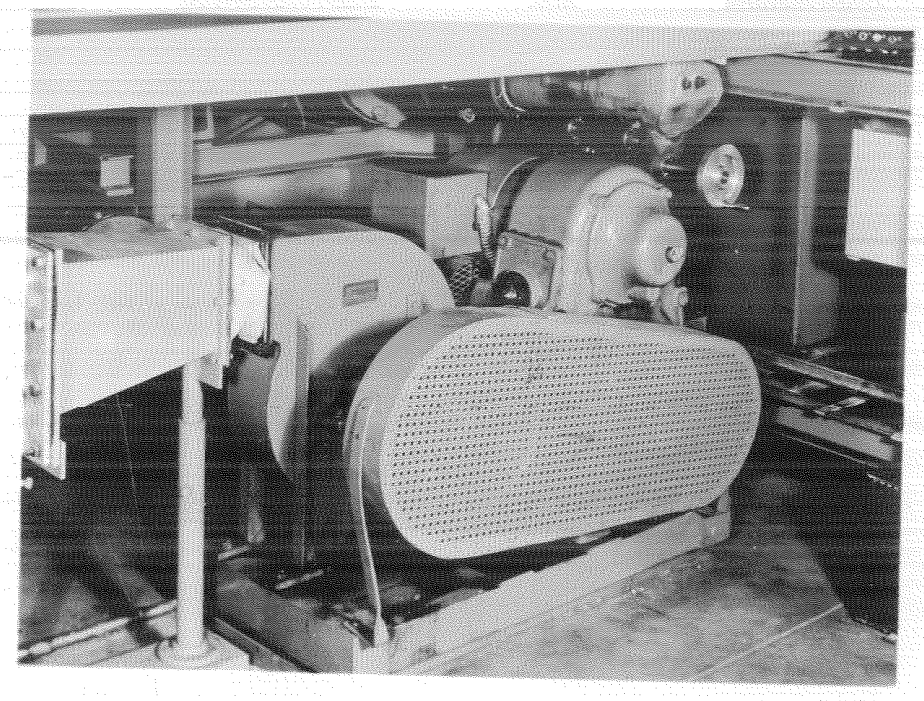

Figure 9. Blower and drive.

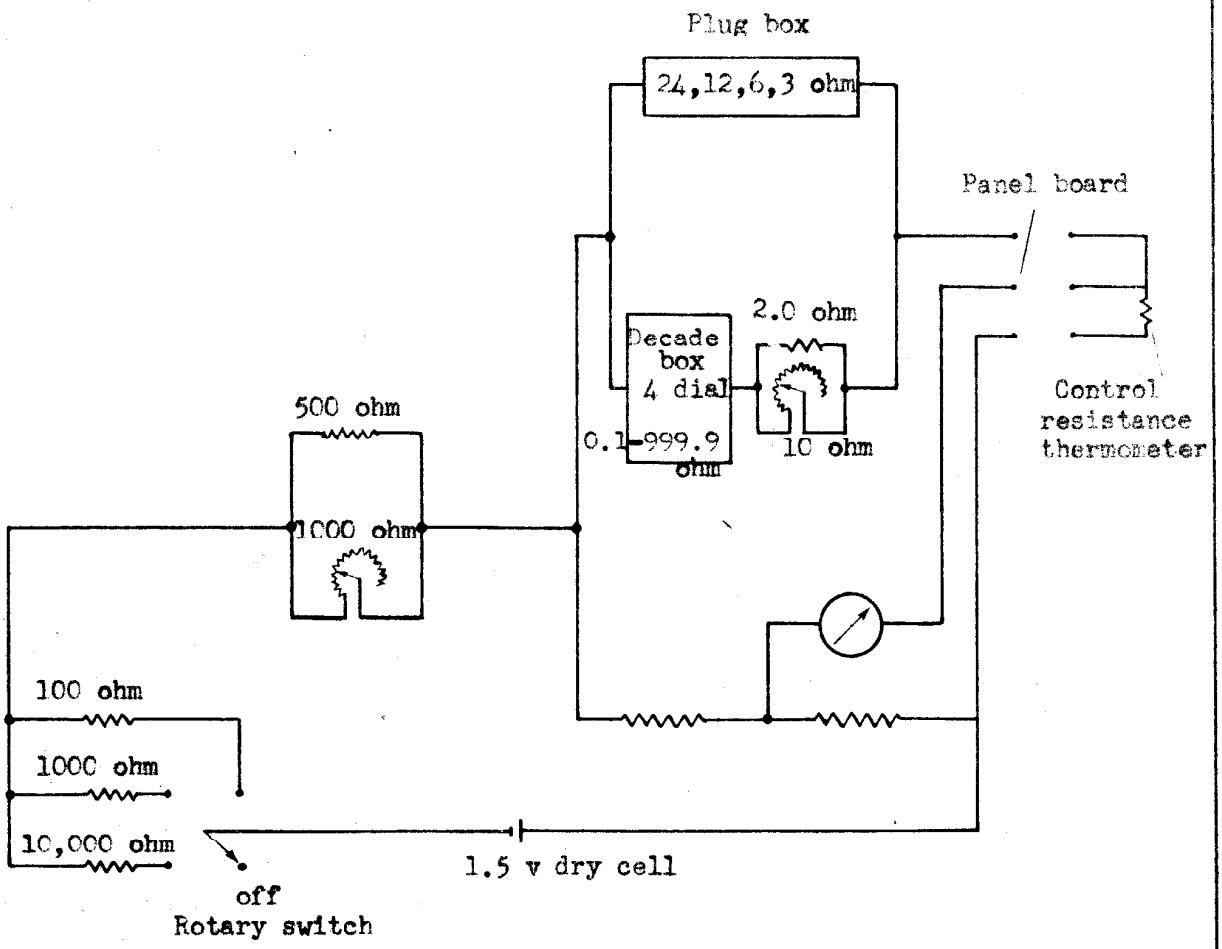

Figure 10. Bridge section of temperature control circuit.

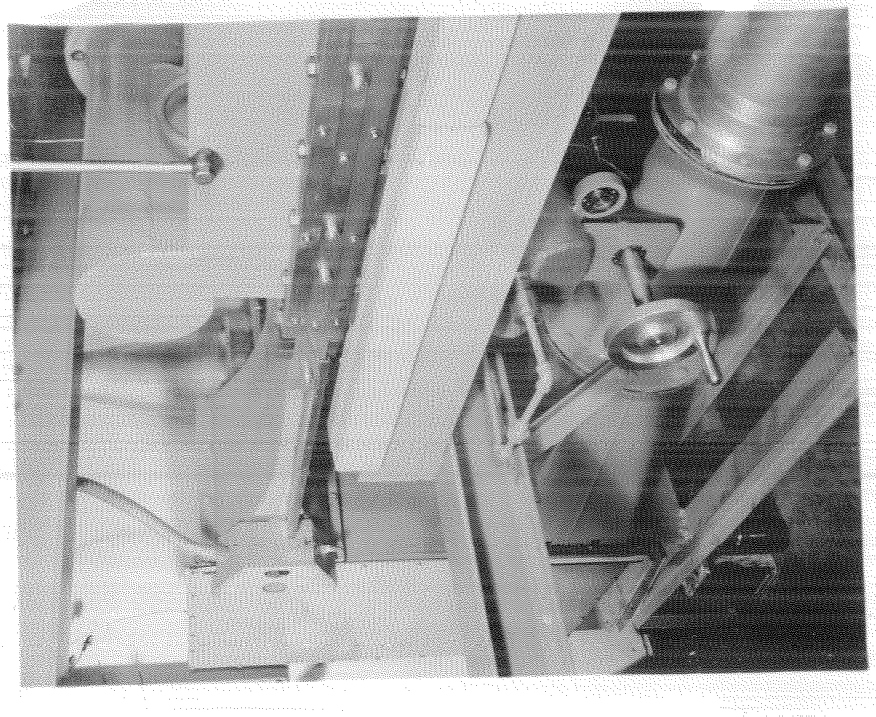

Figure 12. Group of side wall sections in place.

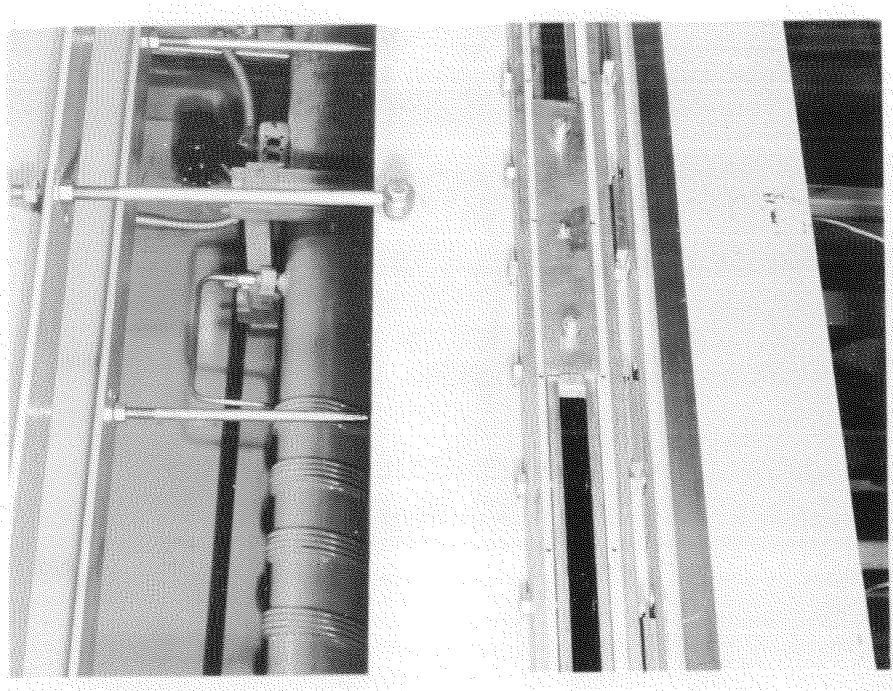

Figure 11. Bakelite side wall section in place.

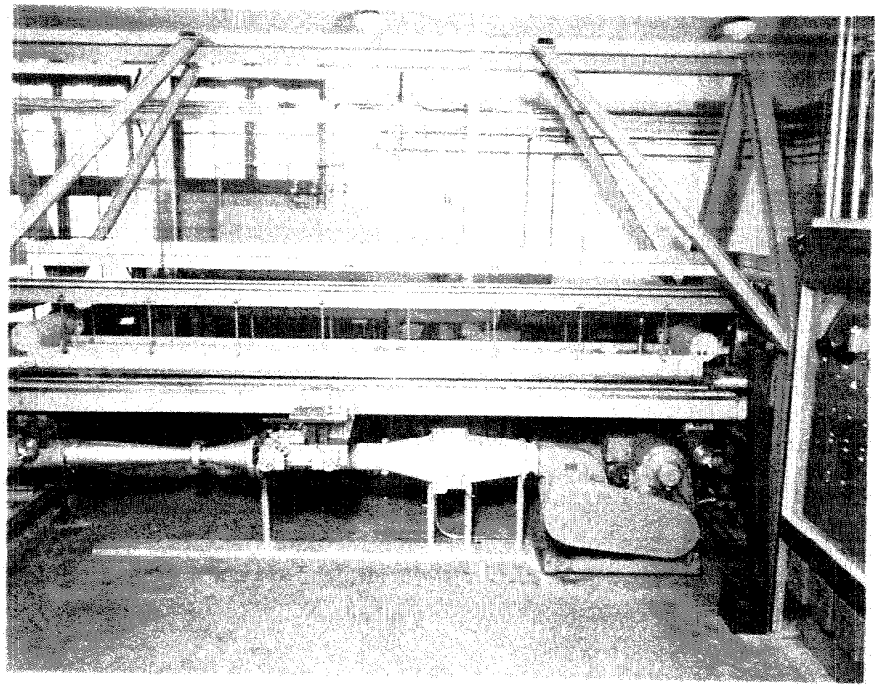

Figure 13. Channel with side walls removed.

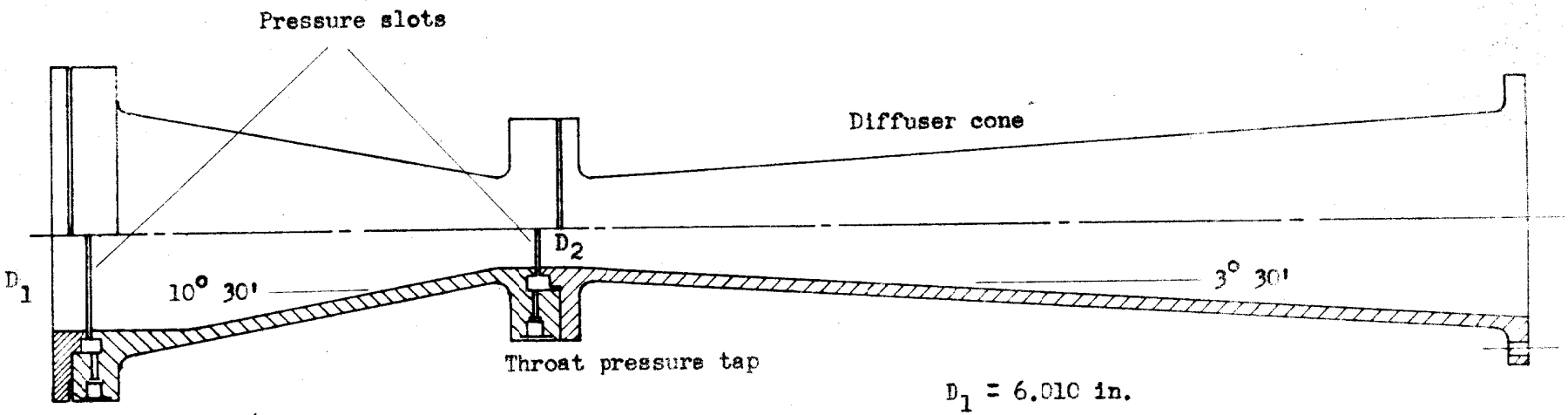

D_1 = 6.010 in.

D_2 = 2.404 in.

Material: Alcoa alloy 43

Finish: Smooth machine after casting

Figure 14. 6-inch Venturi meter

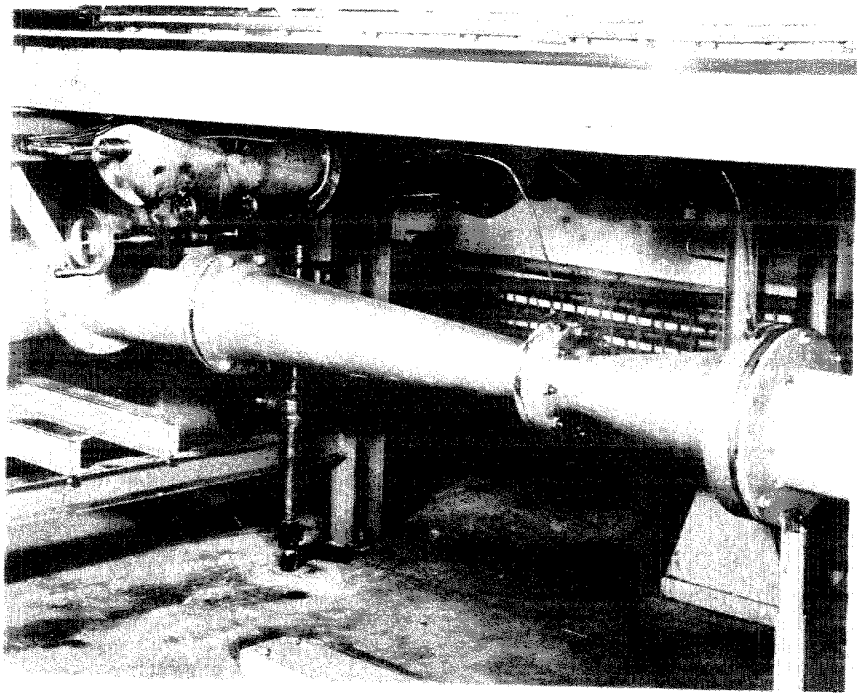

Figure 15. 6-in. venturi meter in position.

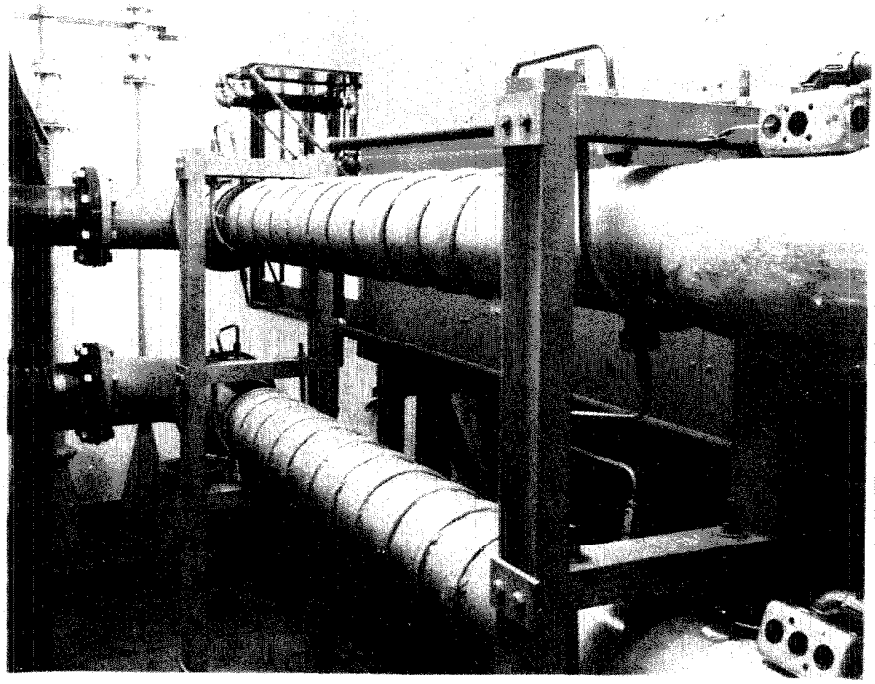

Figure 16. Oil lines leaving baths.

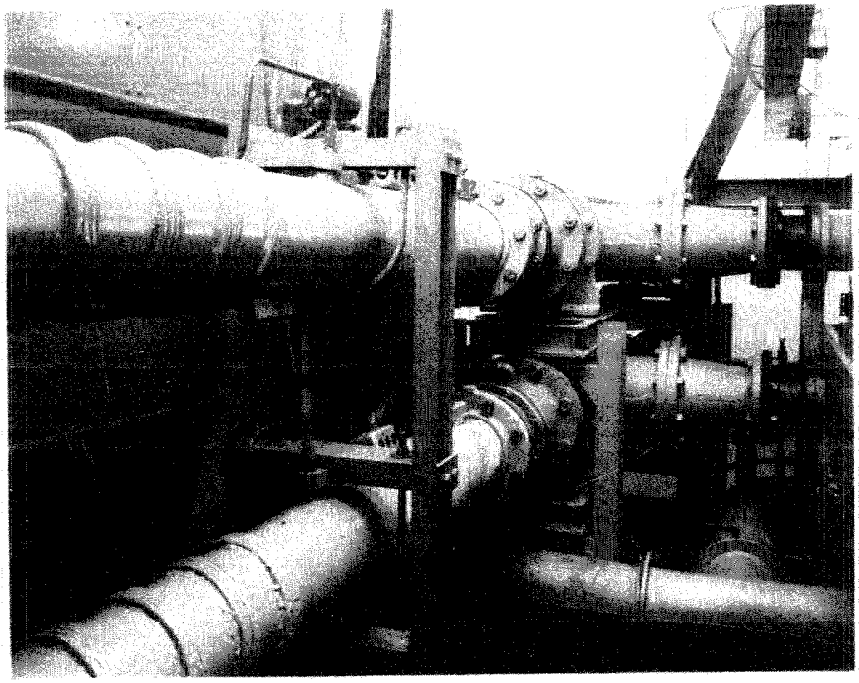

Figure 27. Oil lines entering baths.

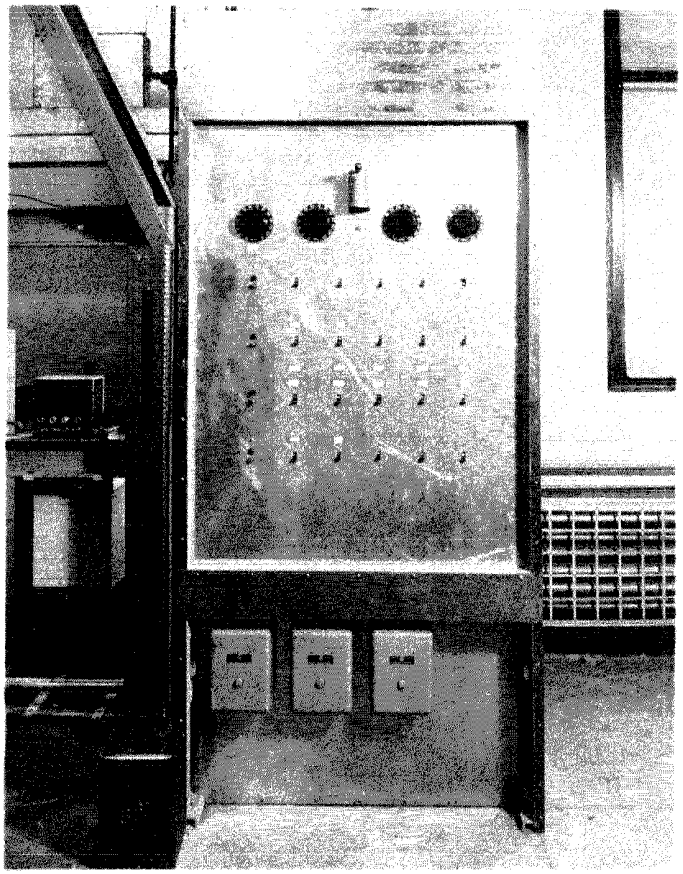

Figure 18. Control panel for air and oil heaters.

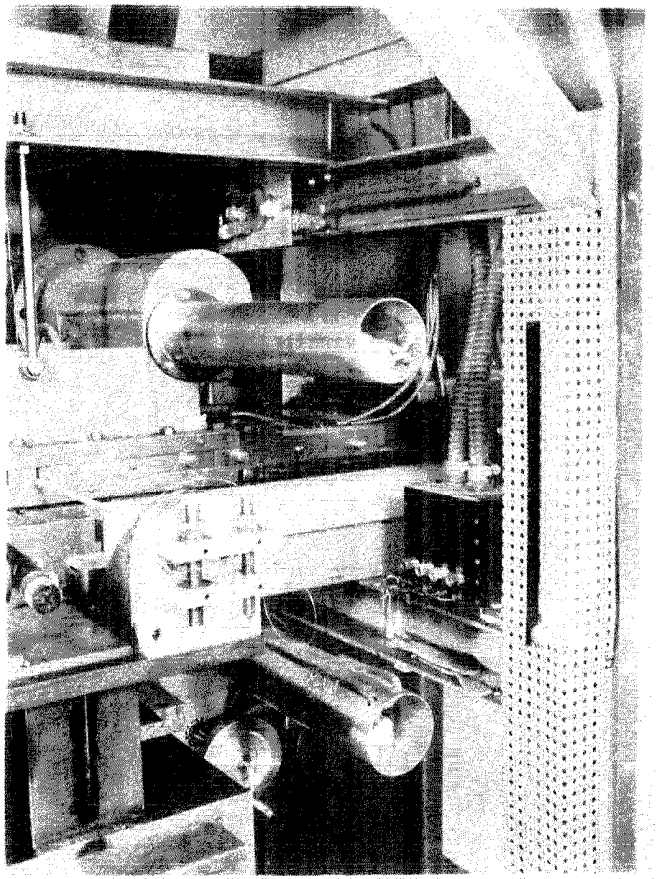

Figure 19. Brass vessel containing control and resistance thermometers for oil bath.

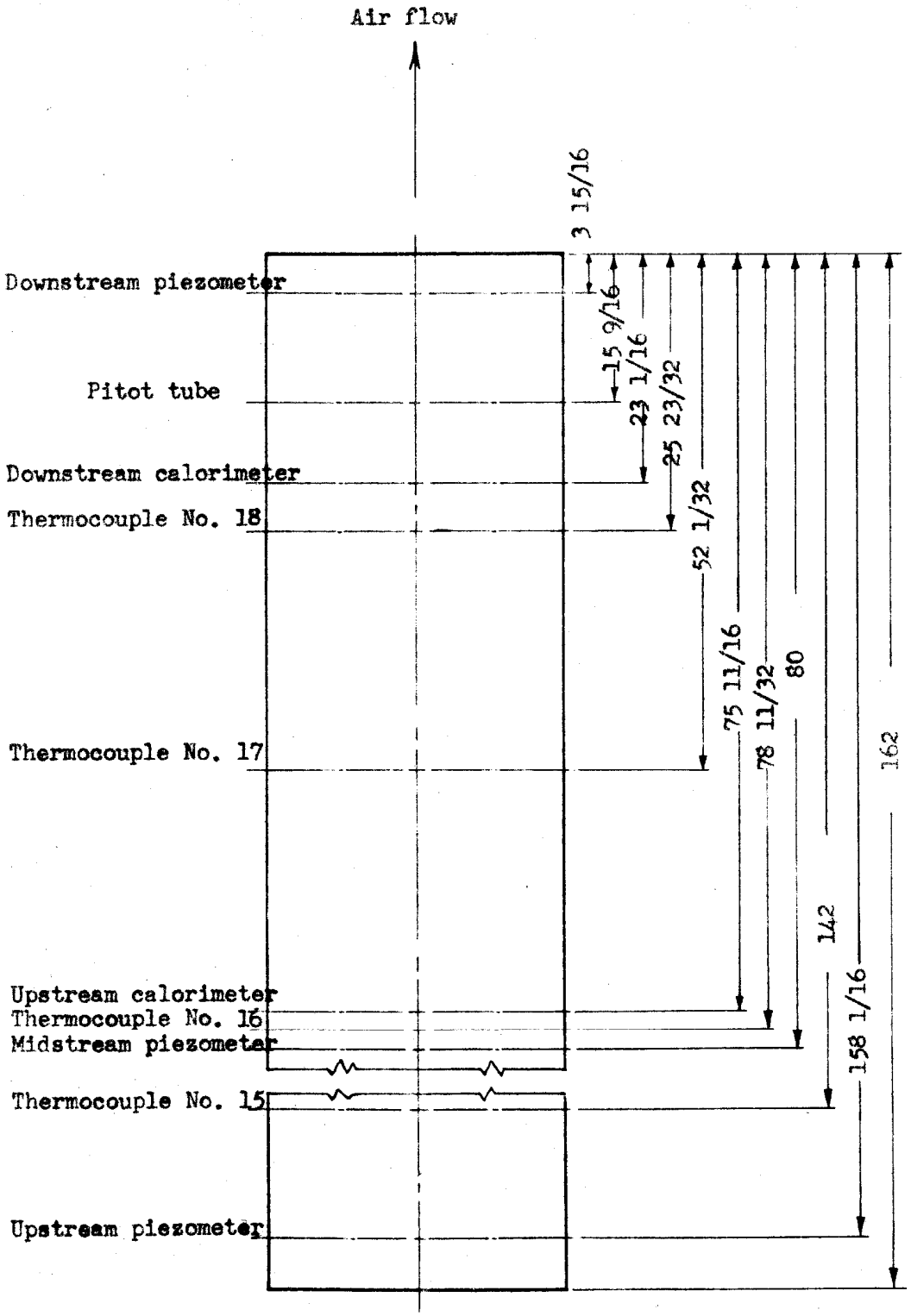

Figure 20. Instrument positions in upper copper plate.

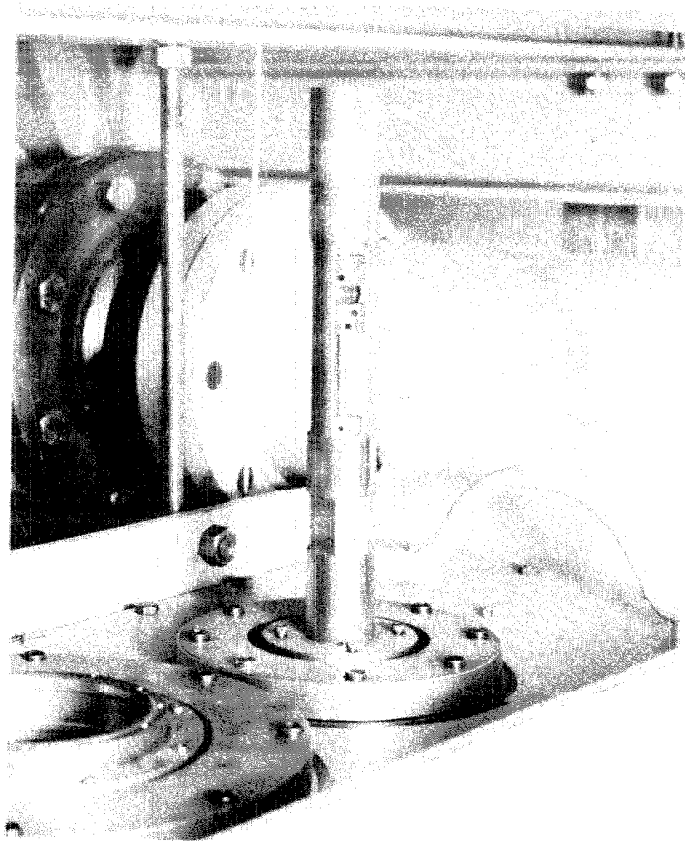

Figure 21. Mounting post for pitot tube.

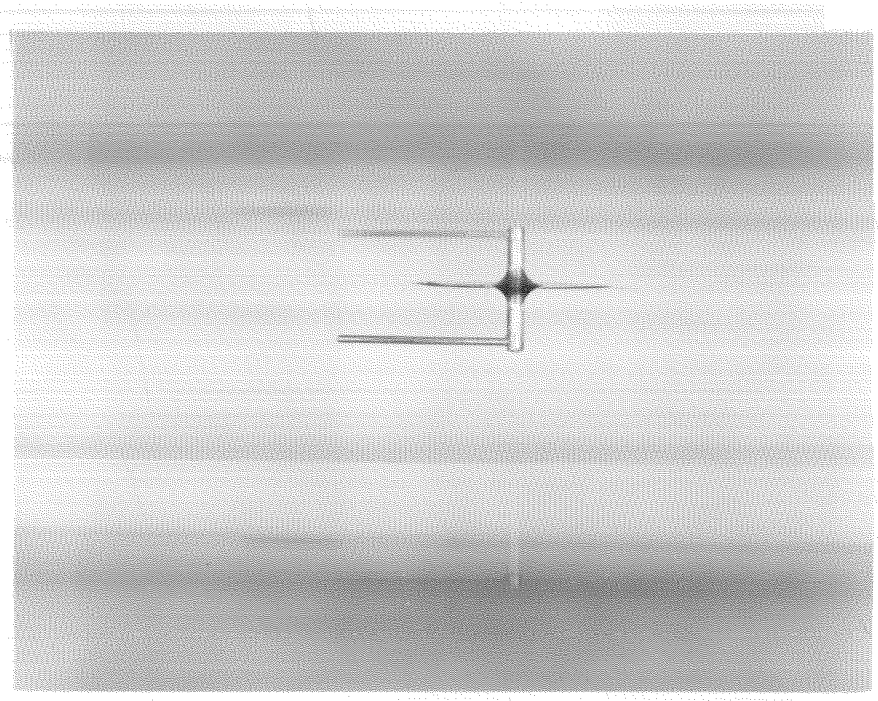

Figure 22. Pitot tube in position.

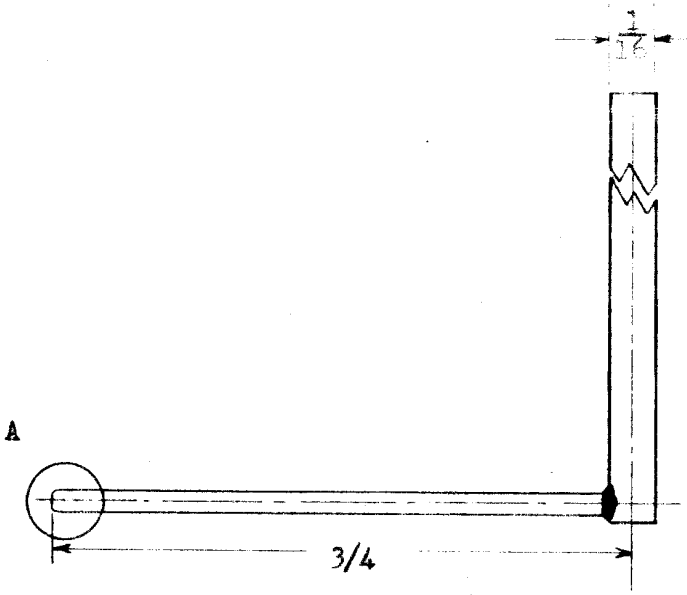

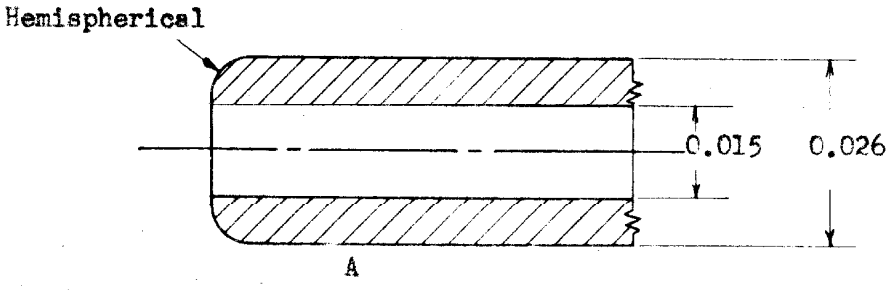

Material: Stainless steel

Figure 23. Dimensions of pitot tube

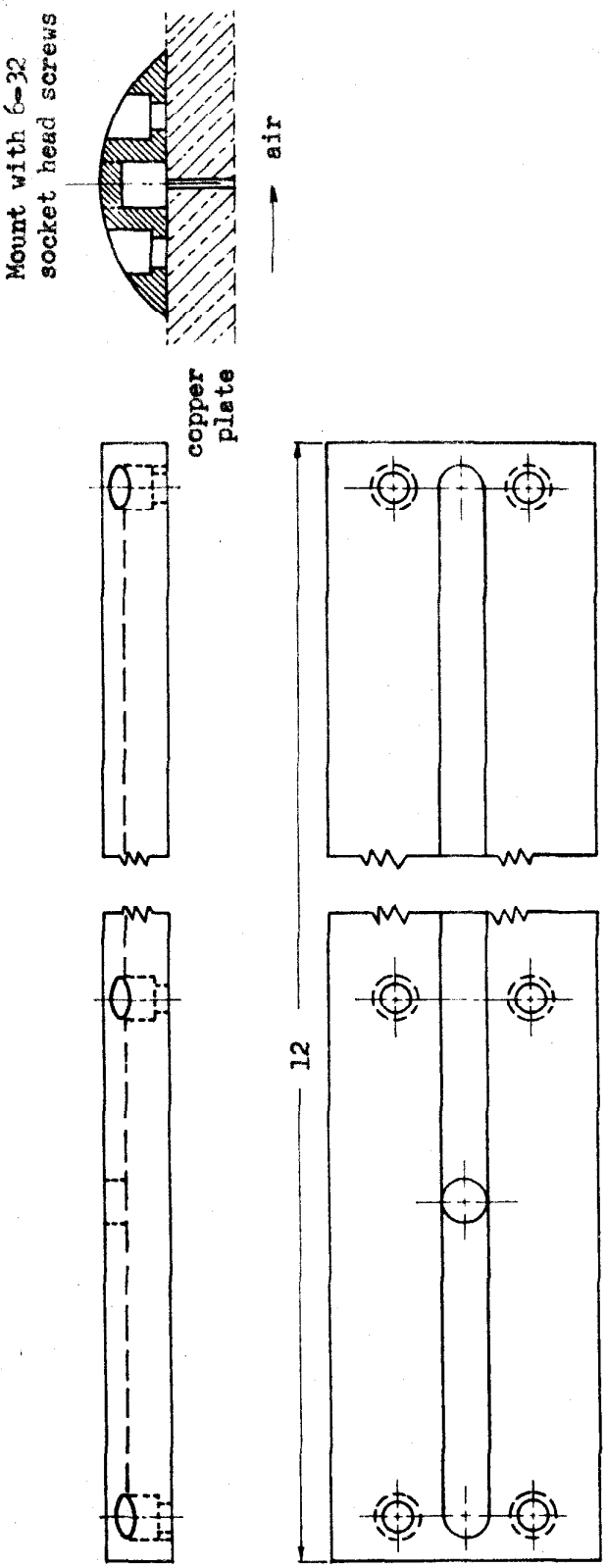

Material: Copper

Figure 24. Piezometer bar.

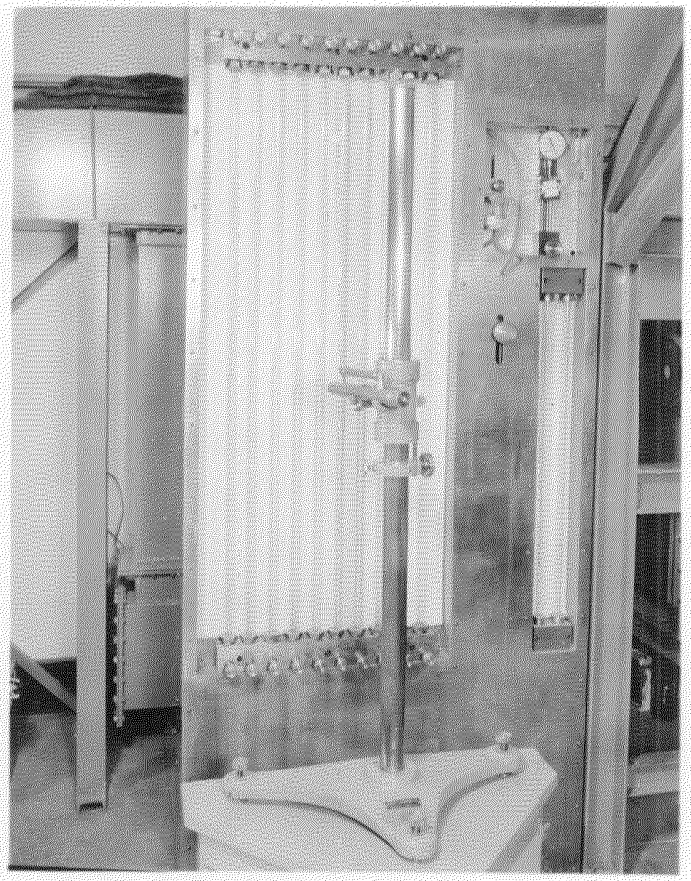

Figure 25. Gang manometer.

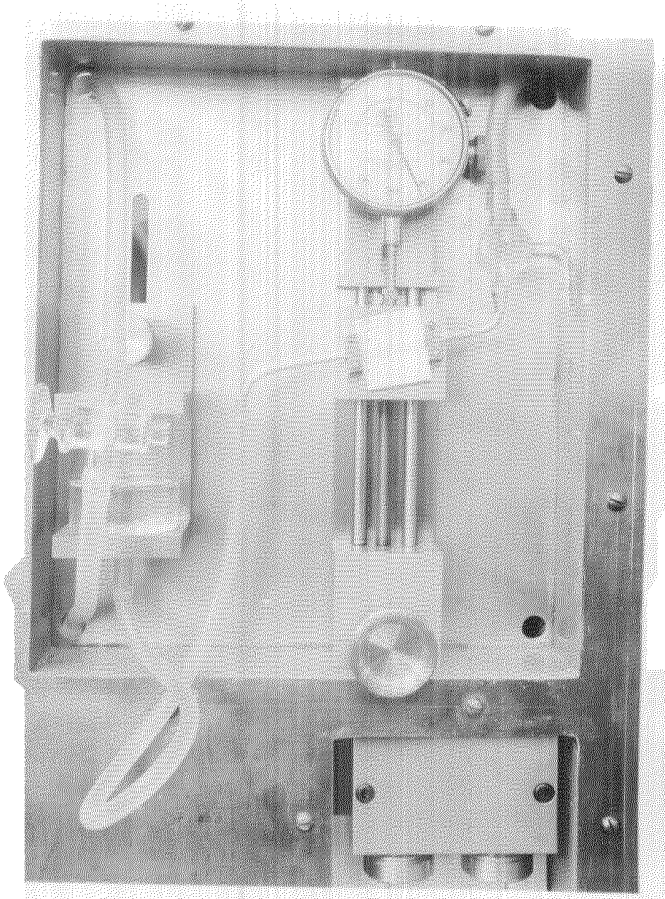

Figure 26. Micromanometer.

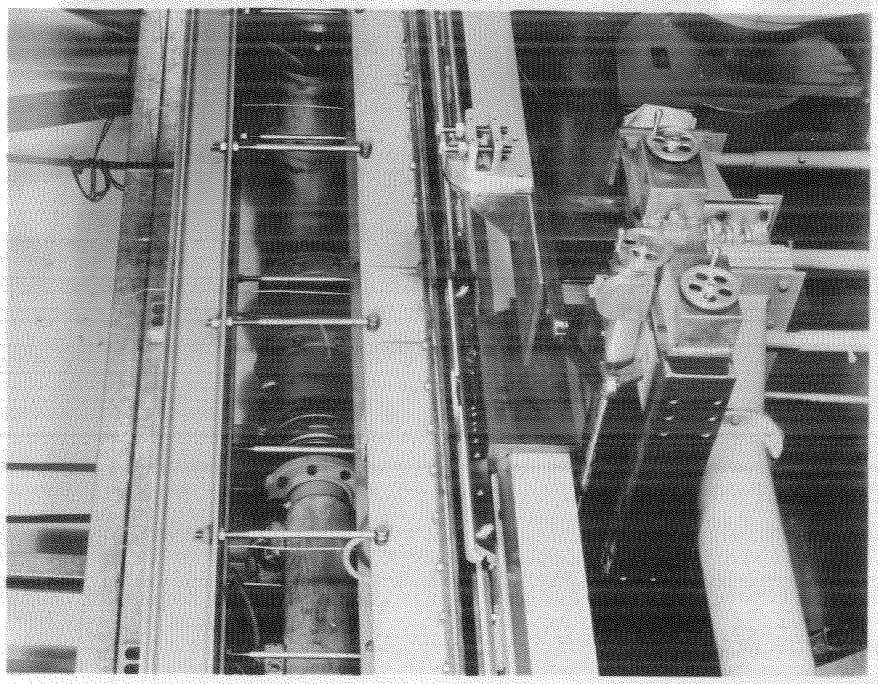

Figure 28. Traverse gear and right hand rail.

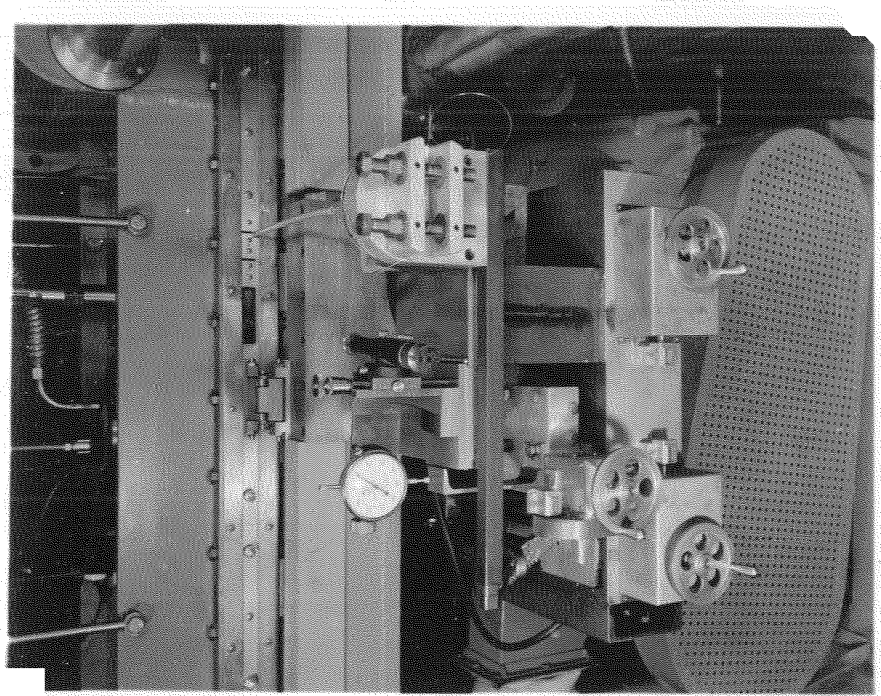

Figure 27. Traverse gear and optical system.

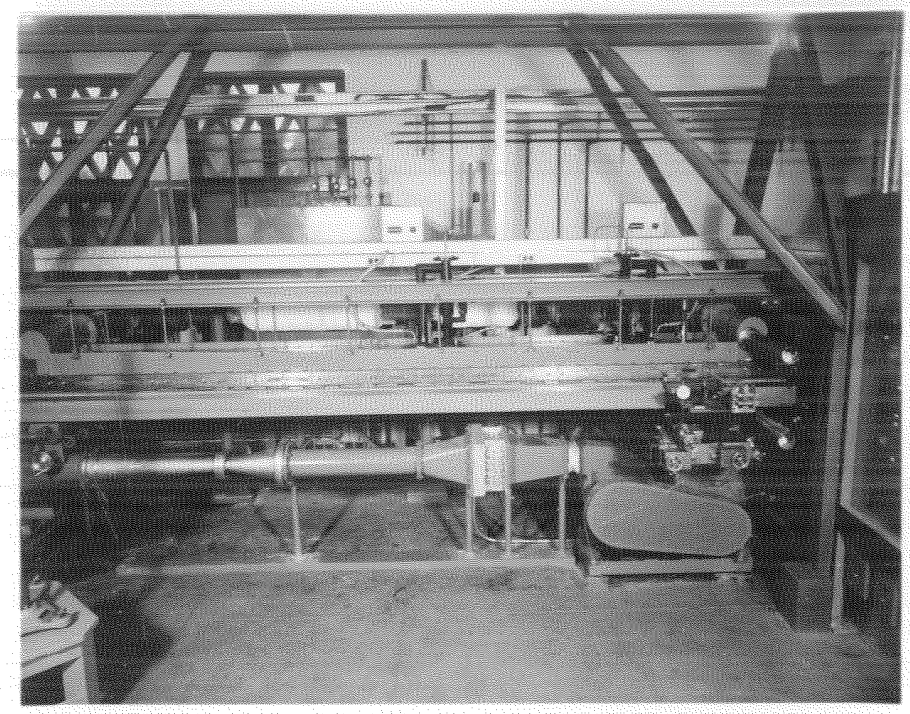

Figure 29. Full length view of right hand rail.

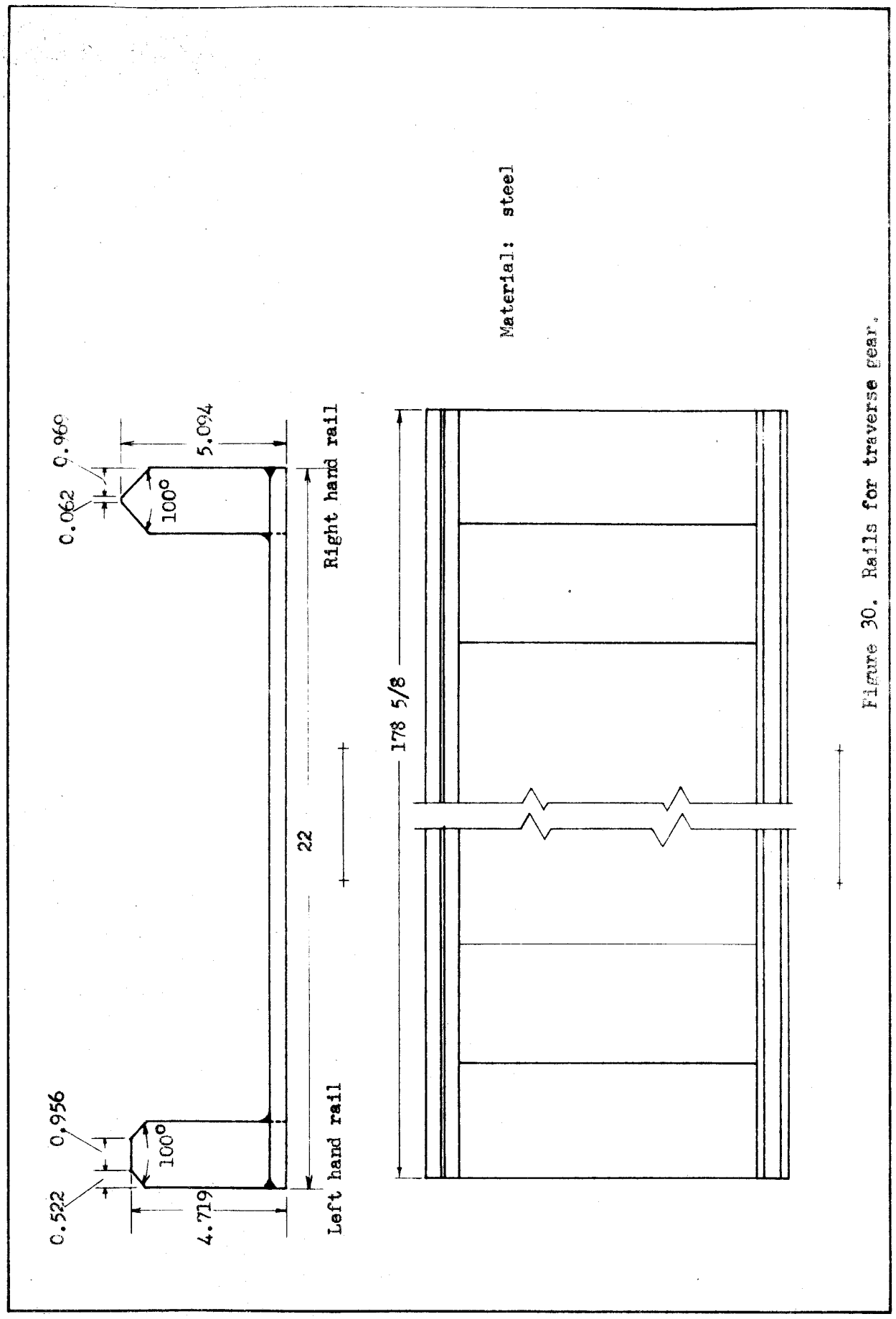

Figure 30. Rails for traverse gear.

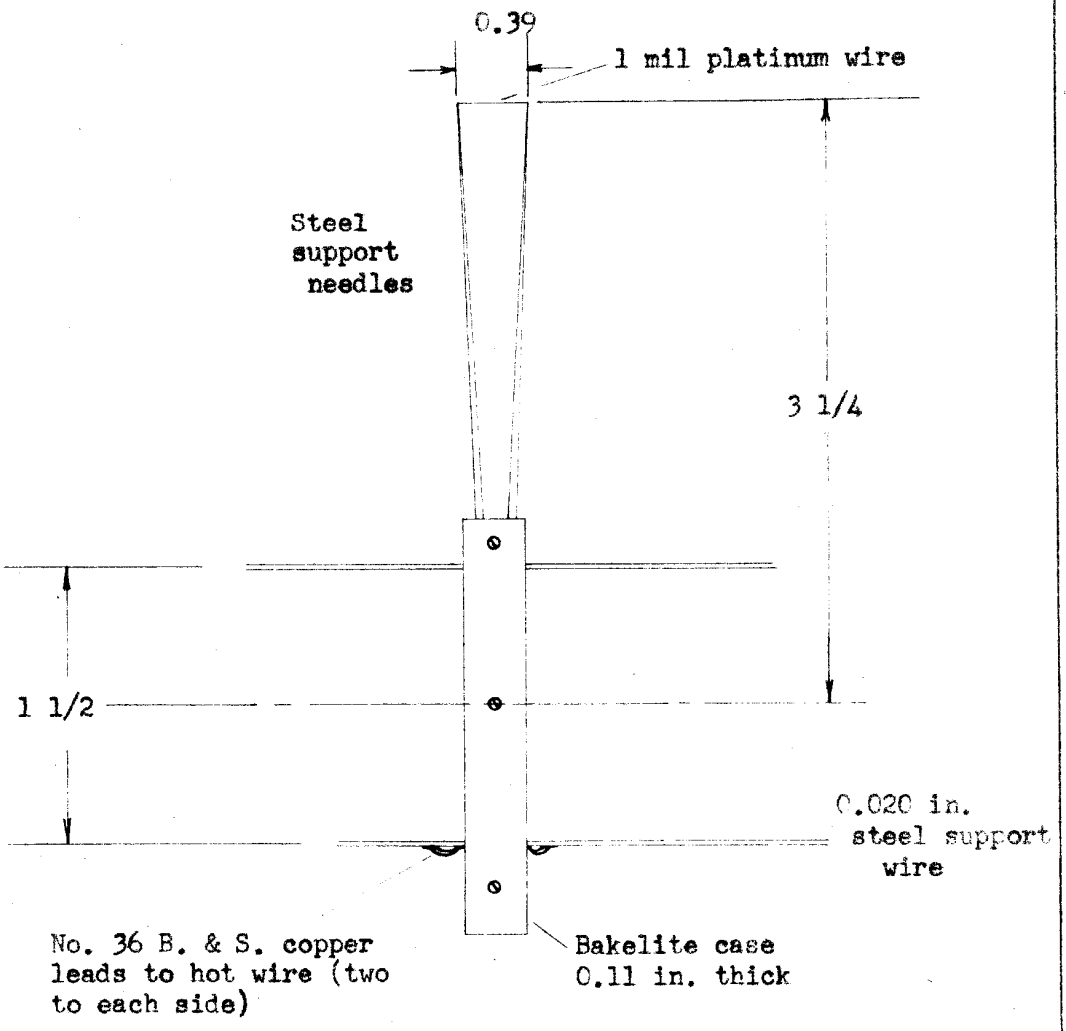

Figure 31. Schematic sketch of hot wire anemometer.

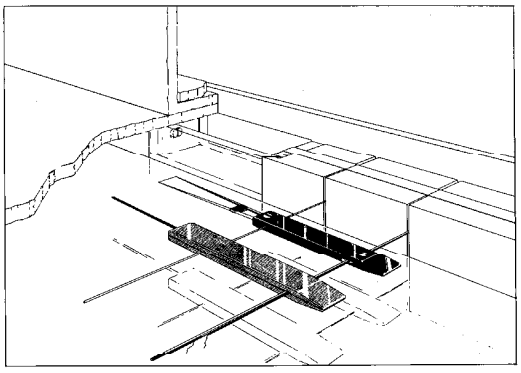

Figure 32. Hot wire anemometer in position.

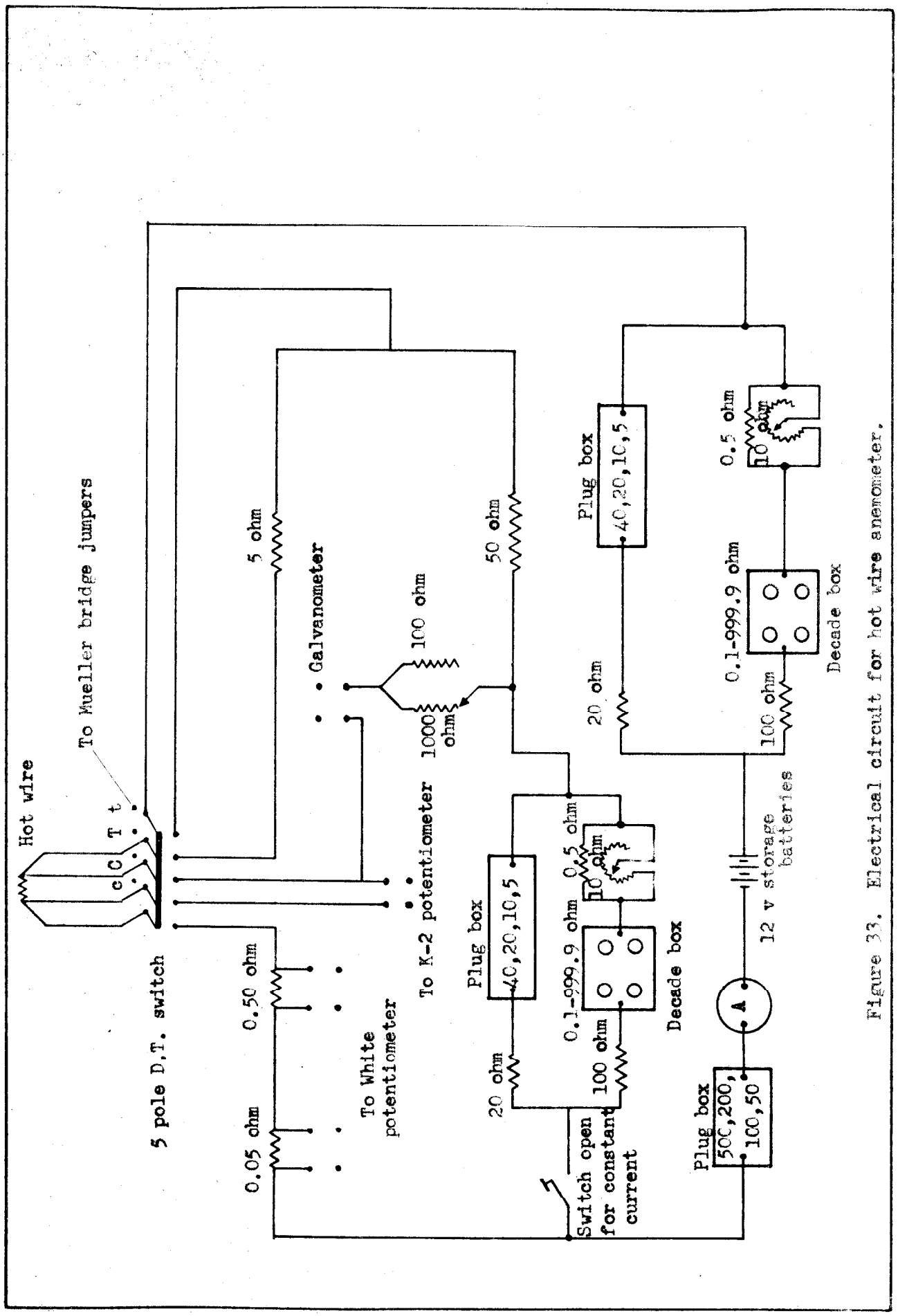

Figure 33. Electrical circuit for hot wire anemometer.

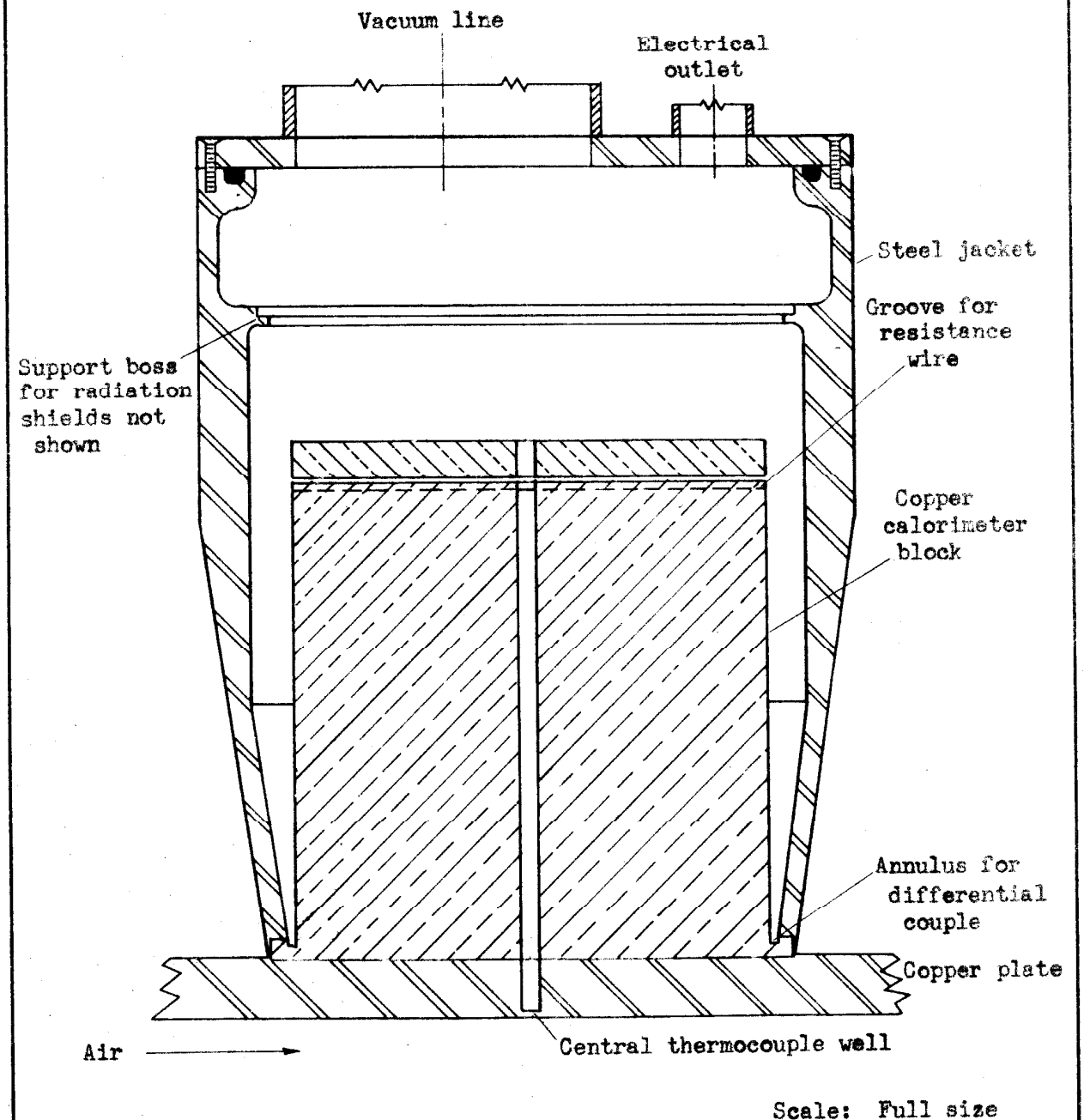

Figure 34. Sectional view of calorimeter

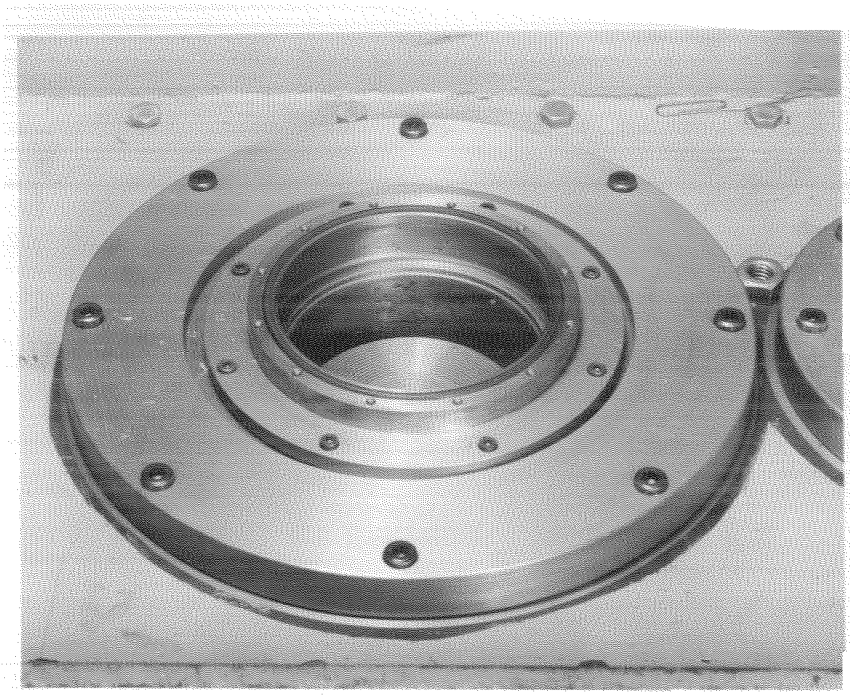

Figure 35. Inside view of calorimeter.

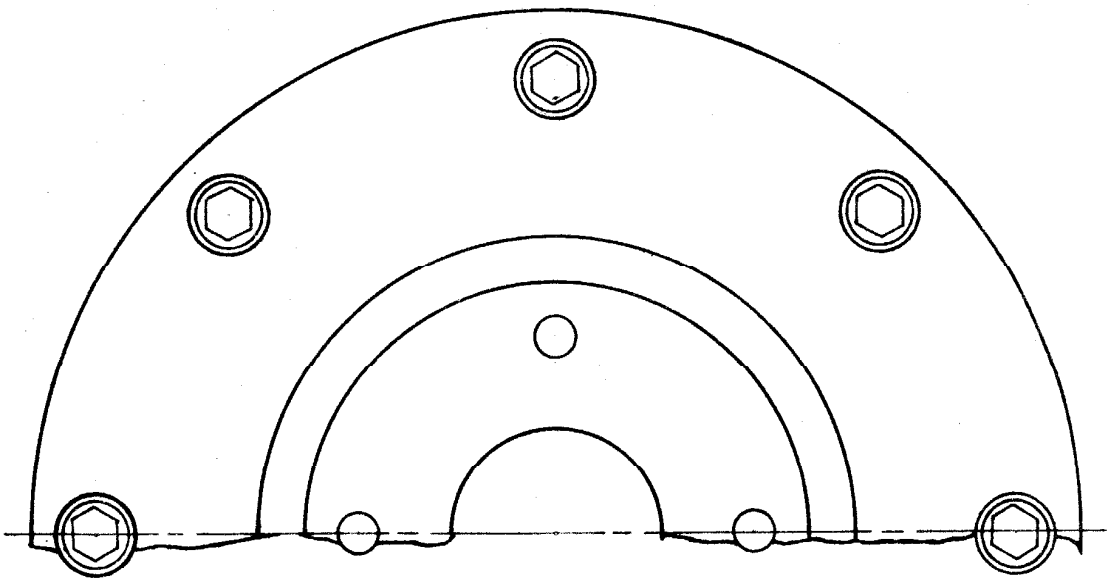

Top view

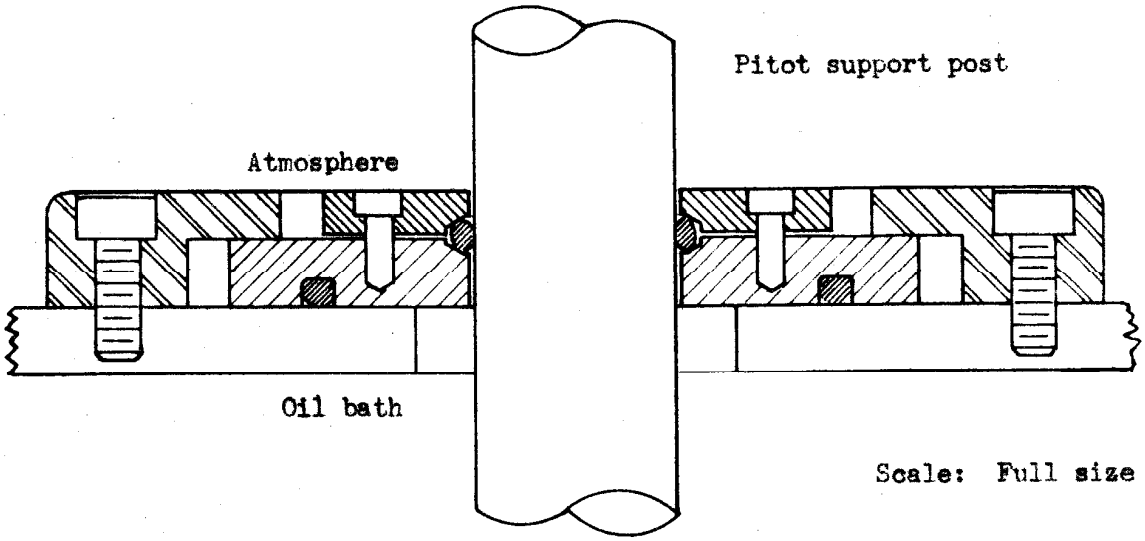

Figure 36. Oil seal ring for pitot post

Figure 37. Metal diffusion pump.

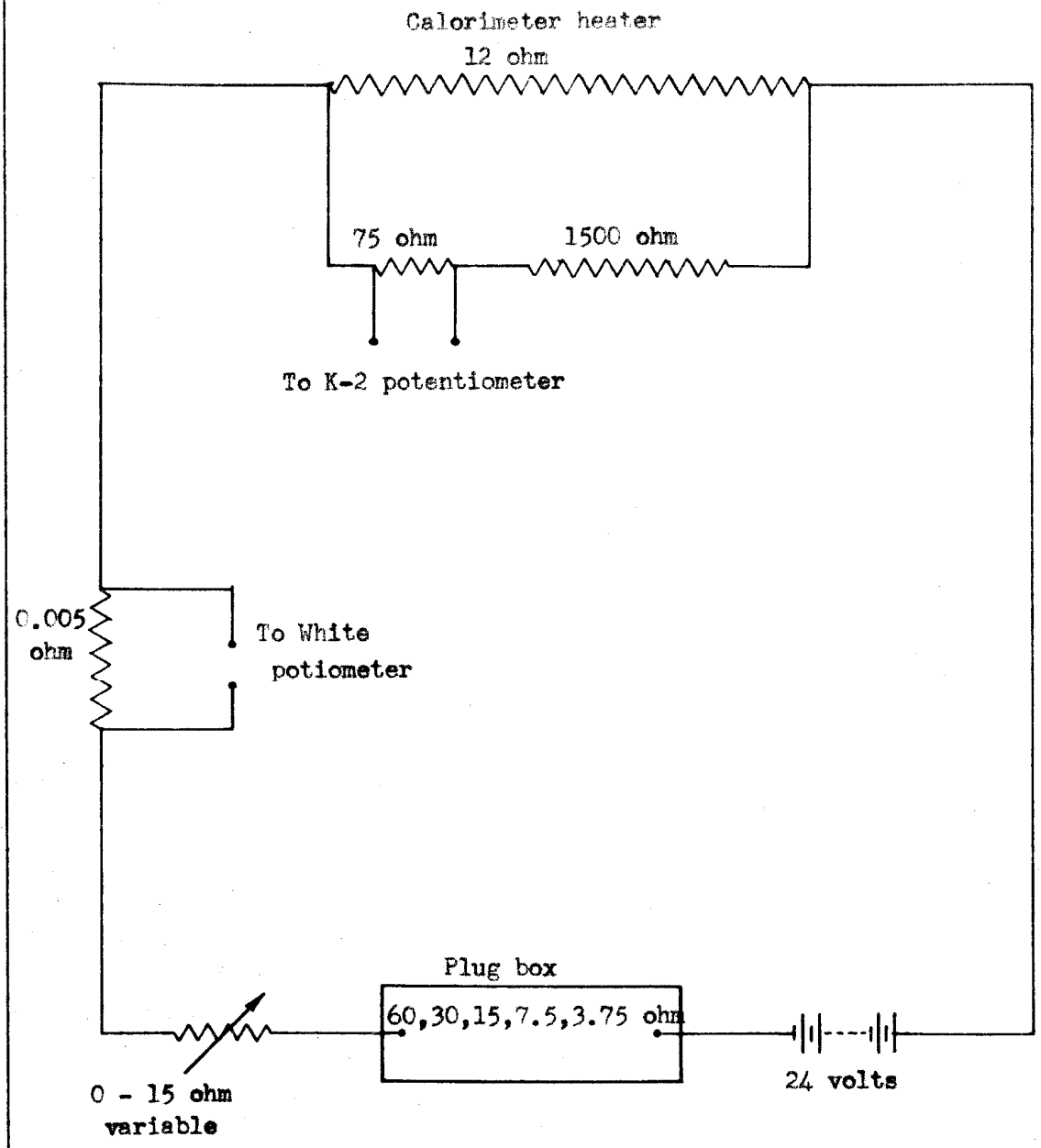

Figure 38. Electrical circuit for calorimeter.

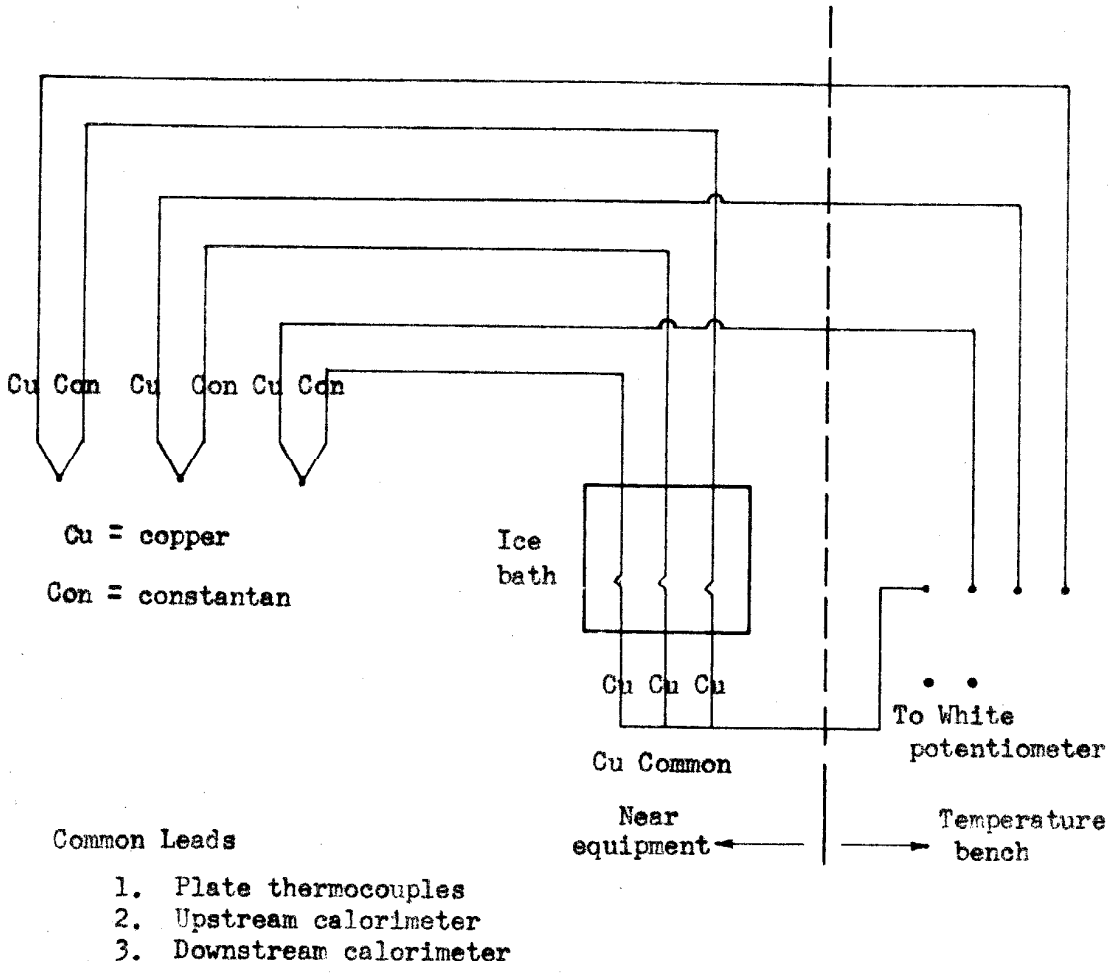

Figure 39. Circuits for thermocouples.

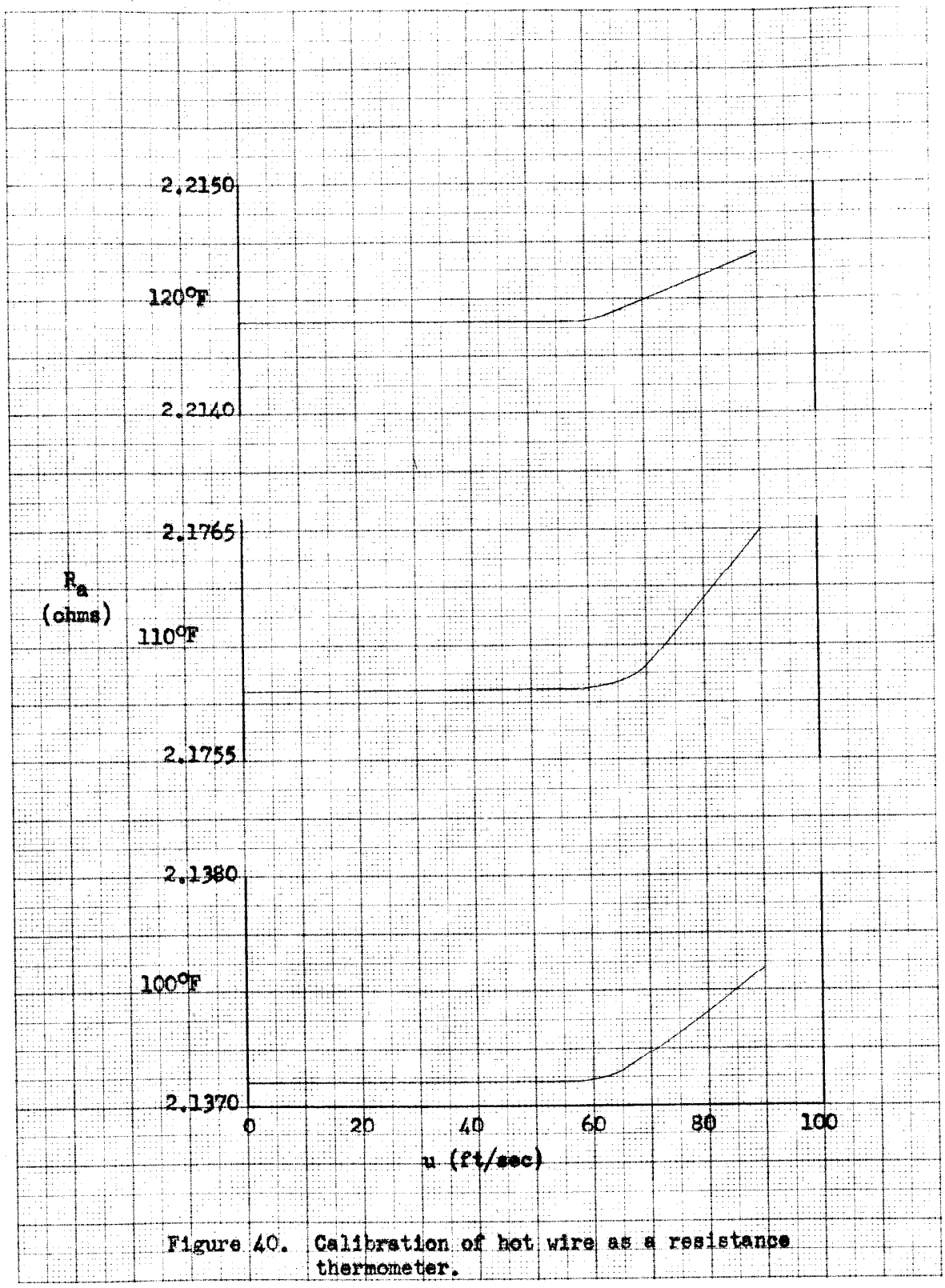

Figure 40. Calibration of hot wire as a resistance thermometer.

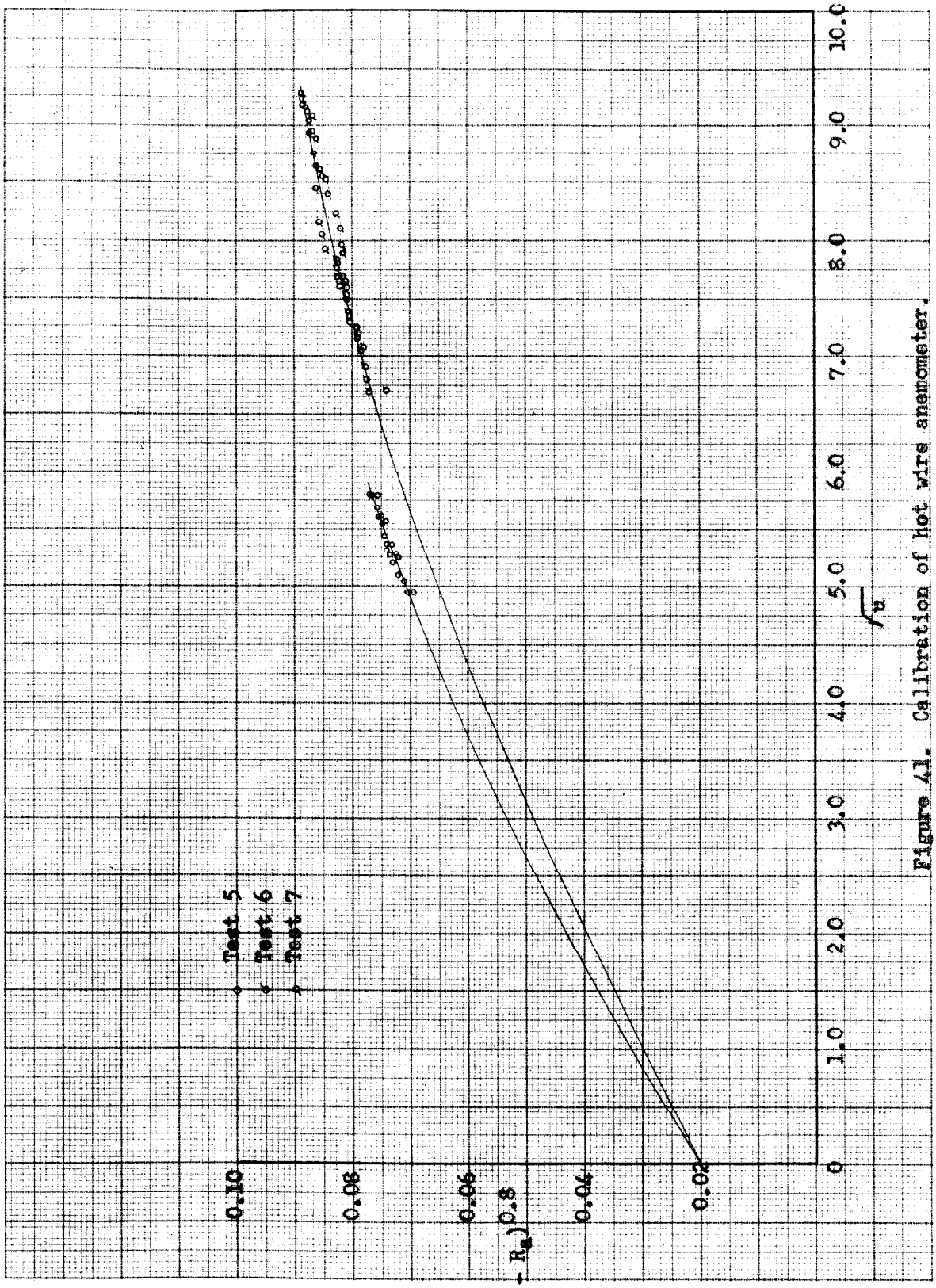

Figure 41. Calibration of hot wire anemometer.

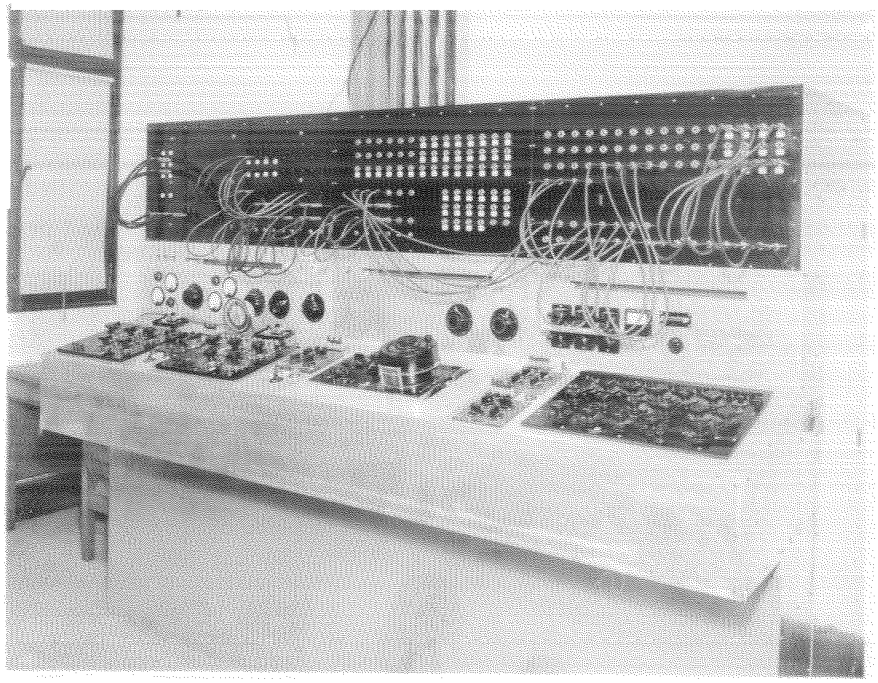

Figure 42. Central temperature bench.

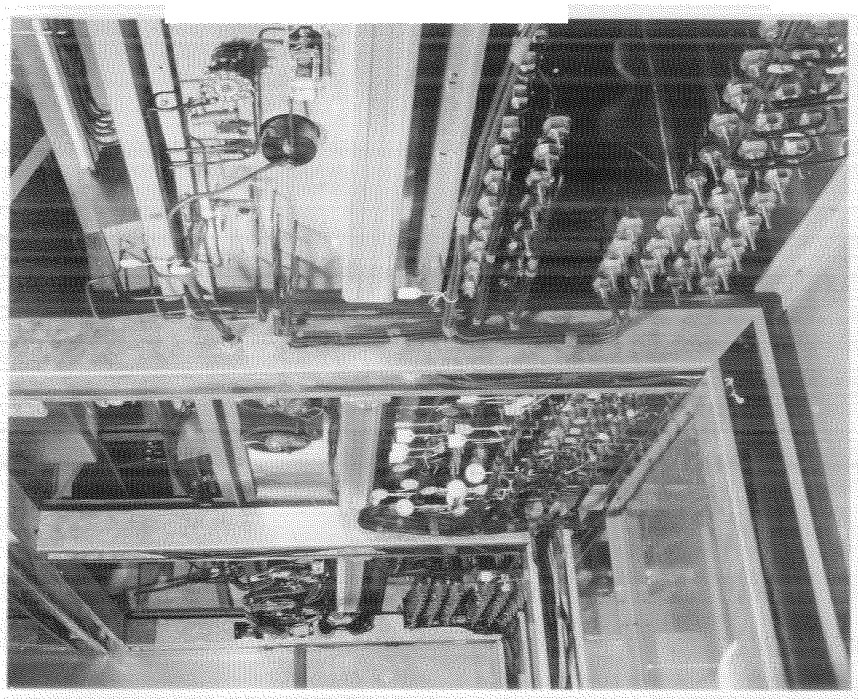

Figure 44. Wiring in temperature bench.

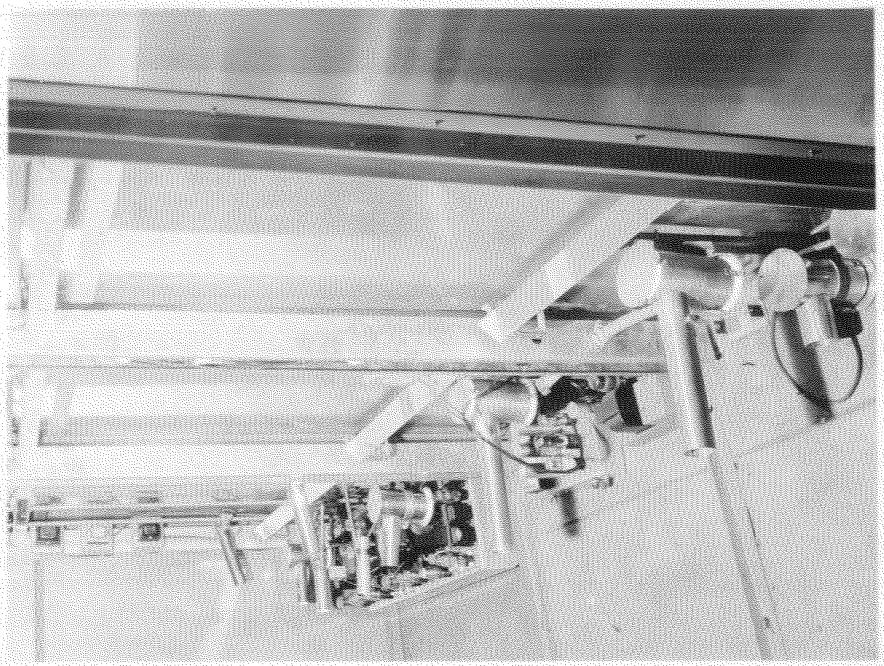

Figure 43. Galvanometer lights in temperature bench.

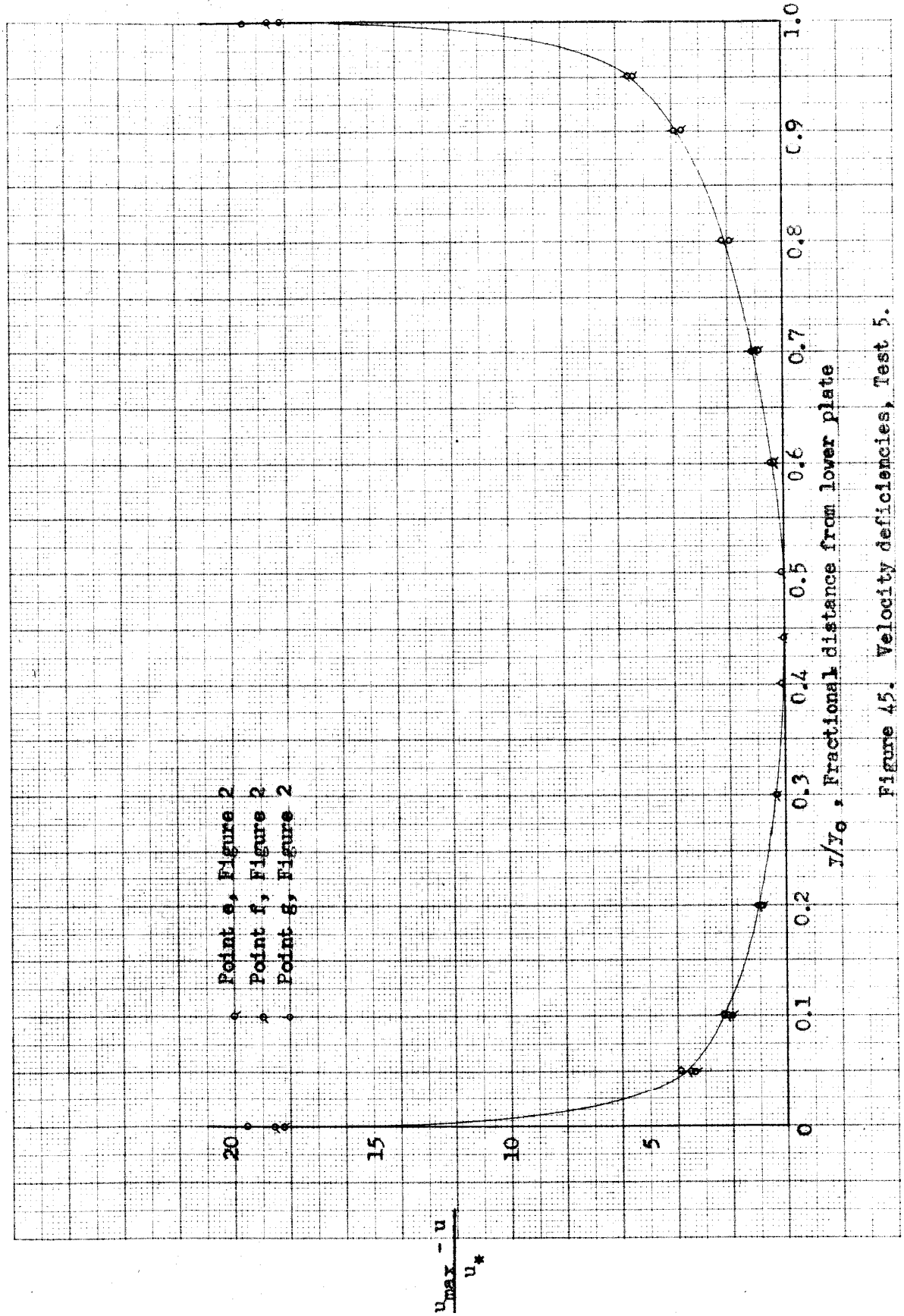

Figure 45. Velocity deficiencies, Test 5.

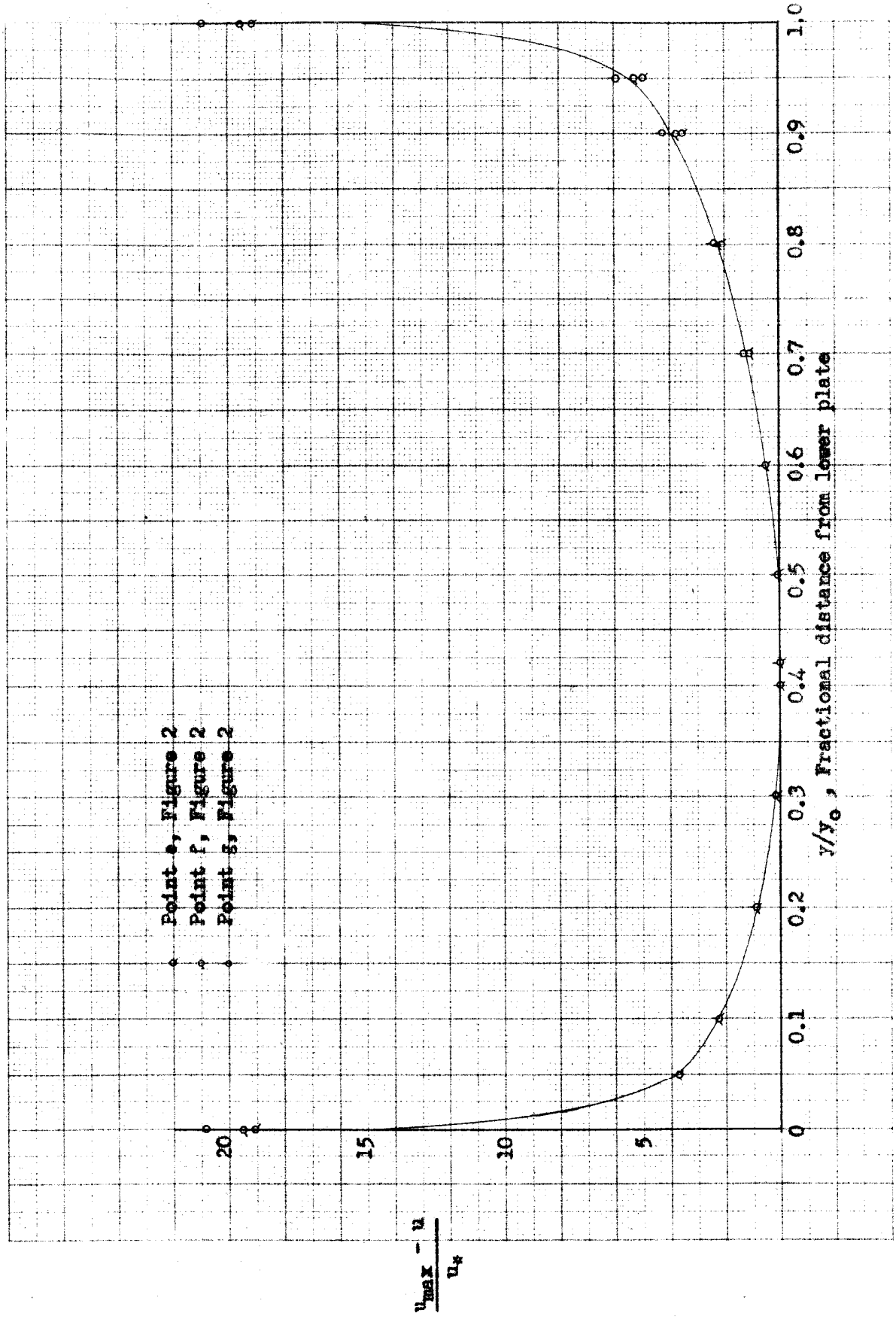

Figure 46. Velocity dificiencies, Test 6.

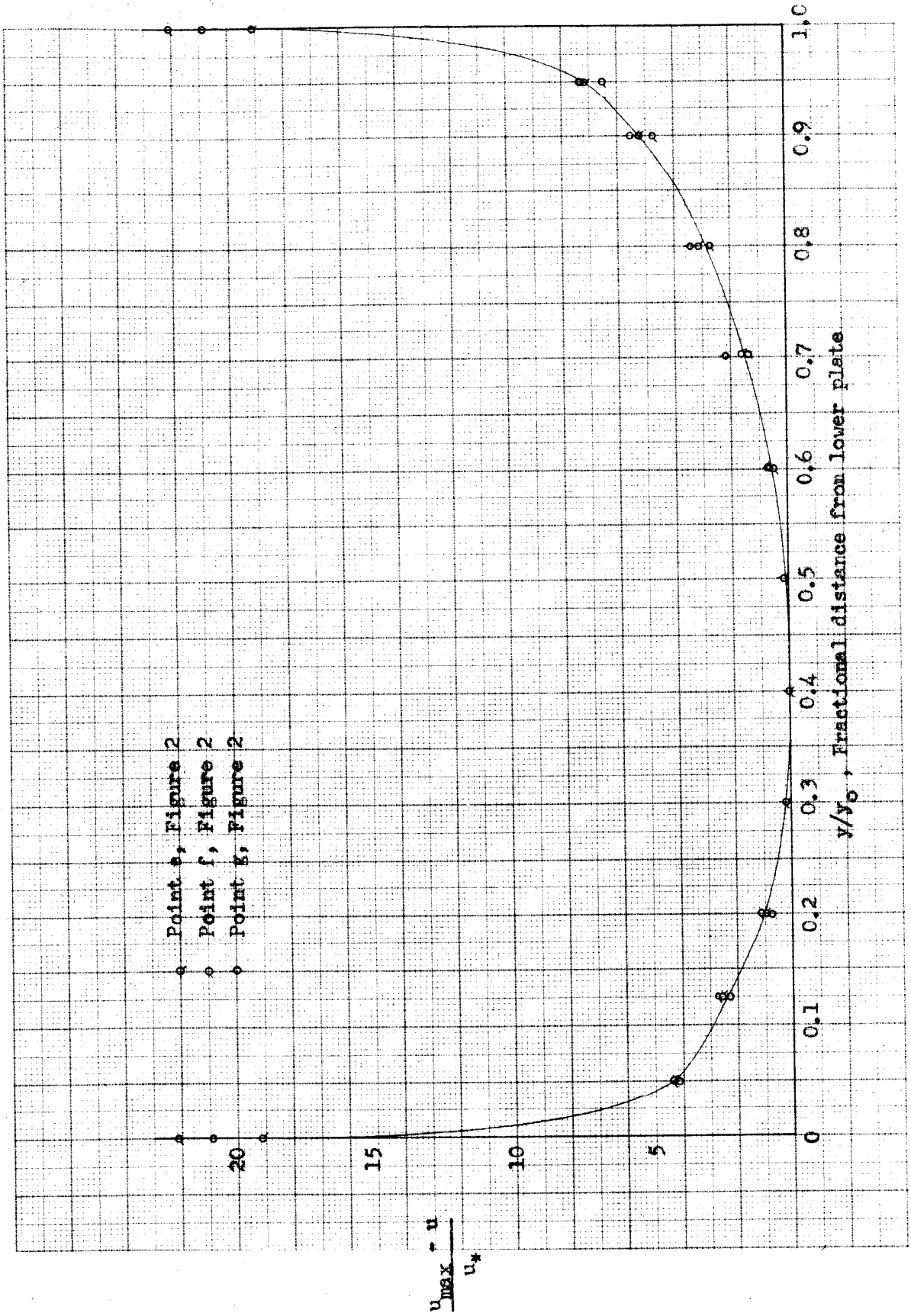

Figure 47. Velocity deficiencies, Test 7.

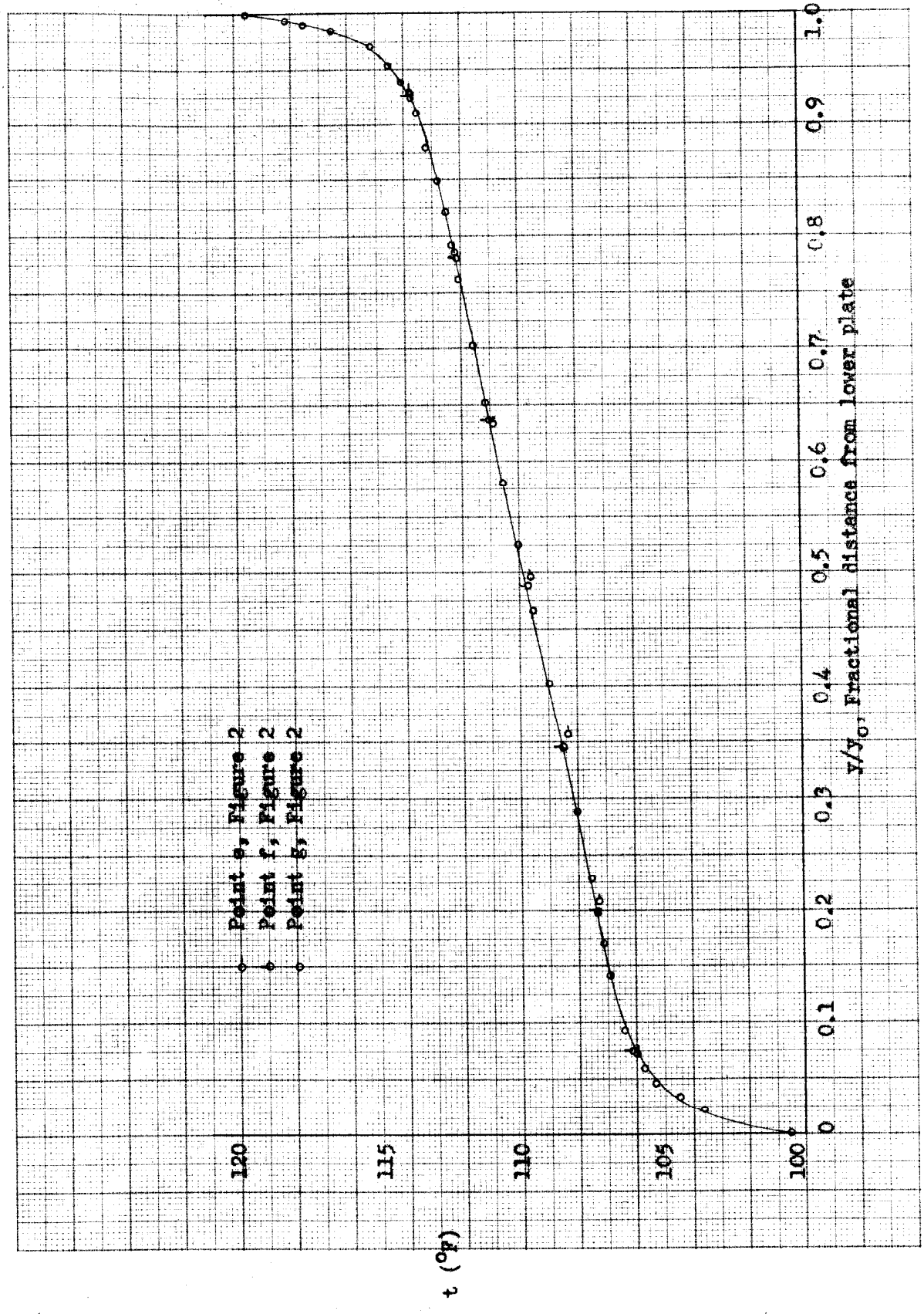

Figure 48. Temperature distribution, Test 5.

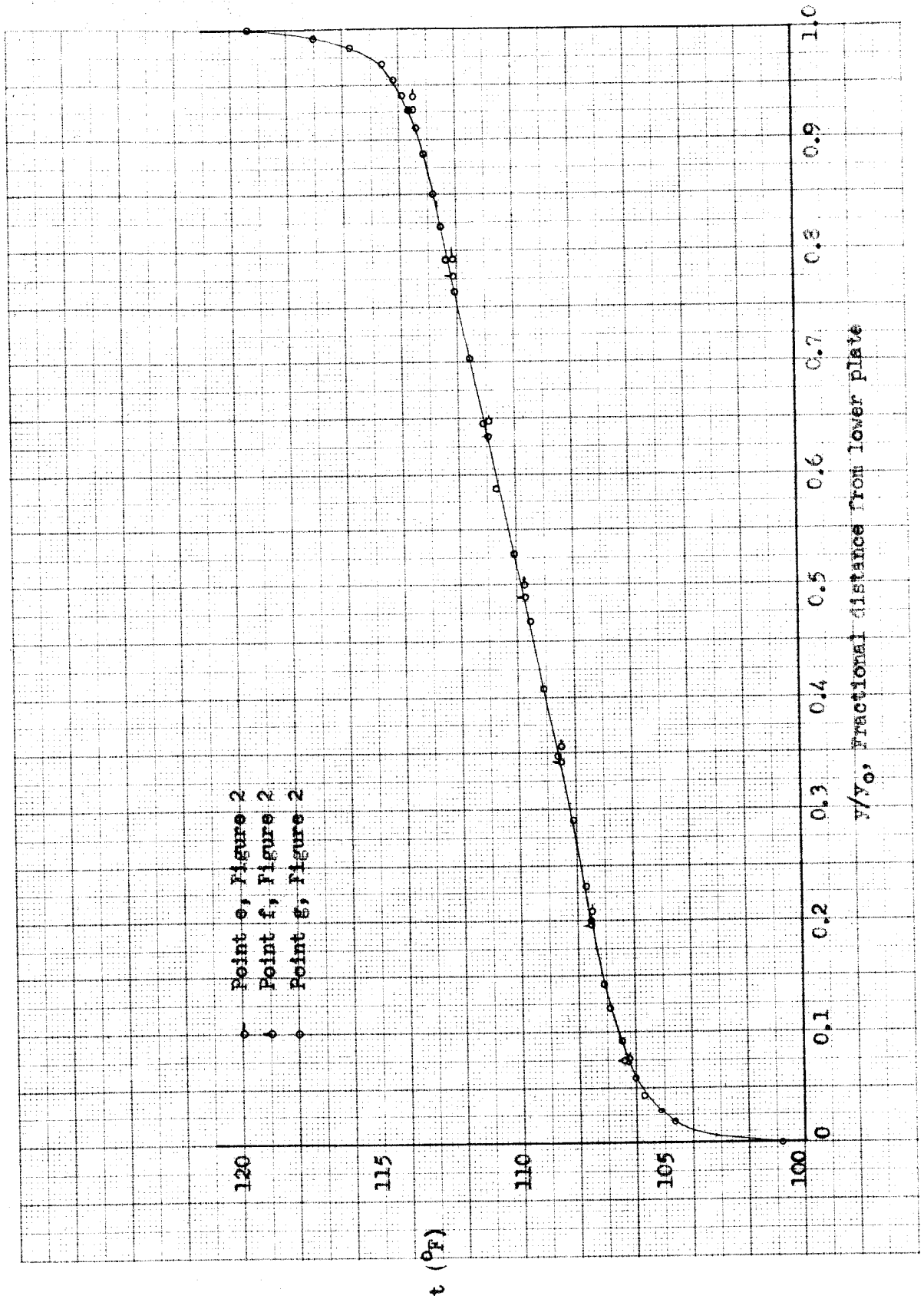

Figure 49. Temperature distribution, Test 6.

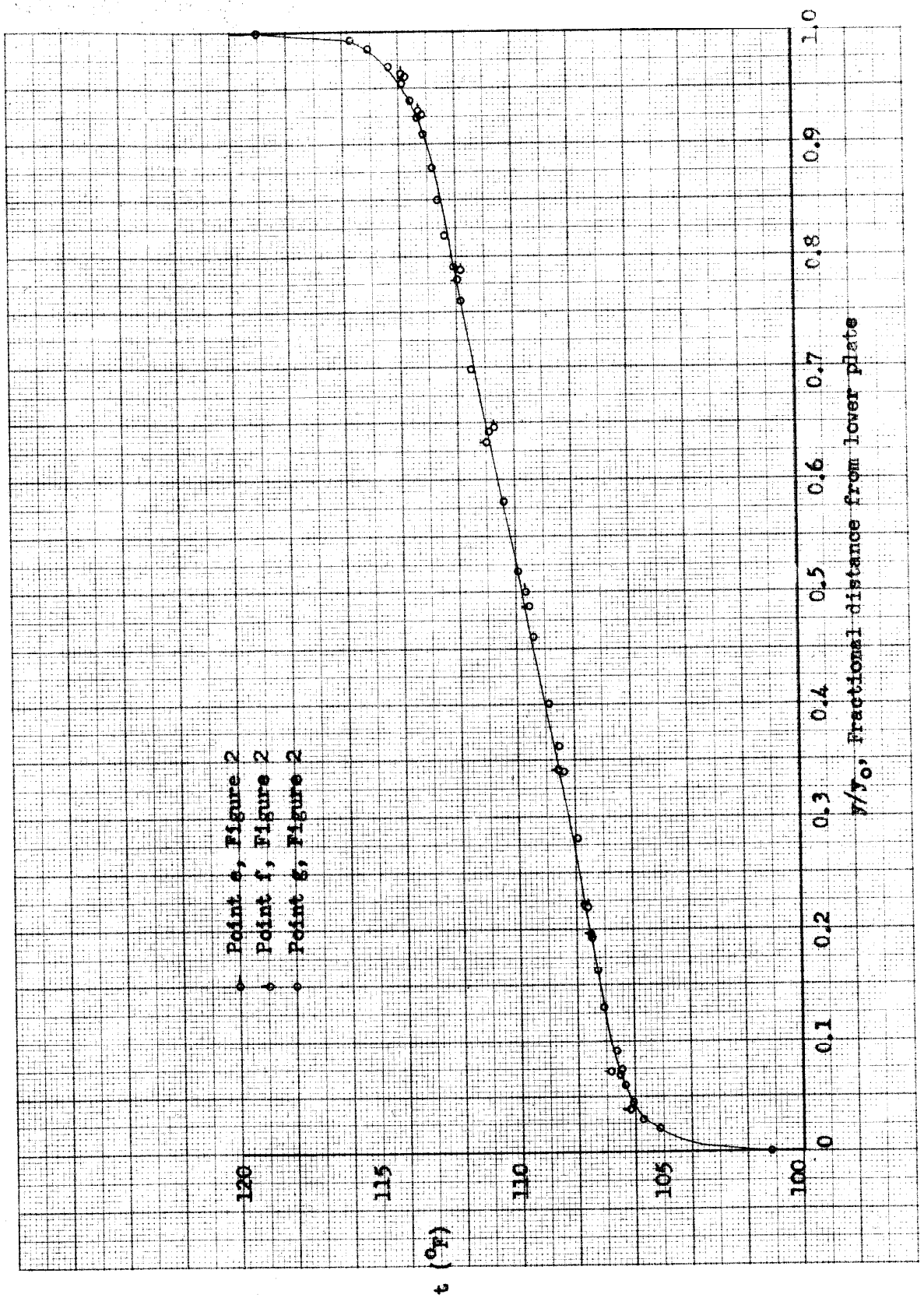

Figure 50. Temperature distribution, Test 7.

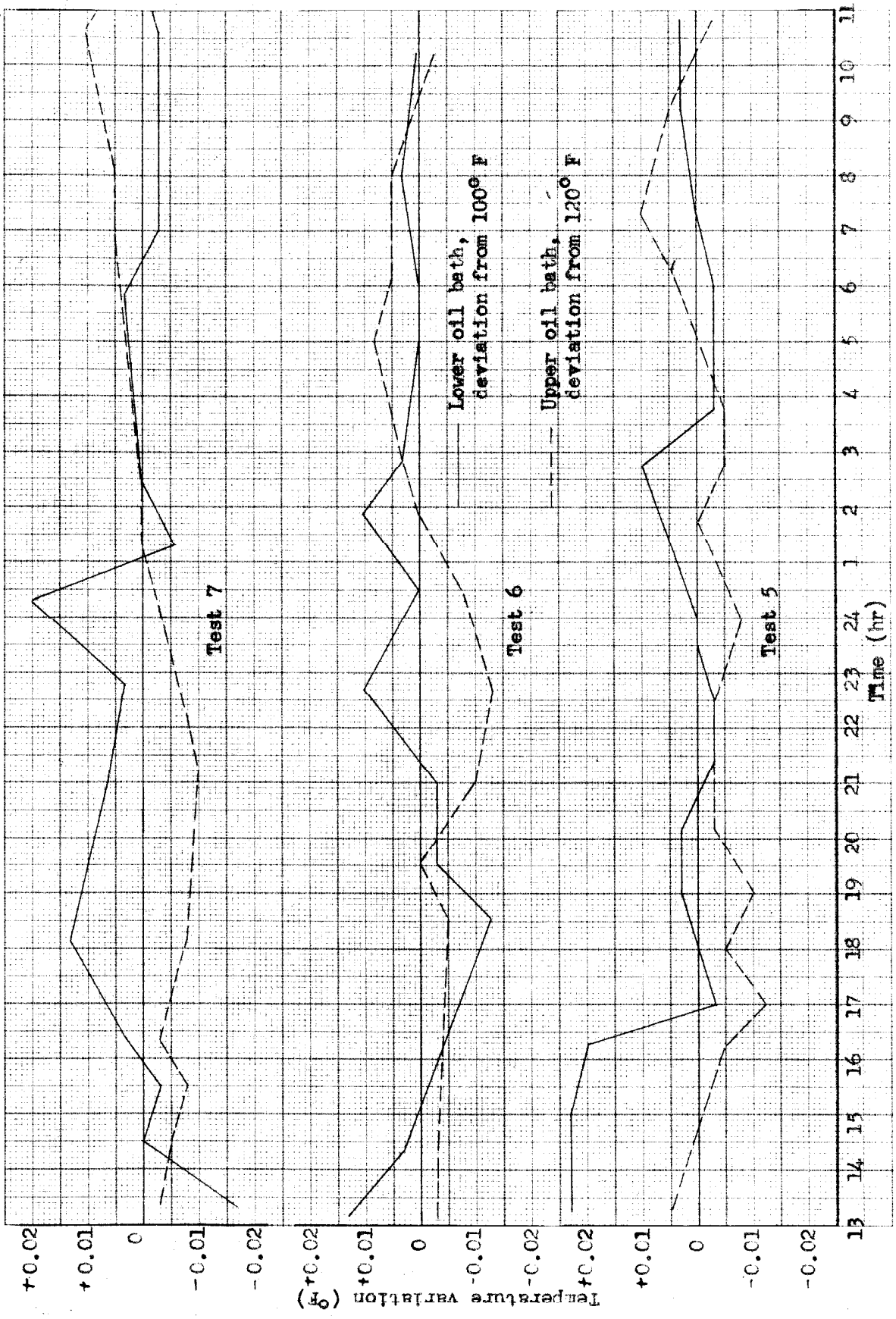

Figure 51. Oil bath temperature variation during Tests 5, 6, and 7.

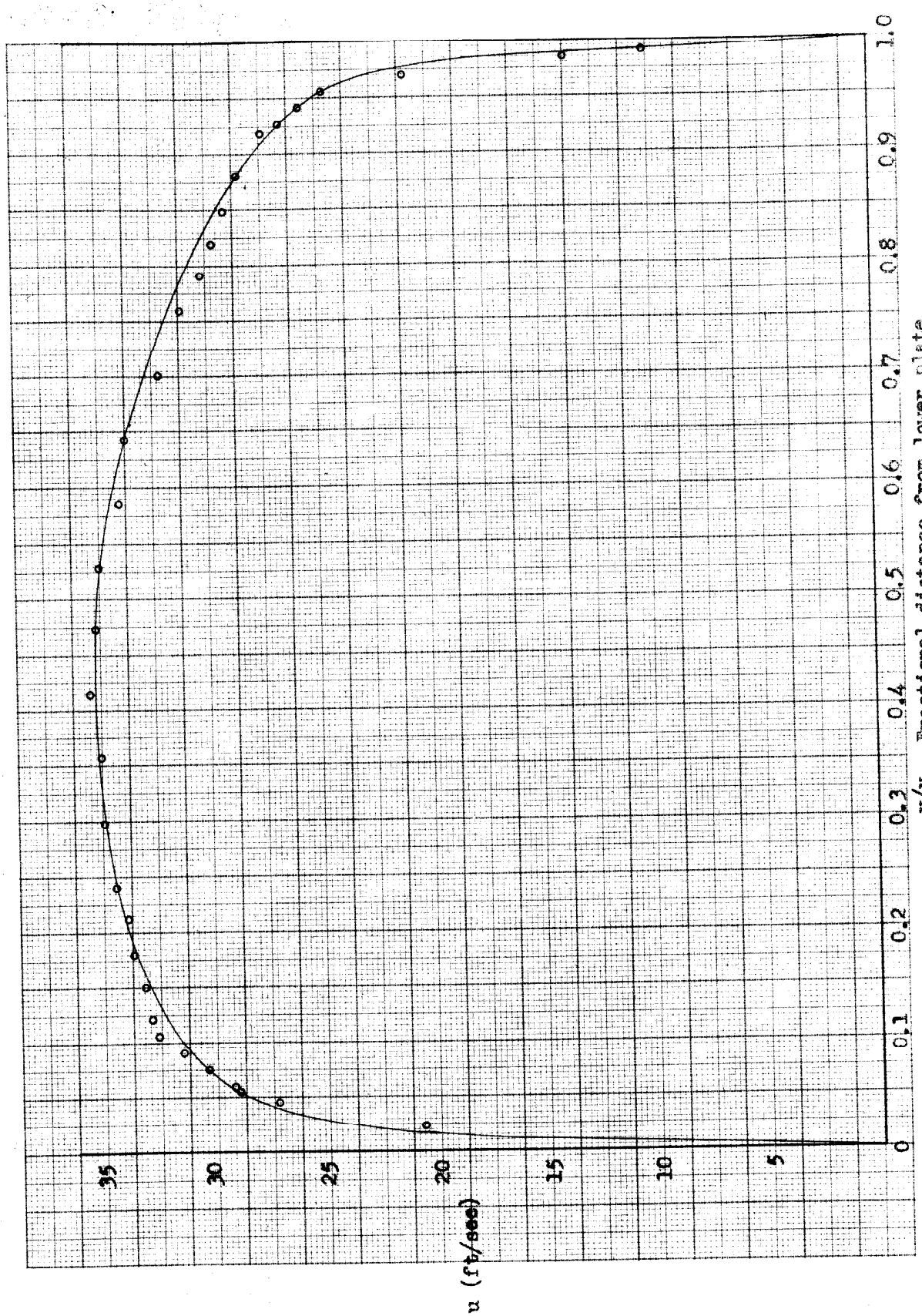

Figure 52. Velocity distribution, Test 5.

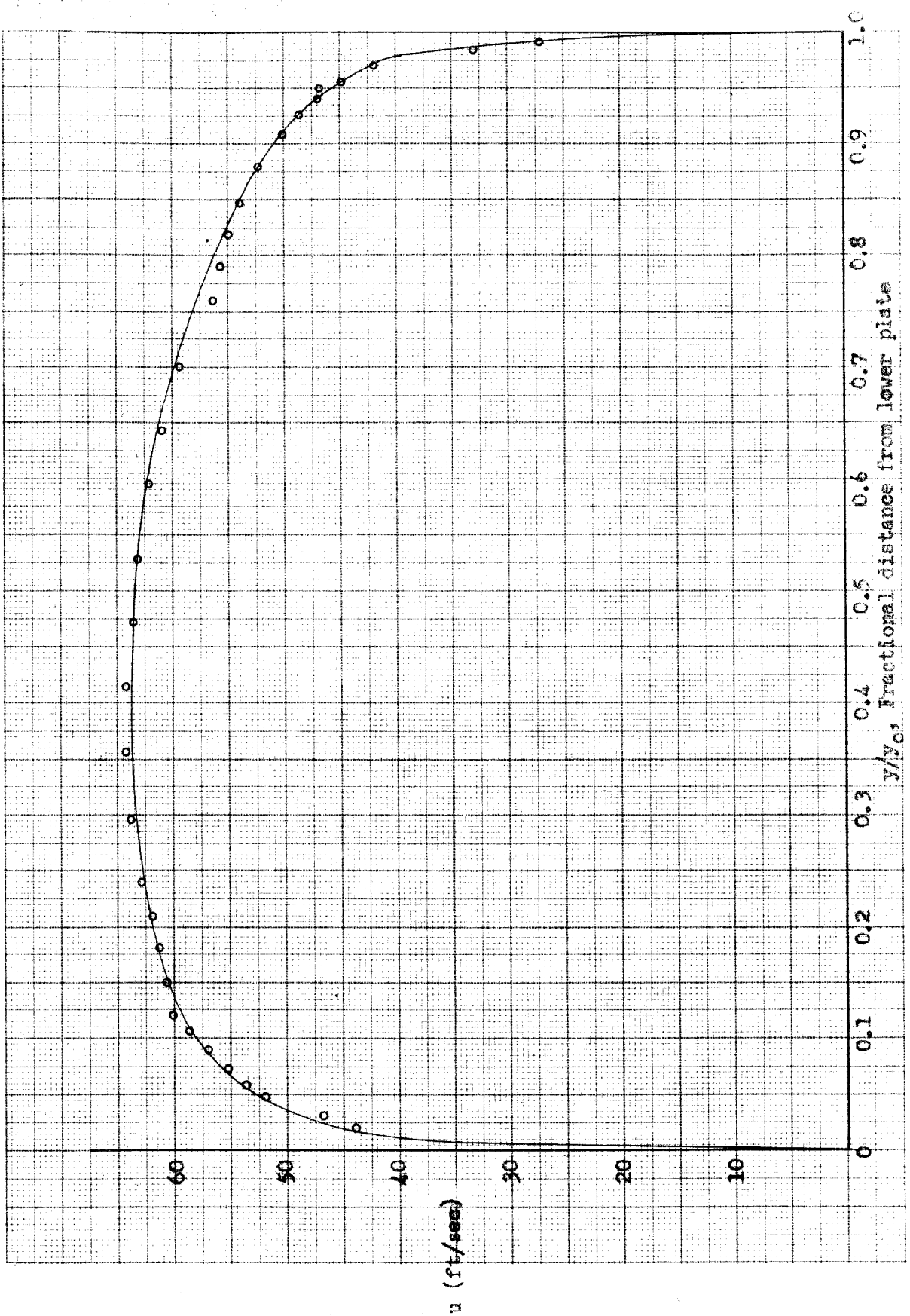

Figure 53. Velocity distribution, Test 6.

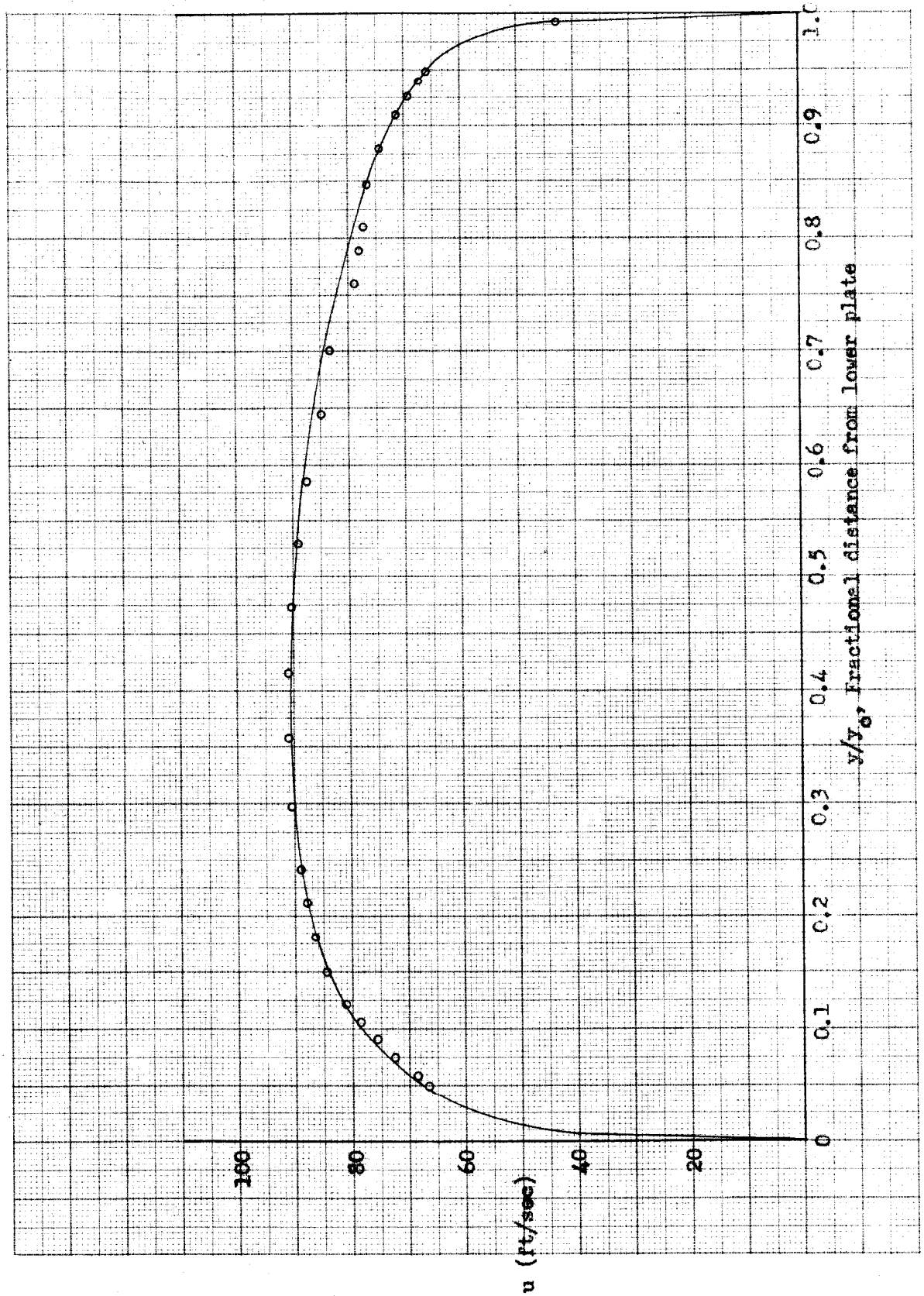

Figure 54. Velocity distribution, Test 7.

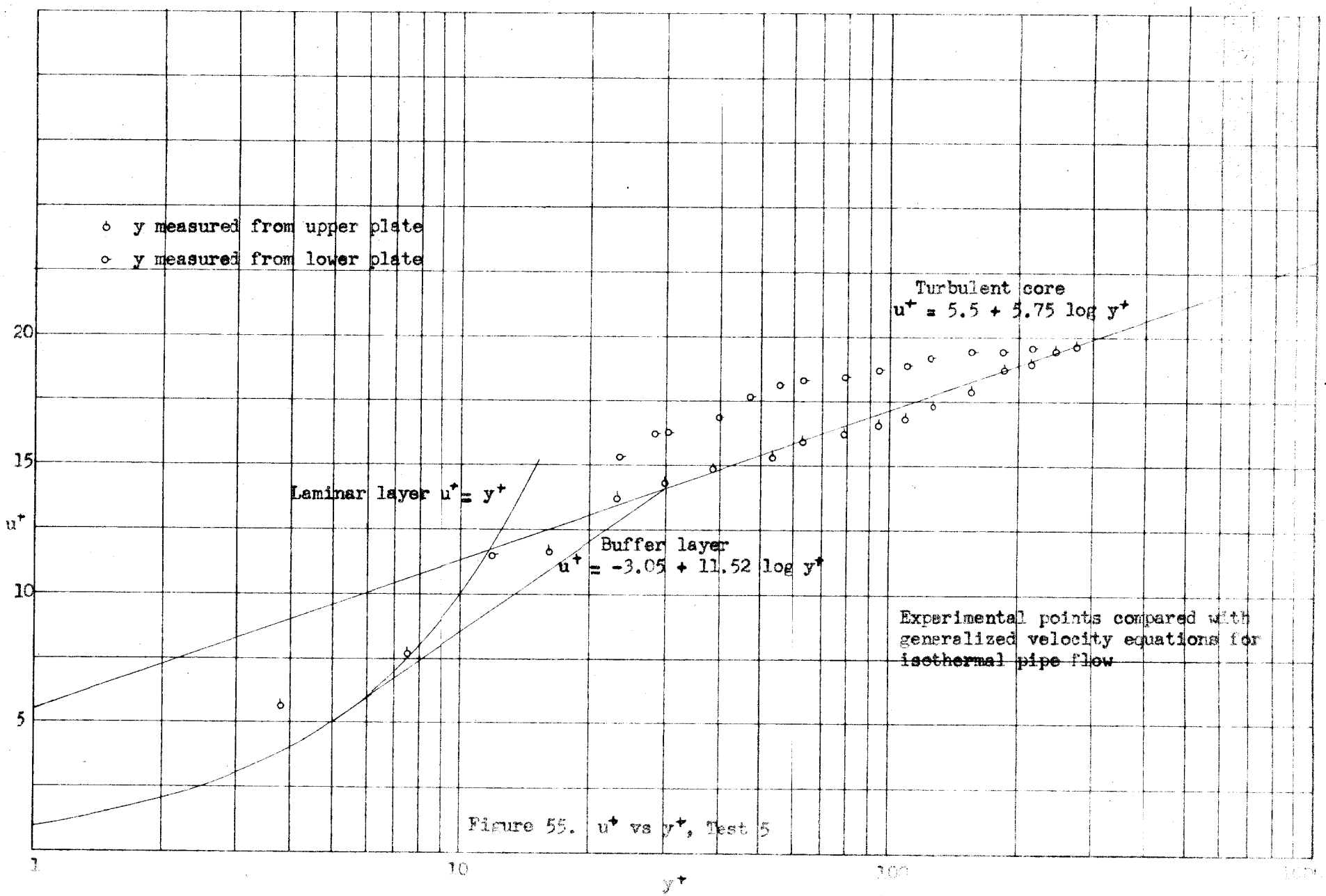

Figure 55. u^+ vs y^+, Test 5

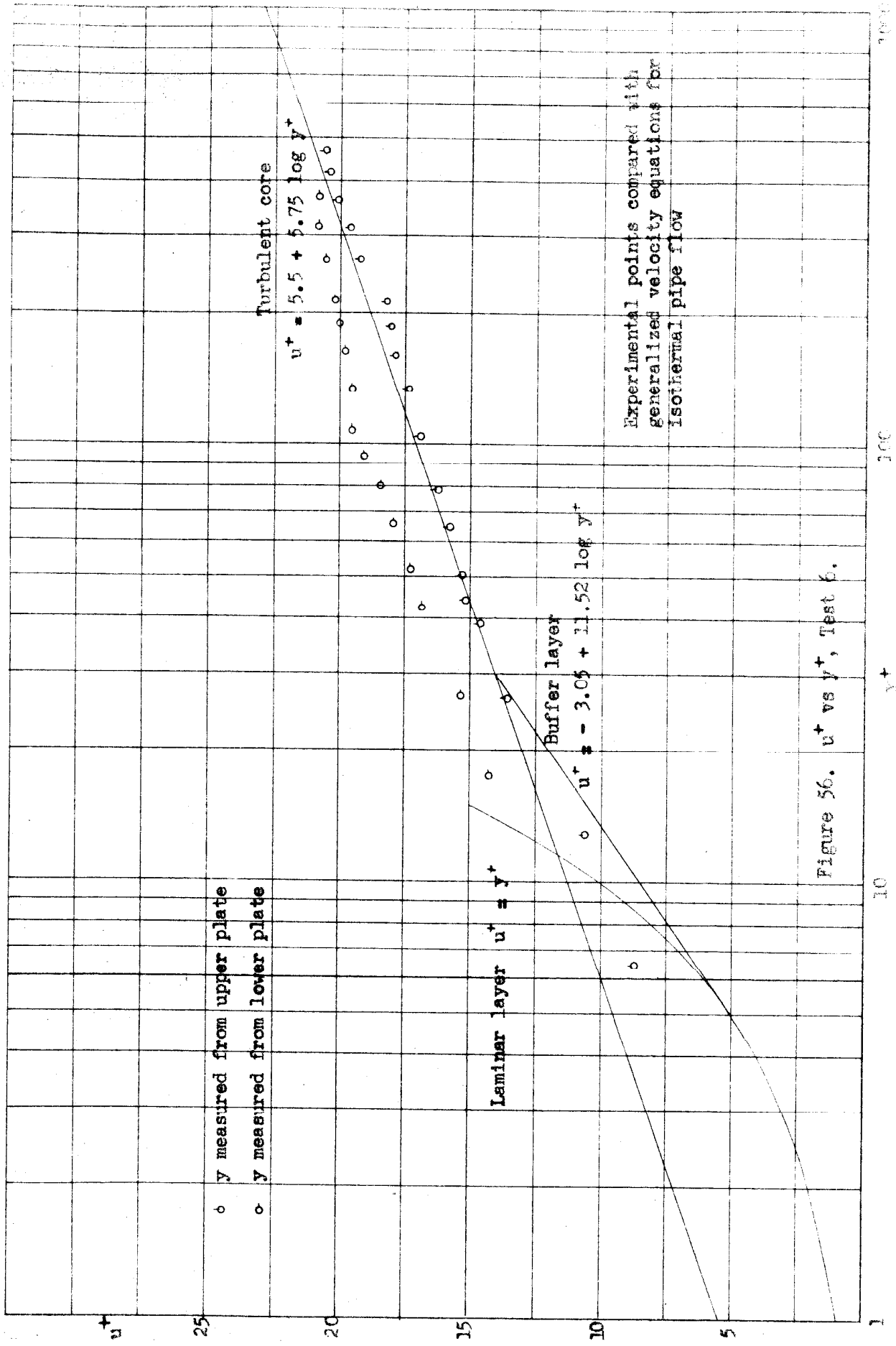

Figure 56. u^+ vs y^+, Test 6.

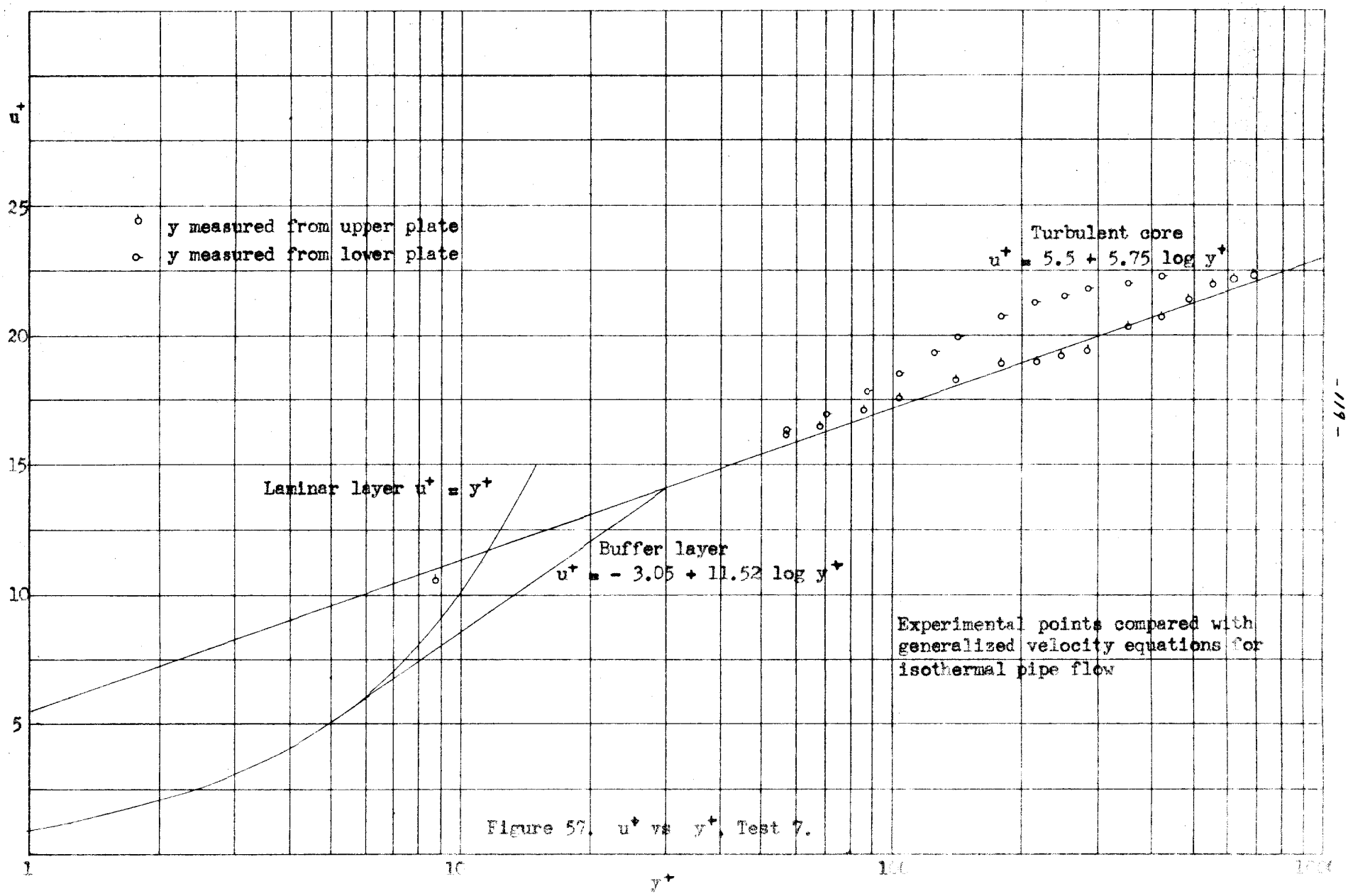

Figure 57. u^+ vs y^+, Test 7.

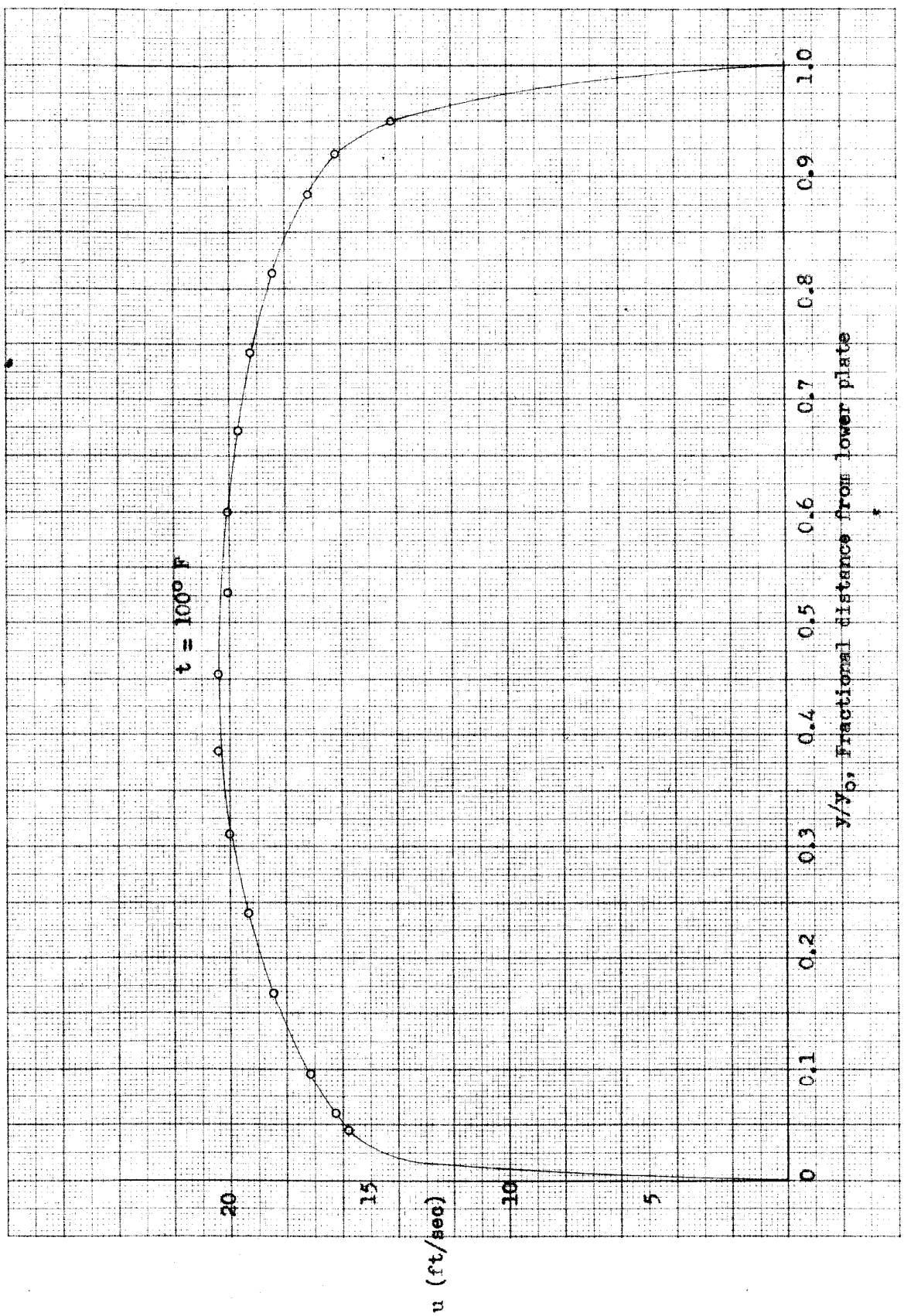

Figure 58. Velocity distribution, isothermal case.

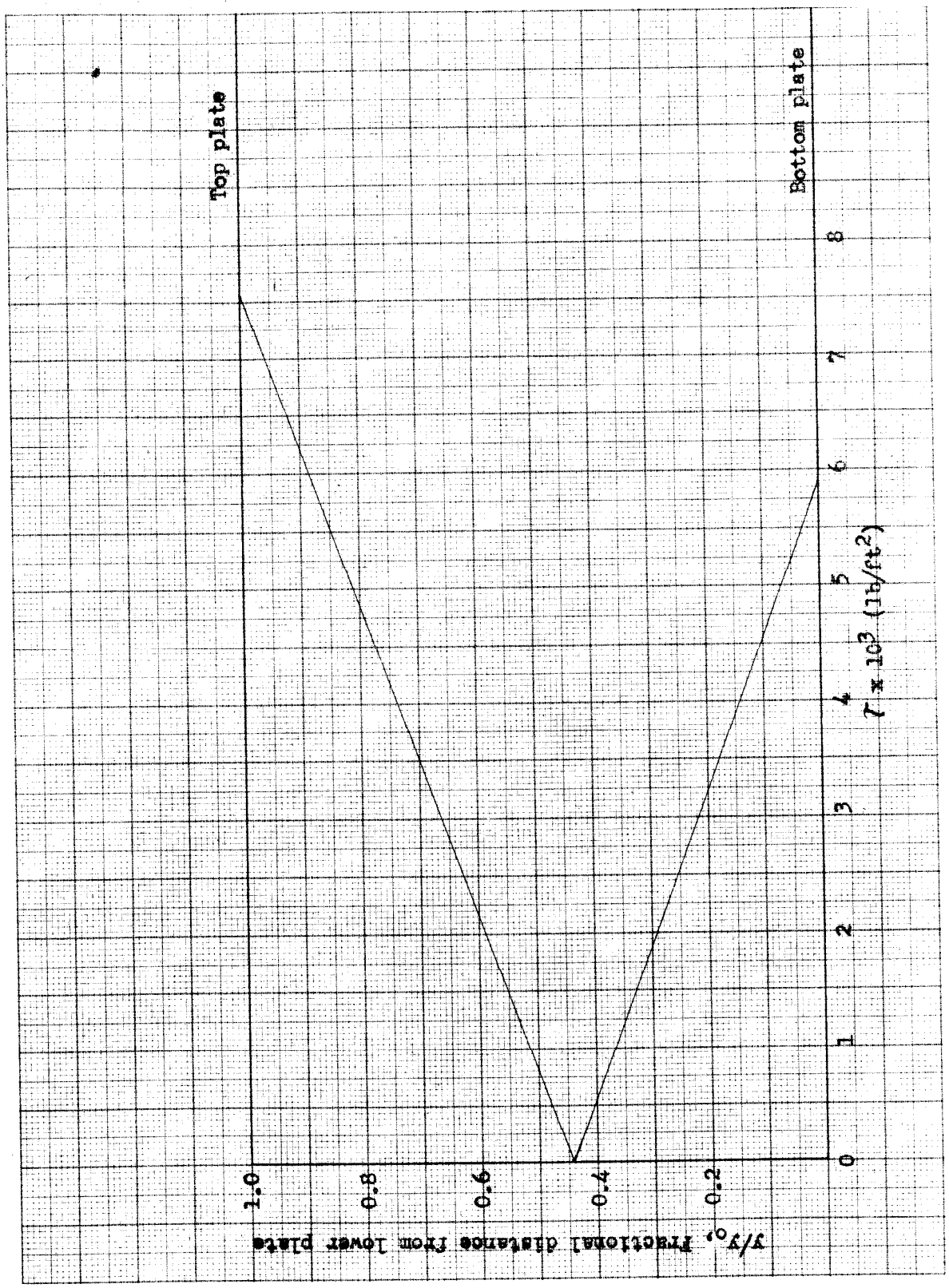

Figure 59. Shear distribution, Test 5.

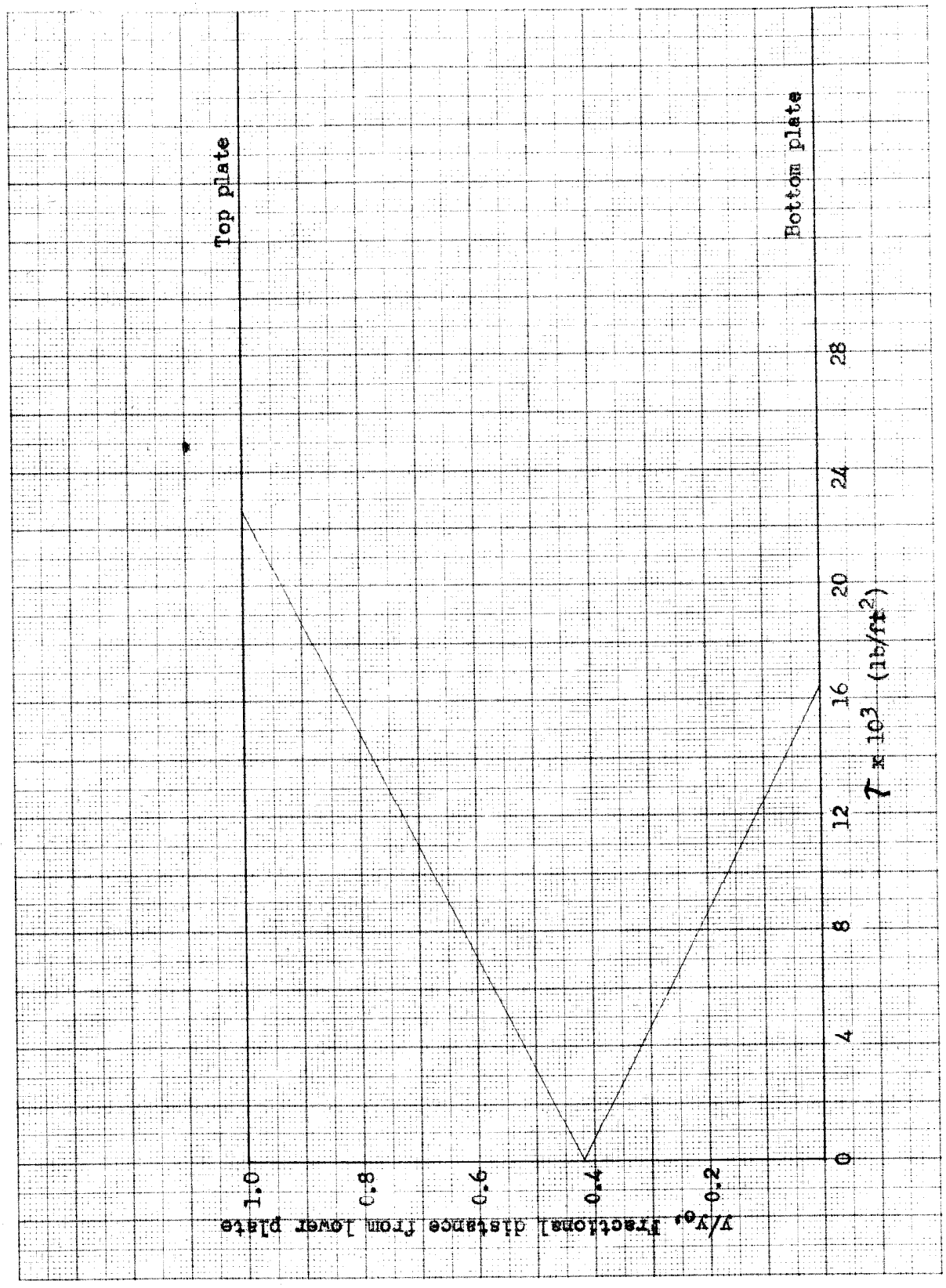

Figure 60. Shear distribution, Test 6.

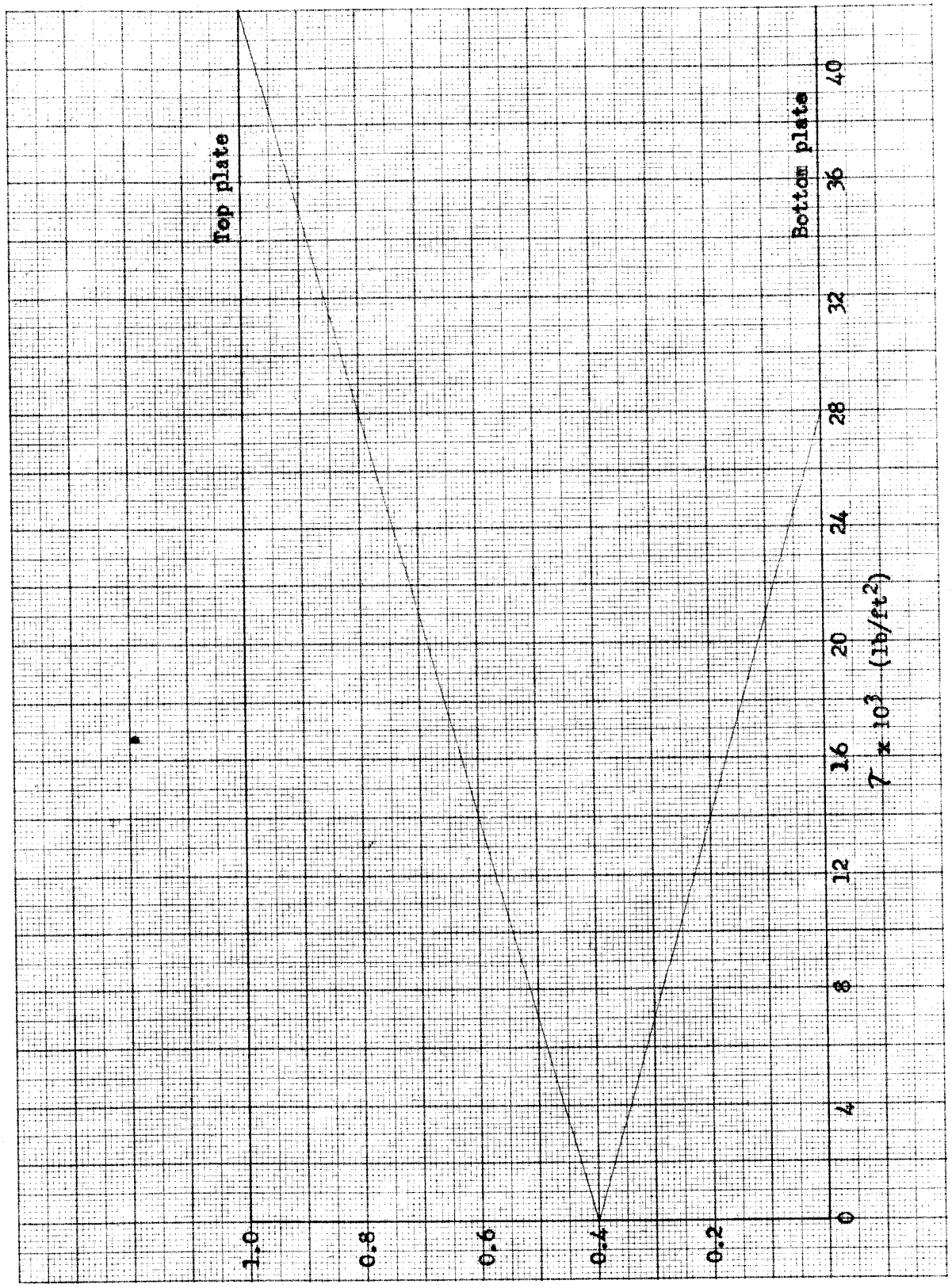

Figure 61. Shear distribution, Test 7.

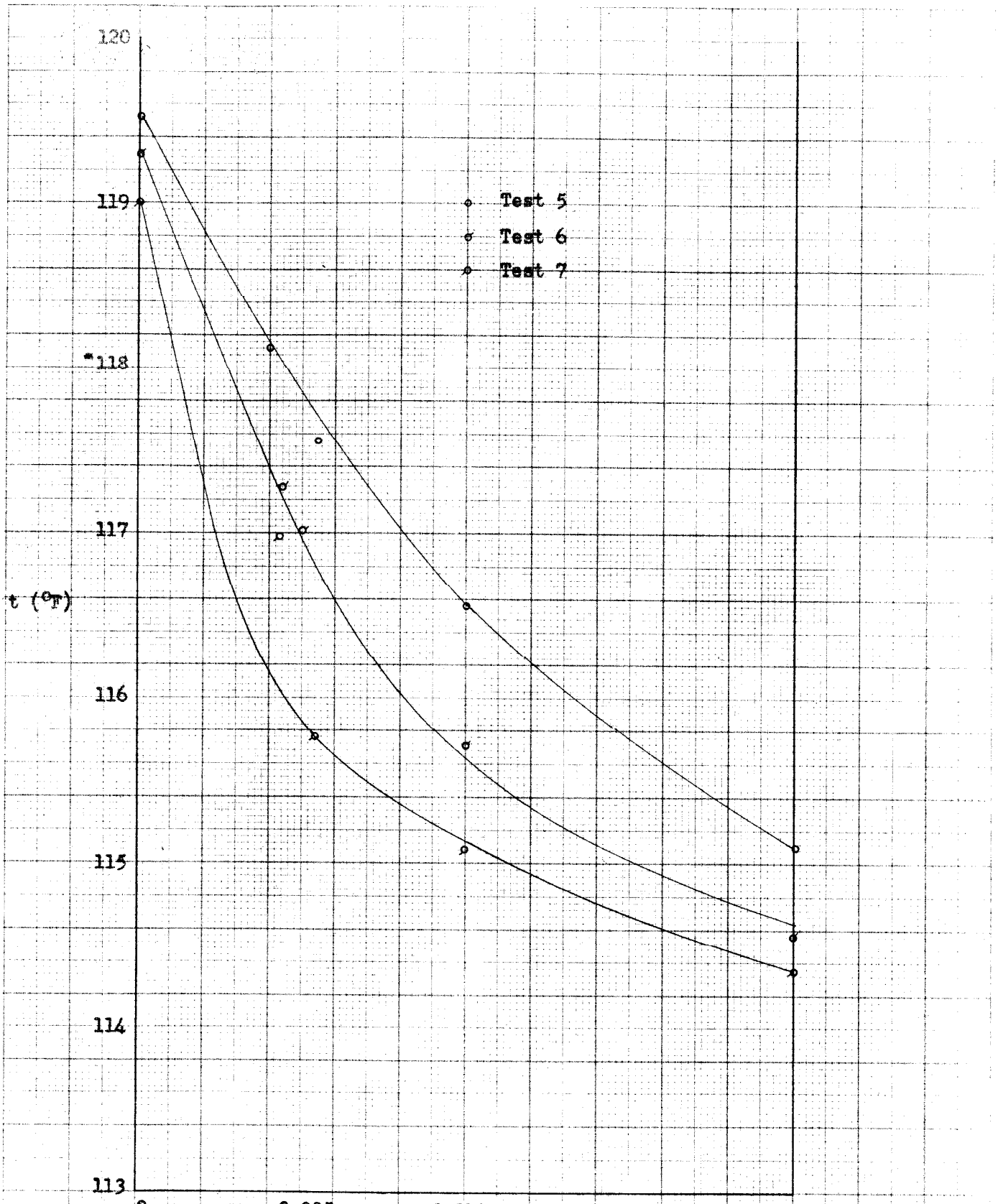

Figure 62. Temperature distribution at upper wall, Tests 5, 6, and 7.

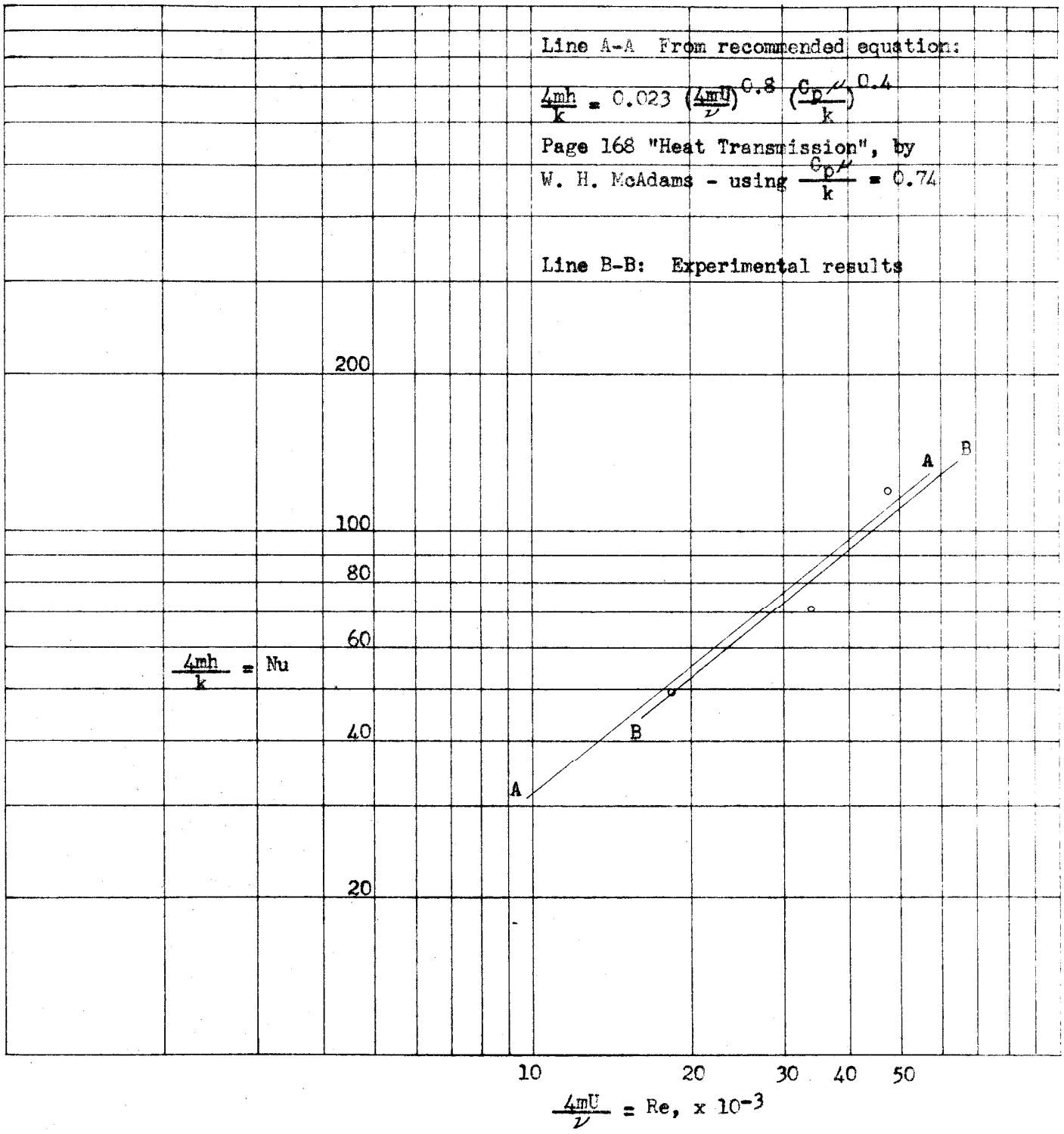

Figure 63. Nusselt number, as derived from dt/dy at upper plate, vs Reynolds number.

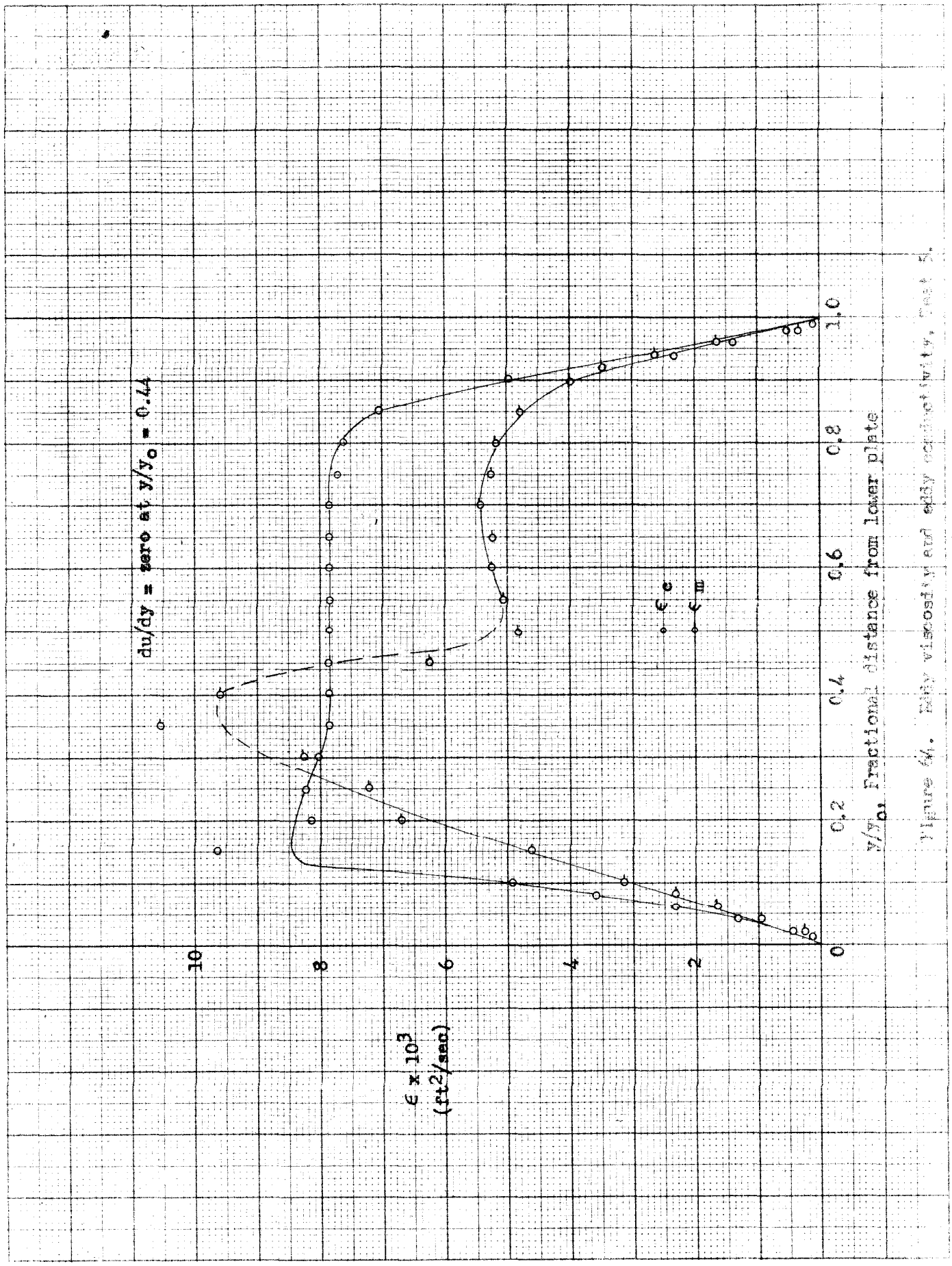

Figure 44. Eddy viscosity and eddy conductivity, run 5.

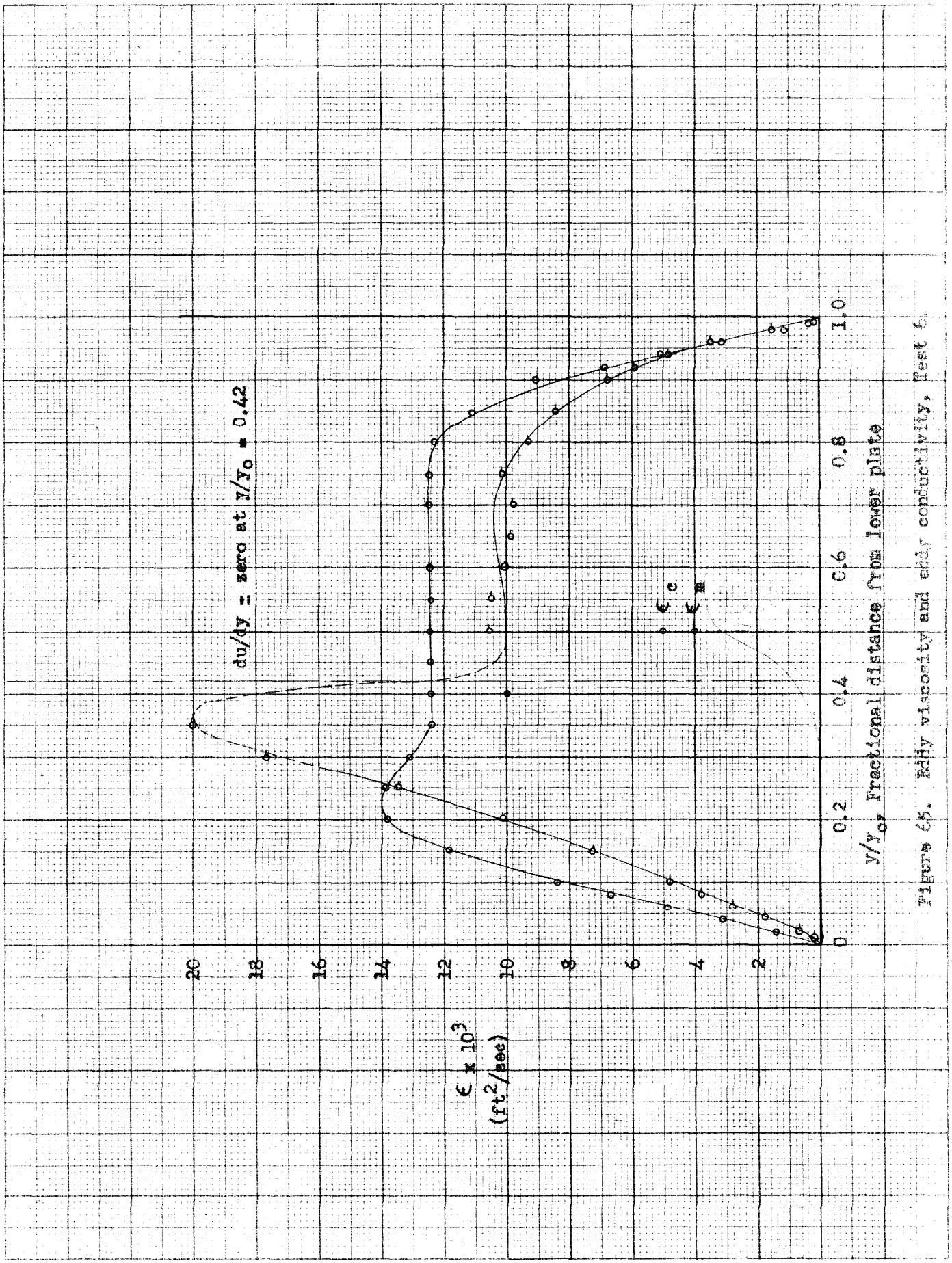

Figure 65. Eddy viscosity and eddy conductivity, Test 6.

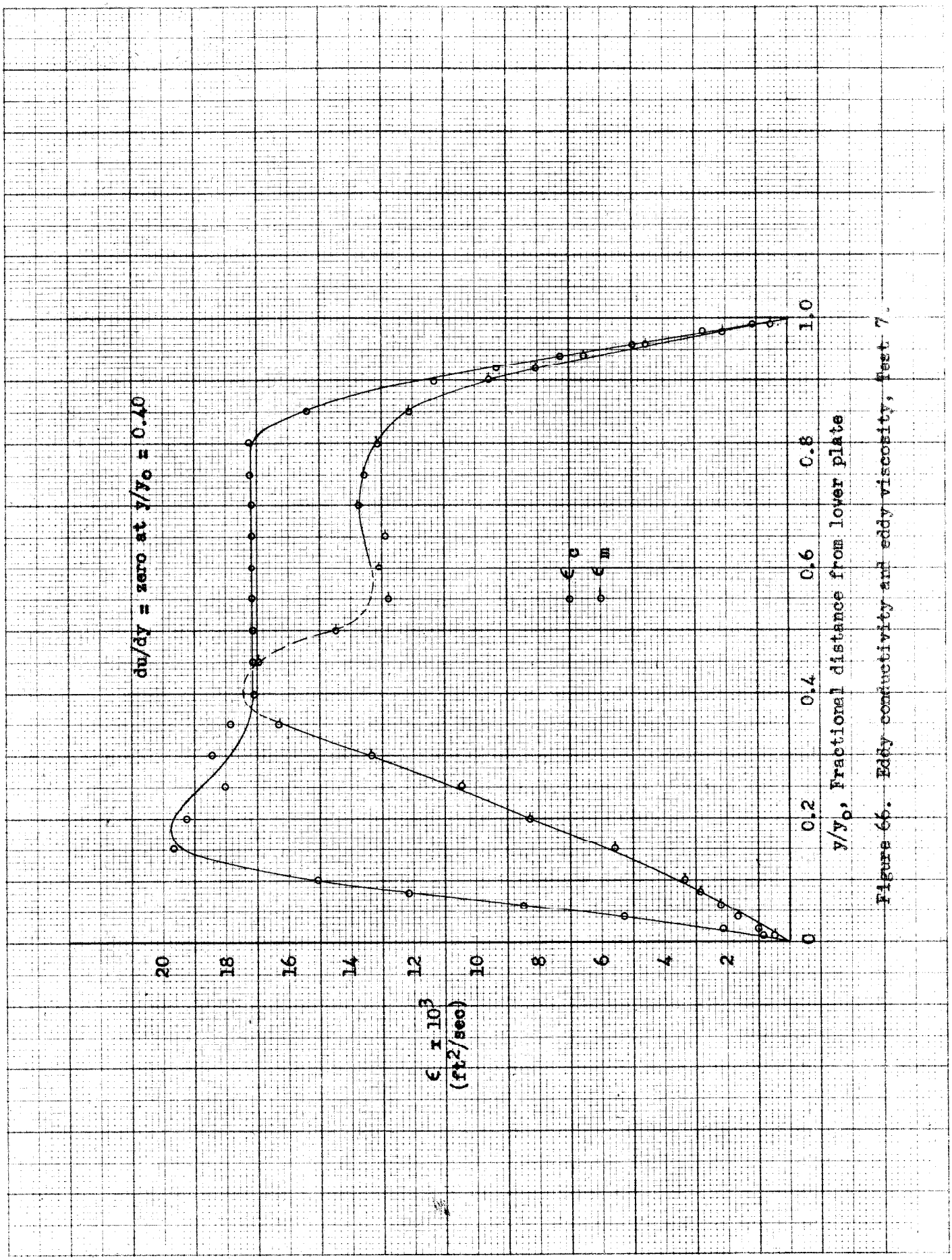

Figure 66. Eddy conductivity and eddy viscosity, Test 7.

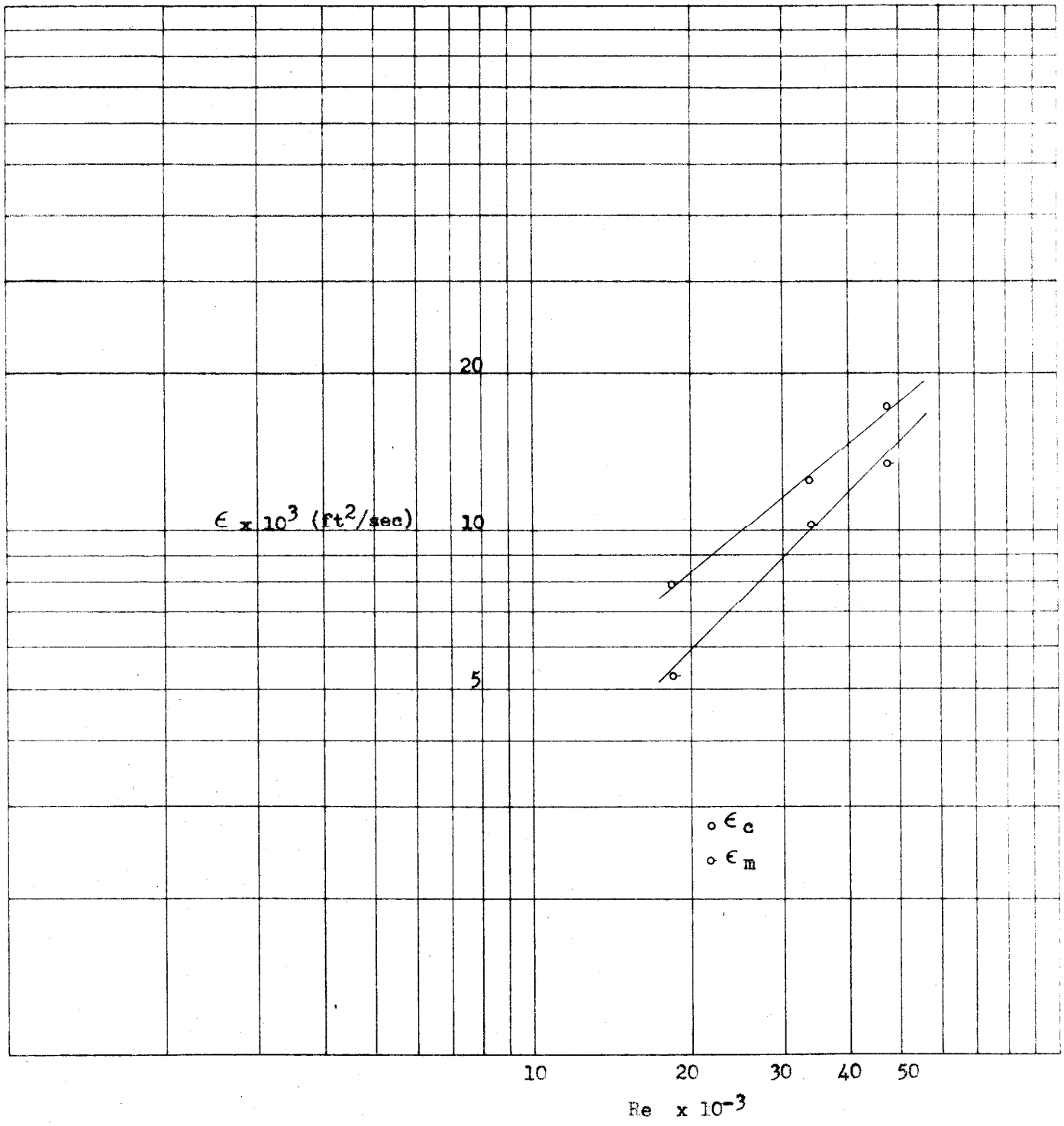

Figure 67. Eddy conductivity and eddy viscosity for central core vs Reynolds number.

APPENDIX

Reprinted from CHEMICAL ENGINEERING PROGRESS *March, 1947*

TEMPERATURE GRADIENTS IN TURBULENT GAS STREAMS

PRELIMINARY STUDIES

By W. H. CORCORAN, B. ROUDEBUSH, and B. H. SAGE

California Institute of Technology, Pasadena, California

ABSTRACT

Equipment is described which permits the measurement of the temperature and velocity distribution in an air stream with essentially two-dimensional flow characteristics. Preliminary results including data describing the temperature and velocity distribution, heat transfer from the wall, and shearing stress are submitted for seven different sets of conditions. The data indicate that within the accuracy of measurement the eddy viscosity and eddy conductivity are equal as was assumed by Theodore von Kármán in his analogy between the transfer of momentum and the thermal transfer of energy. The over-all heat-transfer rate predicted by the Kármán analogy agrees with the experimental results in the case of a symmetrical temperature distribution. However, significant divergences from the heat-transfer rates predicted by the analogy were experienced in the case of nonsymmetrical temperatrue distributions.

The results presented are of a preliminary nature and were of insufficient extent to permit the experimental uncertainty to be established definitely. The detailed study of temperature and velocity distribution together with the associated heat transfer and shearing stress permits a microscopic evaluation of the thermal transfer of energy through a turbulently flowing air stream. The methods employed appear to be capable of refinement, and further study of thermal transfers of energy by these and related methods should permit ultimately the more accurate prediction of the rate of thermal transfers of energy for situations where the transfers of momentum can be predicted from the science of fluid mechanics.

MANY investigators have been interested in the apparent analogy between transfers of momentum and thermal transfers of energy, within flowing fluids. Reynolds (*14*) Prandtl (*13*) Taylor (*15*) and von Kármán (*9*) have each made substantial contributions to this problem, and Boelter (*3*) and co-workers have reconsidered von Kármán's approach and extended it somewhat. In general it appears that at the present time the methods of predicting the thermal transfers of energy across a turbulent stream are comparable in accuracy to the available experimental measurements except in a few isolated cases. The experimental data of Colburn and Coghlan (*4*) and of Eagle and Ferguson (*5*) have been used often in correlations and have been the basis of comparison of methods of prediction suggested by both von Kármán (*9*) and Boelter (*3*) from the momentum transfer analogy.

Because of the relative scarcity of detailed data concerning the thermal transfers of energy within a turbulent gas stream it was believed desirable to initiate additional work in order to permit the extension of the analogy between momentum transfer and the thermal transfers of energy. It was hoped, in common with other investigators, that ultimately a prediction could be made of thermal transfers for nearly all situations for which the transfer of momentum had been established. Recent advances in the science of fluid mechanics, such as are discussed by Gebelein (*6*) Goldstein (*7*) and Bakhmeteff (*2*) lend hope that eventually it may be possible to predict with reasonable accuracy the momentum transfers associated with the flow of fluids through a wide variety of geometric configurations under conditions in which the intensive properties are a function of the spatial coordinates of the fluid. The recent development (*10*) of computing machines suitable for the rapid solution of nonlinear differential equations in terms of particular boundary conditions will permit the application of more elaborate analytical methods to the solution of problems associated with the transfer of material and energy through flowing fluids.

The experimental work of Nikuradse (*11*) is perhaps a classic in the determination of the velocity distribution under turbulent flow conditions. This work which was related primarily to flow in cylindrical tubes has been employed by von Kármán (*9*) and Boelter (*3*) in establishing analytical approximations of the velocity distribution adjacent to the walls of conduits. The velocity distribution has been considered by von Kármán as being divided into three parts. The first, adjacent to the wall, is the laminar sublayer in which the two parameters u and y^+ which are defined (*2*) by the following equations are equal.

$$u^+ = \frac{u}{u^*} = \frac{u}{\sqrt{\frac{\tau_0 g}{\sigma}}} \qquad (1)$$

$$y^+ = \frac{u^* y}{\nu} \qquad (2)$$

The second part of the velocity distribution is considered to be a buffer layer to which von Kármán (*9*) empirically ascribes the following relation between velocity and distance from the wall.

$$u^+ = 5\left[1 + \ln\left(\frac{y^+}{5}\right)\right] \qquad (3)$$

The third is a turbulent core which closely follows a somewhat different logarithmic velocity distribution:

$$u^+ = 5.5 + 2.5 \ln y^+ \qquad (4)$$

In Figure 1 a comparison between Nikuradse's experimental data for uniform flow in smooth circular pipes and the velocity distribution as calculated from Equations (1)-(4) is presented. It is apparent that the data of Nikuradse deviate from Equation (4) at values of y^+ less than 100 and from Equation (3) throughout the greater part of the buffer layer region. Even with this relatively rough approximation of the true velocity distribution in the vicinity of the wall it was shown by both von Kármán (*9*) and Boelter (*3*) that reasonable agreement between the experimental and predicted data could be obtained for the over-

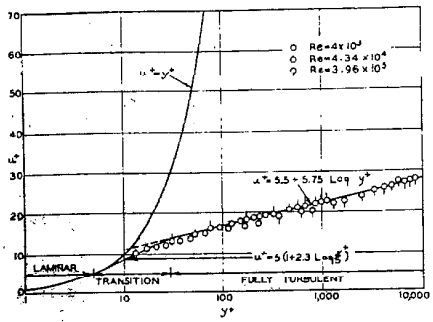

FIG. 1. VELOCITY DISTRIBUTION FOR FLOW IN A CIRCULAR CYLINDER

all heat transfer between a solid phase and a flowing liquid phase.

It is believed that an improvement in the accuracy of predicting heat transfer to a flowing stream may be realized by integrating the basic equations proposed by von Kármán (*9*) and Prandtl (*13*) without assuming simplified velocity distributions or constancy of properties. The following expression presents the basic equation for the thermal transfers through a fluid stream:

$$\frac{\mathring{Q}}{C_p\sigma} = -(K + \epsilon_c)\frac{dt}{dy} \qquad (5)$$

The corresponding equation for the momentum transfer is:

$$\frac{\tau_g}{\sigma} = (\nu + \epsilon_m)\frac{du}{dy} \qquad (6)$$

The variations in thermal conductivity, viscosity, and specific weight for a system of fixed composition may be obtained from a knowledge of the pressure at the point in question and the variation in temperature as derived from the simultaneous solution of Equations (5) and (6). The solution of these differential equations which may be nonlinear when considering the variation of intensive properties with position is tedious with ordinary computing facilities. However, it is believed that with the introduction of more complex computing equipment (*10*) expressions such as Equations (5) and (6) will be useful for the evaluation of the thermal transfers of energy across a flowing stream.

Objective

In order to establish the equality of ϵ_c and ϵ_m in Equations (5) and (6) respectively, as assumed in the analogy proposed by von Kármán, careful simultaneous experimental measurements of velocity and temperature distribution are required. This paper describes certain preliminary experimental equipment that was developed to measure simultaneously temperature and velocity gradients and the corresponding thermal transfers of energy and shear associated with the flowing stream. In addition certain preliminary results are submitted. These measurements leave much to be desired in the way of accuracy but serve to indicate the possibilities of the experimental approach.

Figure 2 shows schematically the arrangement of equipment utilized to determine temperature and velocity distributions in two-dimensional flow of air at Reynolds numbers up to 100,000. Essentially the equipment consists of a centrifugal fan delivering air in a closed circuit through a Venturi meter and the working section. The working section is shown at *A* in Figure 2, and it is 0.75 in. in height and 12 in. in width. A suitable approach section *B* was provided in order to obtain nearly symmetrical flow at the entrance to the working section. The velocity distribution corresponded closely to that anticipated for fully developed turbulence. An exit section *C* which was designed to avoid separation was provided upstream of the entrance to the blower. The Venturi meter *D* was utilized to determine the over-all quantity of air flowing through the system and afforded a useful check of the instruments used to measure velocity at various points in the working section.

The approach section *B* of Figure 2 was 57 in. which is believed sufficient to permit the nearly full development of normal turbulent flow (*2*)(*8*) at a point upstream of the working section. The upper and lower plates of the approach and working sections were maintained at nearly constant predetermined temperatures by rapidly circulating temperature-controlled oil along the outer surfaces of the copper plates as shown at *E* and *F* of Figure 2. The temperature of the air stream was determined as a function of elevation in the working section by means of a small copper-constantan thermocouple so mounted that it could be moved vertically across the section and its position determined with small uncertainty. The velocity was established by means of a Pitot tube arranged so that it could be moved ver- [illegible] section. The [illegible] between the entrance of the approach section and the exit of the working section was ascertained by appropriate piezometer connections located at *G* and *H*. The thermal flux density at the upper wall was established by means of a calorimeter *J* located in the upper plate which permitted the direct measurement of the energy loss per unit area of the plate to the flowing air stream.

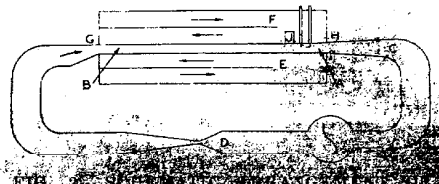

FIG. 2. [illegible] OPERATUS

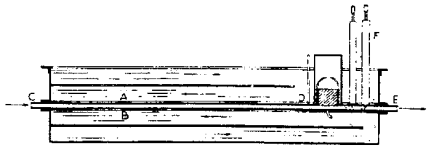

FIG. 3. LONGITUDINAL-SECTIONAL VIEW OF APPROACH AND WORKING SECTIONS

In principle the arrangement described above permitted the measurement of the temperature and velocity distribution and of the energy transfer to the stream per unit area of surface as a function of the temperature difference and bulk velocity of the fluid. From these measurements and the pressure gradient along the channel it is possible to compare values of ϵ_c and ϵ_m established independently from Equations (5) and (6). The equipment described herein is only preliminary in nature and results from an attempt to ascertain if the general approach would yield results of sufficient utility to justify extensive refinement of equipment for more precise measurements.

Description of Equipment

A view of a section taken parallel to the axis of the flow is presented in Figure 3 showing the arrangement of the oil baths in relation to the approach and working sections. The plates, which were made from cold rolled copper, shown at *A* and *B* were employed to separate the oil baths from the flow channel. The oil baths were constructed of welded, low-carbon steel plate, and the faces of the flanges adjacent to the copper plates were machined after the entire assembly had been annealed. It appears from measurements made at the time of assembly that the channel was uniform in section within 0.01 in. throughout the length. The two cop-

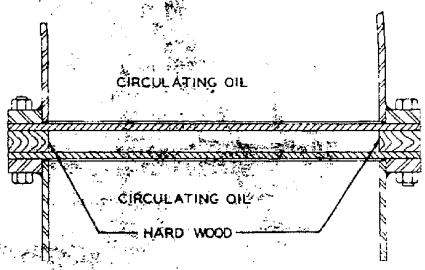

FIG. 4. CROSS-SECTIONAL VIEW OF WORKING SECTION

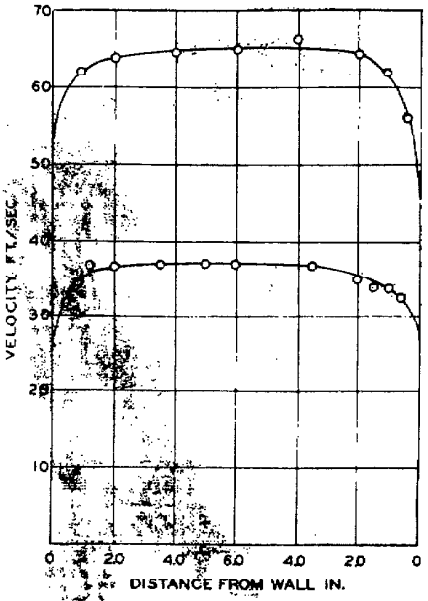

FIG. 5. VELOCITY TRAVERSE ACROSS WIDTH OF WORKING SECTION

per plates were separated at the sides of the section by seasoned hardwood strips (Figure 4). Wood was employed for this purpose in order to avoid excessive conduction between the two plates.

The entrance section consisted of a truncated rectangular pyramid. Traverses at the beginning of the approach section shown at *C* in Figure 3 indicated that the velocity distribution was somewhat more constant with respect to position in the cross section than is the case for fully developed turbulent flow. However, traverses at several points in the approach section indicated that the velocity distribution had become substantially independent of distance in the direction of flow at a point approximately 18 in. upstream from *D* in Figure 3. It is believed that the flow at the working section was nearly two-dimensional. At the exit of the working section at *E* in Figure 3 a traverse across the width indicated approximately constant velocity over the central half of the working section which is shown for two different flow rates in Figure 5. The over-all length of the approach and working section was 6 ft.

The equipment used in making velocity traverses is shown in Figure 6 and was so arranged as to permit the location of the axis of the Pitot tube with an uncertainty of approximately 0.001 in. The end of the Pitot tube is shown in an enlarged view in a part of Figure 6. The tube near the tip had an outside diameter of 0.0176 in. with an axial perforation of 0.010 in. I.D. The leading end of the Pitot tube was honed carefully to insure a symmetrical termination section. The Pitot tube was soldered to the lower part of the sleeve as is shown in Figure 6. The sleeve in turn was soldered to the tube shown in the central part of the traversing equipment. The upper end of this tube was closed and it was provided with a radial opening connecting to the manometer connection shown.

The pressure differential between the Pitot tube and the surrounding air was determined by means of a kerosene-in-glass manometer. The height of the air-hydrocarbon interfaces in the manometer was determined by means of a vertical component cathetometer. An uncertainty of less than 0.3 mm. of kerosene was realized in the measurement of the manometer differentials. In order to decrease the time required for the attainment of equilibrium between the kerosene-in-glass manometer and the flowing stream, arrangements were made for the addition and withdrawal of air from the connecting tubing thus avoiding the need for the flow of relatively large quantities of air through the small Pitot tube. The Pitot tube assembly *F* in Figure 3 is located on the upper plate. Packing was used in the column *A* of Figure 6 to prevent the flow of air from the channel along the axis of the plunger which moved the Pitot tube across the working section. Mechanical limits of *B* of Figure 6 were provided to prevent travel of the Pitot tube to the wall. The position of the Pitot tube was determined by means of a micrometer assembly located at *C* on the upper part of column *A* of Figure 6. The spring *D* [illegible] to return the Pitot tube [illegible] part of the channel upon

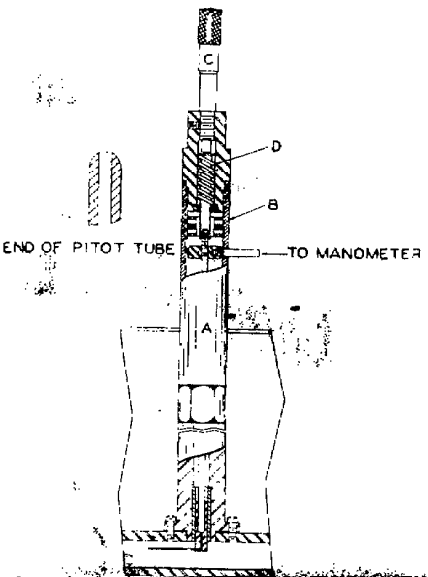

FIG. 6.

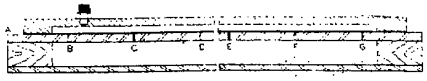

FIG. 7. PIEZOMETER CONNECTIONS FOR WORKING SECTION

retraction of the micrometer anvil. All measurements were taken with an approach from the upper plate in order to avoid hysteresis in the traversing equipment. It was found that a period of as much as 30 min. was required to obtain a determination of the pressure within the Pitot tube relative to that of the surrounding atmosphere.

The static pressure was measured at the beginning of the approach section and at the end of the working section corresponding to points *C* and *E* of Figure 3. The pressure difference between these points was determined by means of piezometer connections attached to the upper plate and by the use of a kerosene-in-glass manometer. The details of the arrangement of the piezometer connections are shown in the sectional view of Figure 7. The holes through the copper plate *A* of Figures 3 and 7 shown at *B* through *G* of Figure 7 were 0.03125 in. I.D. and 0.25 in. in length which corresponds to the optimum length-diameter ratio for such piezometer connections. (*1*) It appears that as a result of the stability of the static pressures the uncertainty in the observed pressure difference was about 0.2 mm. of kerosene.

The static pressure at the same point of the working section as the Pitot tube was determined by a piezometer connection opening into each side of the working section. For most of the measurements reported herein the difference in pressure between the static piezometer connections and the Pitot tube of Figure 6 was determined directly by means of a kerosene-in-glass manometer. In some instances it was determined by

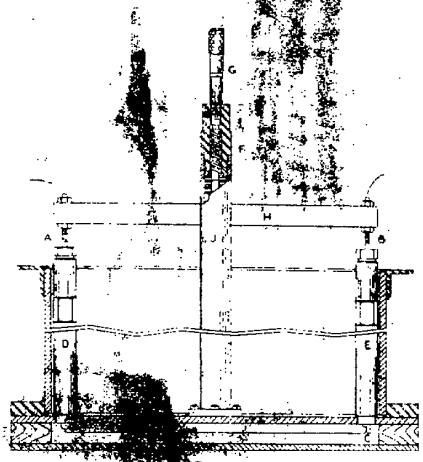

FIG. 8. THERMOCOUPLE SUPPORTS IN THE WORKING SECTION

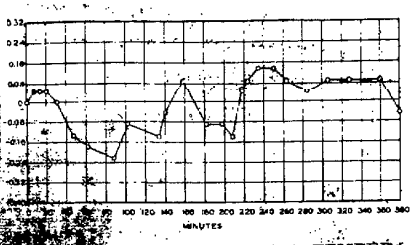

RIATION IN THE TEMPERA-
UPPER PLATE WITH TIME

atmospheric pressure
y.

the temperature at a
points in the flowing
thermocouple was mounted
framework as indicated
8. The thermocouple was
from 0.0037-in. copper
in. constantan wire. The
placed end to end with
coincident and silver sol-
microtechniques in a hydro-
sphere. The tension on the
so adjusted that the cate-
assumed by the wire did not
from a straight line through
of suspension more than
Little flutter of the wire
over the range of flow rates
these investigations, and from
ions of the position of the
function of flow rate for
setting of the microm-
ars that the distance of
couple junction from the
plate was known within 0.003
in. at nearly all of the flow conditions encountered in this study. The thermocouple was calibrated at zero rates of flow by maintaining the temperature of the upper and lower plates constant for a number of different temperature levels. The cold junction was maintained in an agitated ice bath. Materials were individually homogeneous with respect to thermal potential. connected the working section thermocouple to the ice bath and equipment used to measure electromotive force. The electromotive force of the thermocouple was determined by means of a White potentiometer, and it is believed that the values of the electromotive force were accurate within one microvolt at a particular time.

Copper-constantan thermocouples were employed to measure the temperature of the upper and lower plates. The same precaution in the use of homogeneous multiple leads was employed in this instance. It is probable that the temperatures of the copper plates at the points of measurement adjacent to the air stream were known within 0.03° F. The temperatures of the oil baths were controlled by mercury-in-glass regulators actuating electronic relay circuits. However, the thermal transfer between the circulating oil and the copper plates occurring during the measurements made the accurate maintenance of uniform oil temperature difficult.

The leads from the thermocouple were brought out of the tubular supports A and B of Figure 8 through insulated bushings. The constantan multiple lead was continuous from the ice bath to the beginning of the small thermocouple wire at C. The tubular supports A and B passed through packing glands shown at the top of the standards D and E which prevented flow of gas from the working section at these points. The vertical movement of the thermocouple was accomplished through the spring-loaded assembly shown at B. The micrometer G moved the bridge H which was attached to the tubular support A and B. Any slight change in alignment of the parallelogram made of the tubular supports A and B, the bridge H, and the thermocouple did not introduce uncertainties in the location of the juncture because the bridge H and the thermocouple wires remained parallel. Appropriate mechanical limits were provided on the main column J which prevented the thermocouple from being damaged from contact with the walls of the working section.

Figure 9 shows the variations in the upper plate temperature with time during the course of a typical set of measurements. These data indicate gradual changes in the plate temperature resulting from changes in room temperature and in other uncontrolled variables. By increasing the oil velocity and using modulated temperature control, the larger drifts in the

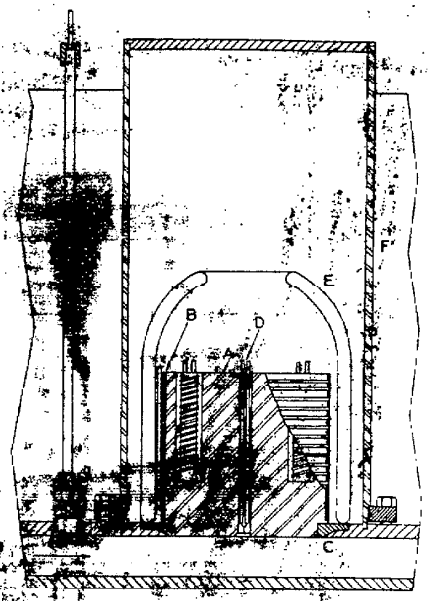

FIG. 10. DETAILS OF CONSTRUCTION OF CALORIMETER

plate temperatures could be eliminated. In the present instance the oil was circulated on the top and bottom sides of plates A and B of Figure 3, respectively, at a velocity of approximately 0.7 ft./sec. At this velocity the oil and air-film coefficients were about equal at a Reynolds number of 10,000 in the working section. The temperatures of the oil baths were determined by means of calibrated mercury-in-glass thermometers.

To determine the rate of heat transfer from the plate into the air stream a block calorimeter was employed. The upper plate was employed. Details of construction are shown in Figure 10. The instrument consists essentially of a copper block A upon which is mounted a noninductive type electric heater B. The lower end of the block is fitted into the upper plate in such a fashion as to be flush with the lower side which was exposed to the flowing air stream. The plate and block were beveled at the point of intersection as shown at C in Figure 10 to decrease the rate of energy transfer between the plate and the calorimeter. In addition the space between the plate and block was filled with an

TABLE 1.—CONDITIONS OF EXPERIMENT MEASUREMENTS

Experiment No.	1	2	3	4	5	6	7
Upper Plate Temp. (° F.)	120.00	120.00	110.00	110.00	110.00	110.00	110.00
Lower Plate Temp. (° F.)	110.00	110.00	100.00	100.00	100.00	100.00	100.00
Bulk Air Temp. (° F.)	114.68	114.45	101.32	101.30	101.39	100.85	100.88
Reynolds Number	18,200	30,500	11,170	14,900	24,200	35,450	50,150
h_c (B.t.u./hr.ft.²)	46.0	71.0	69.5	88.7	126.5	1852	258
c_p (B.t.u./lb.° F.)	0.2401	0.2401	0.2401	0.2401	0.2401	0.2401	0.2401
$k \times 10^4$ (B.t.u. ft./sec. ft.² °F.)	4.05	4.05	3.94	3.94	3.94	3.94	3.94
ρ (lb./ft.³)	0.06905	0.06905	0.0708	0.0708	0.0708	0.0708	0.0708
$\mu \times 10^4$ (lb./ft.²)	6.10	14.0	2.98	4.47	10.8	22.7	43.5
$\mu/g \times 10^4$ (lb.sec./ft.²)	3.91	3.91	3.87	3.87	3.87	3.87	3.87

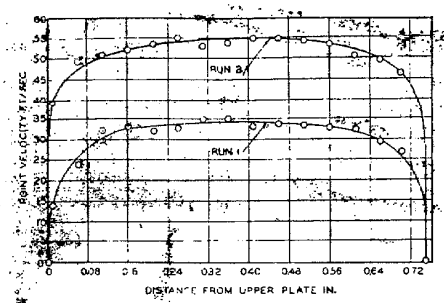

FIG. 11. VELOCITY TRAVERSE IN WORKING SECTION FOR TWO RATES OF FLOW

insulating material in order to decrease still further the energy transfer between the [illegible] copper-constantan thermocouples [illegible] installed in the calorimeter block. The upper part of the calorimeter assembly was enclosed in the vacuum jacket *E*. The calorimeter and vacuum jacket were placed in a metal jacket *F* which extended above the surface of the upper oil bath. The energy input to the calorimeter was determined by potentiometric techniques such as are described by Osborne and co-workers. (*12*) An uncertainty of less than 0.1 per cent was realized in the measurement of the rate of energy input into the calorimeter. In carrying out the calculations the mean area between the aperture in the plate and the area of the face of the calorimeter block was used. This calorimeter technique appeared [illegible] satisfactorily and [illegible] the determination of the rate of heat transfer to the flowing stream with an uncertainty of approximately 0.5 per cent.

To determine the bulk flow rate Venturi meters were installed as shown in Figure 2. The meters were of conventional design with approximately a 7-degree exit cone. They were calibrated by means of velocity traverses at the entrance to the approach section. The differential static pressures between the upstream and throat sections of the Venturi meters were measured by means of kerosene-in-glass manometers used in conjunction with a vertical component cathetometer.

Procedures

To make the desired velocity, temperature, and flux measurements, the upper and lower plates *A* and *B* of Figure 3 were brought to predetermined temperatures. The air flow was started then and the inlet-air temperature was adjusted roughly by means of auxiliary heaters to a predetermined value. As a result of the increased transfer of energy between the plates caused by the flowing air stream some adjustment in the oil-bath temperature was necessary then to maintain the desired temperatures of the plate surfaces. The calorimeter was adjusted then so that the temperature of the exposed end of the calorimeter block was equal to that of the contiguous plate.

After dynamic equilibrium had been obtained, the rate of energy supplied to the calorimeter, the temperature of the upper and [illegible] and the pressure differences [illegible] approach and working sections were determined as a function of time. After completion of a set of measurements at one velocity the rate of flow was changed and the series of measurements repeated.

The results [illegible] only preliminary [illegible] obtained with the equipment [illegible] been described. The experience obtained indicated that certain revisions and modifications of equipment were desirable. However, the data obtained are indicative of the possibilities of this approach and in general appear to be at least semi-quantitatively applicable. For this reason a tabulation of data has been included that has been obtained as well as a graphical presentation of certain derived functions. The information can be divided into two categories: experiments 1 and 2 involve conditions in which the bulk temperature of the incoming air was approximately midway between the temperatures of the upper and lower plates. In the second set of measurements involving experiments 3 to 7 the bulk temperature of the air entering the approach section closely approximated the temperature of the lower plate. For the sake of brevity the graphical presentation of derived results has been limited primarily to experiments 1 and 2.

In Figure 11 the air velocity is shown as a function of the distance from the upper plate for two different rates of flow. The corresponding temperature traverses are shown in Figure 12. In these instances the bulk air temperature entering the working section was 115° F. and the upper-and-lower-plate temperatures were 120° and 110° F. respectively. The corresponding values of Reynolds number for the two measurements were 19,750 and 33,100 respectively. These values of Reynolds numbers were computed for the average state of the air flowing at the working section. Table 1 records the pertinent information concerning the [illegible] measurements [illegible] and 12. Also in Table 2 the experimental values of [illegible] temperature are tabulated as functions of the distance from the upper plate. Data are recorded in Tables 1 and 2 for other conditions than are contained in Figures 11 and 12. The work reported as experiments 3 to 7, inclusive, refers to investigations made with the [illegible] air nearly equal to the lower plate temperature. [illegible] coefficients [illegible] tion associated with the flow [illegible] channel for the measurements recorded in Figures 11 and 12 are [illegible] in Figure 13. Values for the [illegible] measurements presented in [illegible] are shown in Figure 14. In both Figures 13 and 14 the theoretical curves as predicted by von Kármán for flow between parallel plates are included. The experimental [illegible] represented by means of the [illegible]

$$\frac{\tau_0 g}{\sigma V^2} \qquad (7)$$

[illegible] velocity, V, is the bulk velocity as measured by the Venturi meter and is to be differentiated from the velocity, U, as determined in the vertical Pitot [illegible] traverse. The Reynolds number plotted as the abscissa in Figures 13 and 14 is based on the bulk velocity.

The heat-transfer number has been defined by Kármán (*9*) in the following fashion:

$$C_H = \frac{}{\rho U \Delta} \qquad (8)$$

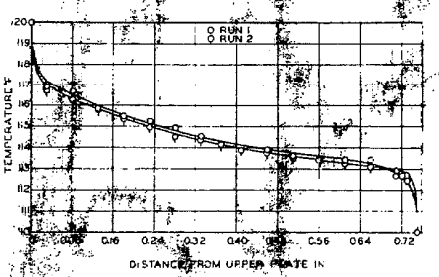

FIG. 12. TEMPERATURE TRAVERSE AT WORKING SECTION FOR TWO RATES OF FLOW

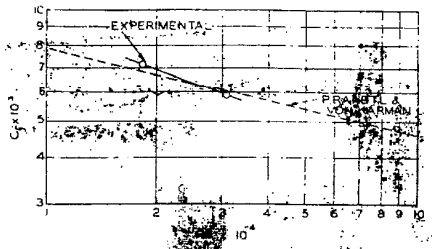

FIG. 13. FRICTION COEFFICIENTS FOR NEARLY SYMMETRICAL TEMPERATURE DISTRIBUTION

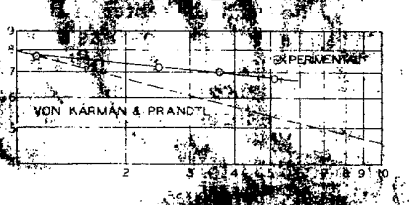

FIG. 14. FRICTION [illegible] NONSYMMETRICAL [illegible] TRIBU[illegible]

Kármán relates the heat-transfer number to the friction factor and properties of the fluid by the following expression which is applicable for most gases at states remote from the critical state.

$$\frac{1}{C_H} = \frac{2}{C_f} + 5\left(\frac{2}{C_f}\right)^{1/2}\{Pr - 1 + \ln[1 + 5/6(Pr - 1)]\} \quad (9)$$

Prandtl suggested the equation

$$\frac{1}{C_H} = \frac{2}{C_f} + \left(\frac{2}{C_f}\right)^{1/2}(Pr - 1) \quad (10)$$

Values of the heat-transfer number C_H as a function of Reynolds number obtaining in the working section are presented in Figure 15. It is apparent that for the conditions involved in experiments 1 and 2 for which the bulk temperature corresponds to the temperature of the central part of the flowing stream, the computed values from von Kármán (9) agree with the calorimetric values. In Figure 16 similar information is presented for measurements made under conditions where the bulk temperature corresponds more closely to the temperature of the lower plate. In this instance the experimentally determined heat-transfer number is somewhat larger than that obtained from the predictions of von Kármán (9). For both Figures 15 and 16 it is to be noted that curve *D* shows points plotted as functions of the Reynolds number based on the actual bulk velocity since the experimental coefficients of friction associated with the computations were obtained on the basis of the bulk flow. The relation between C_H and C_f is given by Equation (9).

The information recorded in Tables 1 and 2 permits the evaluation of the eddy viscosity by application of Equation (6) and the fact that the shear stress decreases linearly with distance from the wall to zero at the center. By suitable graphical operations the eddy viscosity ϵ_m was computed for experiments 1 and 2. The results of these computations are shown in Figure 17. As would be expected the eddy viscosity is somewhat higher velocity. The center of the flow chan[illegible] shown as a dotted cur[illegible] certainties in the velo[illegible] ment.

From the information submitted in Figures 12 and 17 it is possible from Equation (5) to evaluate the rate of thermal transfer of energy normal to the flowing stream as a function of position in the stream. These data

TABLE 2.—EXPERIMENTAL VELOCITY AND TEMPERATURE GRADIENTS

Distance from Upper Plate (in.)	Velocity (ft./sec.)	Distance from Upper Plate (in.)	Temperature (° F.)
Experiment 1			
.010	14.0	.030	117.01
.060	24.3	.080	116.62
.110	31.5	.130	115.95
.160	32.5	.180	115.51
.210	32.6	.230	115.19
.260	33.2	.280	114.88
.310	34.6	.330	114.53
.360	34.7	.370	114.20
.410	33.7	.410	114.03
.460	33.[illegible]	.460	113.92
.510	33.4	.510	113.70
.560	32.7	.560	113.54
.610	31.9	.610	113.45
.660	29.3	.660	113.31
.700	26.4	.710	112.80
		.720	112.72
		.730	112.48
Experiment 2			
.010	39.2	.030	116.93
.060	49.0	.080	116.30
.110	50.5	.130	115.81
.160	52.0	.180	115.35
.210	53.5	.230	115.02
.260	54.2	.280	114.61
.310	53.2	.330	114.40
.360	54.2	.370	114.18
.410	54.8	.410	113.98
.460	54.5	.460	113.75
.510	54.2	.510	113.55
.560	53.3	.560	113.40
.610	51.0	.610	113.33
.660	49.6	.660	113.14
.700	46.5	.710	112.96
		.720	112.81
		.730	112.76
Experiment 3			
.010	9.5	.050	105.5
.020	11.6	.060	105.2
.040	15.3	.085	104.3
.050	16.2	.110	103.35
.100	18.6	.135	102.8
.200	20.5	.160	102.4
.300	21.5	.210	101.80
.375	21.6	.310	100.80
.450	21.3	.350	100.55
.550	20.2	.385	100.30
.650	18.5	.410	100.20
.700	16.3	.510	100.00
		.610	100.00
		.710	100.00
Experiment 4			
.010	14.2	.050	105.20
.015	16.2	.060	104.80
.020	17.3	.080	104.10
.025	19.2	.100	103.45
.030	20.3	.150	102.60
.040	22.5	.200	101.95
.050	22.9	.300	101.05
.075	24.4	.375	100.65
.100	24.8	.400	100.45
.160	26.3	.500	100.13
.200	26.3	.600	[illegible]
.240	28.1	.650	[illegible]
.300	28.2	.700	[illegible]
.375	28.8	.750	[illegible]
.400	29.0		
.450	28.8		
.500	27.0		
.550	26.5		
.600	25.[illegible]		
.650	23.4		
.675	22.8		
.700	21.6		
.710	20.9		

TABLE 2.—*Continued*

Distance from Upper Plate (in.)	Velocity (ft./sec.)	Distance from Upper Plate (in.)	Temperature (°F.)
	Experiment 5		
.010	21.2	.050	105.15
.015	26.8	.060	104.95
.020	20.9	.080	103.95
.040	33.4	.100	103.11
.080	37.4	.150	102.50
.160	41.3	.200	101.99
.240	43.9	.300	101.00
.320	45.7	.375	100.45
.375	45.7	.400	100.30
.420	45.5	.500	100.02
.480	44.7	.600	100.01
.560	42.8	.650	100.01
.640	38.4	.700	100.00
.680	35.0	.750	100.00
.707	31.4		
	Experiment 6		
.015	43.9	.060	102.95
.030	50.1	.070	103.55
.040	52.3	.080	102.70
.050	52.9	.100	102.42
.060	55.2	.125	102.10
.120	61.3	.150	101.75
.220	66.6	.200	101.30
.300	69.0	.250	100.85
.375	70.5	.300	100.60
.480	68.6	.400	100.25
.530	66.5	.500	100.06
.580	63.5	.600	100.00
.630	59.4	.650	100.00
.670	55.4	.700	100.00
.690	52.3	.750	100.00
.707	50.2		
	Experiment 7		
.015	66.0		103.2
.020	68.7	.070	102.9
.040	75.3	.080	102.7
.060	75.3	.100	102.4
.080	82.7	.125	102.0
.100	84.8	.150	101.7
.150	89.6	.200	101.25
.170	91.1	.250	100.80
.220	95.0	.300	100.55
.270	97.1	.400	100.15
.375	100.2	.500	100.05
.460	99.1	.550	100.00
.530	93.8	.600	100.00
.560	94.8	.650	100.00
.580	89.3	.700	100.00
.600	87.7		
.650	84.5		
.670	81.7		
.690	78.0		
.710	74.3		

do not involve the calorimetric determination of energy added to the stream at the boundary. In Figure 18 curves are indicated showing the thermal transfers of energy as a result of eddy conductivity and of both eddy and molecular conductivity. It is apparent that as the wall is approached the importance of the conduction increases and, at the wall it accounts for the entire transfer. The behavior near the wall has been indicated by means of dotted curves since some uncertainty exists as to the temperature gradients in this region. However, the extrapolation of the curves representing the thermal transfers of energy normal to the flowing stream at a significant distance from the wall agree with the independently determined calorimetric values shown as $\mathring{Q}_w$. The high rate of heat transfer for experiment 7 is almost entirely the result of the higher eddy conductivity under these conditions. These results appear to indicate that the hypothesis of von Kármán (*9*) which states that the eddy viscosity and the eddy conductivity are equal numerically appears to be valid within the accuracy of the experimental work herein reported. Similar calculations can be made for the other data recorded in Tables 1 and 2 and for the most part reasonable agreement with the calorimetric measurements is obtained. However

instance the rate of heat transfer decreases to a low value at a point in the vicinity of the lower plate since the bulk air temperature at the inlet of the approach section was close to the lower-plate temperature.

The authors wish to emphasize that these measurements are preliminary and are subject to uncertainties. For that reason no attempt has been made to carry forward the analysis of the results as far as would be justified if the uncertainty in the measurements were known. The extent of the measurements were limited sufficiently to make an evaluation of the uncertainty difficult. Therefore no indication of the probable error in the several variables has been made.

Acknowledgments

R. R. Bowles, E. Cate, Q. Elliott, and T. L. Kirtley obtained a number of the measurements reported here and their assistance is acknowledged.

Nomenclature*

C_f = coefficient of friction, dimensionless, $= f = \frac{2\tau_0 g}{\sigma V^2}$

C_H = heat transfer number, dimensionless, $= \frac{\mathring{Q}}{C_p \sigma U \Delta t}$

C_p = isobaric heat capacity, $\frac{B.t.u.}{\text{lb. °F.}}$

g = acceleration due to gravity, ft./sec.^{2}

k = thermal conductivity of fluid, $\frac{B.t.u.\ ft.}{\text{sec. ft.}^2\ °F.}$

K = thermometric conductivity

ln = logarithm to the base e

log = logarithm to the base 10

m = hydraulic radius, ft.

Pr = Prandtl number, dimensionless, $= \frac{\mu C_p}{k}$

$\mathring{Q}$ = rate per unit area of thermal transfer of energy, $\frac{\text{B.t.u.}}{\text{sec. ft.}^2}$

$\mathring{Q}_e$ = rate per unit area of thermal transfer of energy, based on ϵ, $\frac{\text{B.t.u.}}{\text{hr. ft.}^2}$

$\mathring{Q}_{\epsilon+k}$ = rate per unit area of thermal transfer of energy, based on ϵ and k, $\frac{\text{B.t.u.}}{\text{hr. ft.}^2}$

* Throughout this paper the force-length-time system of dimensions has been employed. All quantities are expressed in

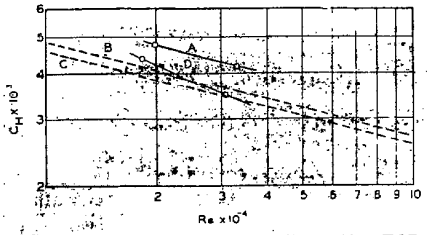

FIG. 15. HEAT-TRANSFER NUMBER FOR NEARLY SYMMETRICAL TEMPERATURE DISTRIBUTION

A—Experimental; B—von Kármán; C—Prandtl; D—von Kármán's analogy using experimental C_f

$\mathring{Q}_w$ = heat transfer per unit area at upper plate of channel, $\frac{\text{B.t.u.}}{\text{hr. ft.}^2}$

Re_U = Reynolds number based on bulk velocity, U, $= \frac{4_m U}{\nu}$

Re_V = Reynolds number based on bulk velocity, V, $= \frac{4_m V}{\nu}$

t = time average temperature at any point y, °F.

u = time average velocity at any point y, ft./sec.

u^* = friction velocity, ft./sec. $= \sqrt{\frac{\tau_0 g}{\sigma}}$

u^+ = velocity to friction velocity ratio, dimensionless, $= \frac{u}{u^*}$

U = bulk velocity based on integrated Pitot tube measurements made in central portion of working section, ft./sec.

V = bulk velocity based on Venturi meter measurements, ft./sec.

$X = \frac{\text{ft.}^2}{\text{sec.}} = \frac{k}{C_p \sigma}$

y = distance from wall, ft.

y^+ = friction distance parameter, dimensionless, $= \frac{yu^*}{\nu}$

Δ = difference notation

ϵ_o = eddy conductivity, ft.^{2}/sec.

ϵ_m = eddy viscosity, ft.^{2}/sec.

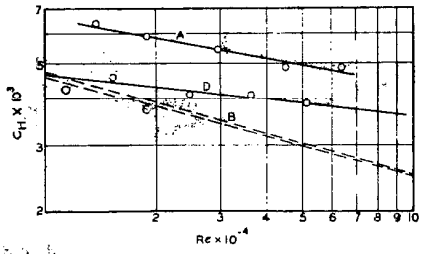

FIG. 16. HEAT-TRANSFER NUMBER FOR NEARLY SYMMETRICAL TEMPERATURE DISTRIBUTION

A—Experimental; B—von Kármán; C—Prandtl; D—von Kármán's analogy using experimental C_f

μ = absolute viscosity of fluid, lb.sec./ft.^{2}

ν = kinematic viscosity of fluid, ft.^{2}/sec.

ρ = density of fluid, lb.sec.^{2}/ft.^{4}

σ = specific weight, lb./ft.^{3}

τ = shearing stress at any point y, lb./ft.^{2}

τ_0 = shearing stress at wall, lb./ft.^{2}

Literature Cited

1. Allen, C. M., and Hooper, L. J., *Trans. A.S.M.E.*, 54, (1932); paper HYD-54-1.
2. Bakhmeteff, B. A., "The Mechanics of Turbulent Flow," Princeton University Press, (1936).
3. Boelter, L. M. K., Martinelli, R. C., and Jonassen, F., *Trans. A.S.M.E.*, 63, 447, (1941).
4. Colburn, A. P., and Coghlan, C. A., A.S.M.E. Annual Meeting, Dec. 2-6, (1940).
5. Eagle, A., and Ferguson, R. M., *Proc. of Royal Society*, 127a, 540, (1930).
6. Gebelein, H., "Turbulenz." Julius Springer, (1935) Berlin.
7. Goldstein, S., "Modern Developments in Fluid Dynamics, *I* and *II*, Oxford University Press, (1938).
8. von Kármán, Th., "Turbulence and Skin Friction," *J. of Aeron. Sciences*, 1, (1934).
9. von Kármán, Th., *Trans. A.S.M.E.*, 61, 705, (1939).
10. Kuehni and Peterson, "A New Differential Analyzer," *Trans. A. I. E. E.*, 63, 221, (1944).
11. Nikuradse, J., V.D.I., *Forschungsheft*, 356, 36, (1932).
12. Osborne, N. S., and Van Dusen, M. S., *Bur. of Standards, Bull.* 14, 133, (1917); Scientific Paper No. 301.
13. Prandtl, L., Physikalische *Zeitschrift*, 29, 487, (1928).
14. Reynolds, O. S., *Proc. Manchester Literary and Philosophical Society*, 14, 7, (1874); *Collected Papers*, I, 81.
15. Taylor, G. I., Great Britain Advisory Committee for Aeronautics, Reports and Memoranda, No. 272, 2, 423 (1916-1917).

Presented at the Regional Meeting, San Francisco, California, August 25-28, 1946.

Discussion

J. Howard Arnold (California Research Corp., Richmond, Calif.): It is about twenty-five years now since Whitman introduced chemical engineering to his two-film theory of material transfer, and I think it is somewhat longer since chemical engineers became aware of the function of films or boundary layers in heat transfer. I am glad to see this paper bring out the availability and the flexibility of the Prandtl and Kármán equations, and by inference at least the Colburn and Sherwood analogies to these equations for material transfer.

As I stated yesterday, I believe that equations such as these are not very familiar to most chemical engineers, in spite of the fact they represent the only really [illegible] theoretical equations in this field. Further work, such as Professor Sage has reported, is of great importance in improving these equations, or securing other equations that are better, so that we may have equations that utilize the proper physical picture and give us adequate representation of the data, and no longer have to depend on correlations based solely on dimensional analysis.

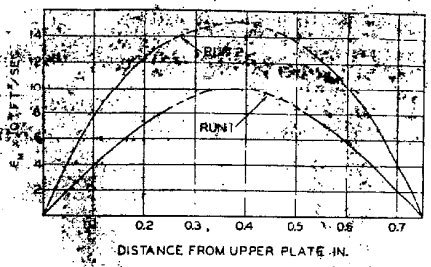

FIG. 17. EDDY VISCOSITY IN FLOWING STREAM

B. H. Sage (California Institute of Technology, Pasadena): I concur with the comments that have been presented to the meeting by Mr. Arnold. It is hoped that in the not too distant future, as the result of the application of such or other analogies, the chemical engineer will be in as good a position in predicting the thermal transfer of energy and the transfer of material as is the engineer in the application of fluid mechanics to the prediction of transfers of momentum in situations wherein there is no change in the intensive properties of the fluid from point to point in the flowing system. At the present time there is insufficient information concerning even fluid mechanics to predict with accuracy the coefficient of friction under circumstances where there are large changes in the viscosity and specific weight from point to point in the system.

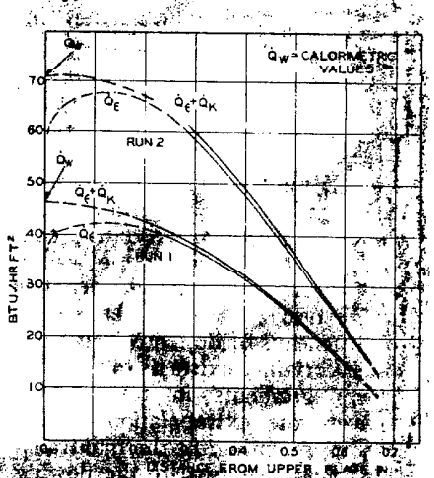

FIG. 18. THERMAL TRANSFER OF ENERGY ACROSS THE FLOWING STREAM

PART II. THERMODYNAMIC PROPERTIES OF METHANE AT LOW TEMPERATURE

Reprinted from INDUSTRIAL AND ENGINEERING CHEMISTRY, Vol. 36, Page 825, September, 1945

Thermodynamic Properties of Methane at Low Temperature

W. H. CORCORAN, R. R. BOWLES[1], B. H. SAGE, AND W. N. LACEY
California Institute of Technology, Pasadena, Calif.

IN THE solution of many engineering problems the use of detailed thermodynamic data is very convenient. Frequently such data are not readily available and must be obtained from measured physical and thermal properties by lengthy calculations. Thermodynamic properties of methane above 70° F. have been tabulated by several authors. Corresponding information for temperatures below 70° F. is not so easily available. Keesom and Houthoff (*4*) presented a temperature-entropy diagram for methane covering the temperature range from 100° to 270° K. and the pressure range from 1 to 40 atmospheres. The thermodynamic quantities were determined by utilizing information from a single source (*5*). The results are given in metric units and no tabulated data are shown. Subsequent experimental work has afforded increased information on the physical and thermal properties of methane.

It has, therefore, seemed desirable to utilize the more recent methane data in preparing a temperature-entropy diagram for the low temperature region, in terms of English units. The thermodynamic properties of methane from 70° to −230° F. and from atmospheric pressure to 1400 pounds per square inch absolute have been derived from data existing in the literature and are presented in tabular and graphical form.

[1] Present address, Standard Oil Company of California, El Segundo, Calif.

METHODS

Molal heat capacities at zero pressure were determined from fundamental vibrational frequencies given by Vold (*9*). At zero pressure the isobaric heat capacity is given by the equation

$$C_{P_0} = ab\left[\frac{3}{2} + \frac{3}{2} + 1 + \sum_{i=1}^{3n-5}\left(\frac{\theta_i}{T}\right)^2 \frac{e^{\frac{\theta_i}{T}}}{\left(e^{\frac{\theta_i}{T}} - 1\right)^2}\right] \qquad (1)$$

The first two terms within the bracket are concerned with translational and rotational energy, respectively; the third term is related to the difference between the isobaric and isochoric heat capacities. The characteristic temperature, θ_i, is obtained by multiplying the vibrational frequency by hc/k in consistent units. Since the methane molecule has five atoms, it possesses nine degrees of vibrational freedom and hence the limits for the last term

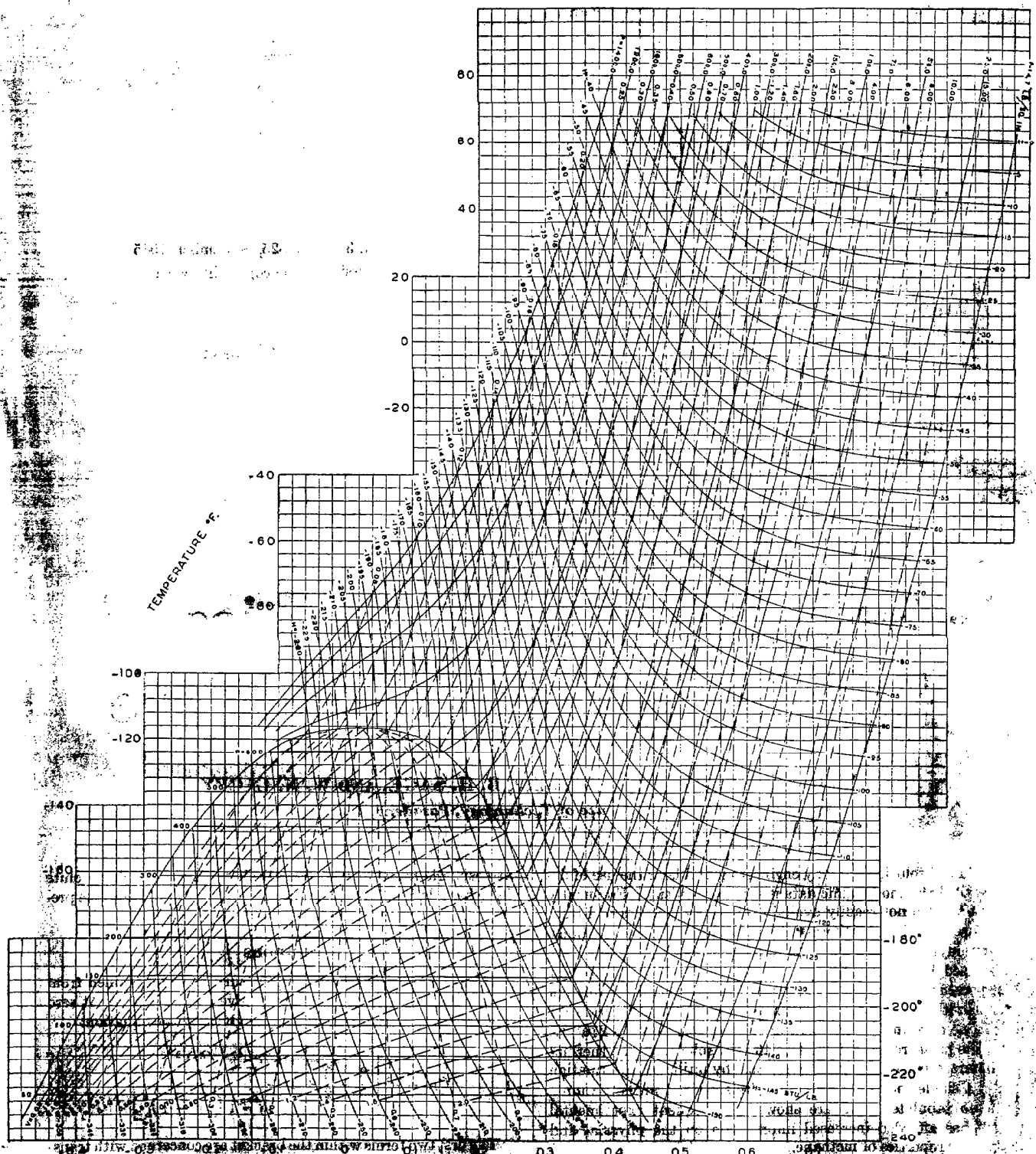

Figure 1. Temperature-Entropy Diagram of Methane in Low-Temperature Region

Table I. Thermodynamic Properties of Methane in the Single-Phase Region[a]

P	70° F. H	70° F. V	70° F. S	40° F. H	40° F. V	40° F. S	10° F. H	10° F. V	10° F. S	−20° F. H	−20° F. V	−20° F. S	−50° F. H	−50° F. V	−50° F. S	−80° F. H	−80° F. V	−80° F. S	−110° F. H	−110° F. V	−110° F. S
0	5.26	.....	....	−10.44	.....	....	−25.67	.....	....	−41.32	.....	....	−56.50	...	...	−71.58	...	...	−86.50	...	...
14.696	4.80	24.064	1.0086	−10.93	22.701	0.9794	−26.53	21.310	0.9472	−41.94	19.935	0.9133	−57.21	18.552	0.8774	−72.45	17.173	0.8390	−87.52	15.775	0.7976
25	4.45	14.122	0.9439	−11.30	13.311	0.9130	−26.96	12.502	0.8808	−42.40	11.689	0.8468	−57.72	10.873	0.8107	−73.04	10.053	0.7721	−88.21	9.225	0.7305
[illegible]	3.70	7.040	0.8571	−12.18	6.637	0.8259	−28.90	6.219	0.7934	−43.50	5.808	0.7592	−58.97	5.390	0.7227	−74.52	4.974	0.6836	−89.91	4.548	0.6418
[illegible]	2.90	4.677	0.8058	−13.00	4.402	0.7744	−28.90	4.125	0.7417	−44.60	3.847	0.7072	−60.19	3.564	0.6704	−76.04	3.281	0.6308	−91.60	2.987	0.5880
100	2.15	3.496	0.7694	−13.85	3.290	0.7374	−29.90	3.079	0.7046	−45.70	2.869	0.6697	−61.48	2.645	0.6325	−77.[illegible]	2.438	0.5924	−93.54	2.208	0.5487
150	0.60	2.317	0.7166	−15.60	2.174	0.6846	−31.90	2.031	0.6512	−47.98	1.887	0.6157	−64.07	1.738	0.5778	[illegible]	1.587	0.5[illegible]	−96.99	1.4280	0.4916
200	−1.00	1.7256	0.6685	−17.40	1.619	0.6464	−33.90	1.509	0.6125	−50.25	1.397	0.5763	−66.78	1.283	0.5376	[illegible]	[illegible]	[illegible]	[illegible]	1.0390	0.4478
300	−4.18	1.1356	0.6245	−21.07	1.062	0.5909	−38.03	0.9854	0.5559	−55.09	0.9072	0.5182	−72.35	0.8254	0.4776	[illegible]	0.7398	0.4321	−10[illegible].00	0.6585	0.3809
400	−8.95	0.8407	0.5848	−24.60	0.7833	[illegible]	−42.25	0.7283	0.5138	−60.08	0.6622	0.4744	−78.16	0.5967	0.4323	−97.65	0.5268	0.3829	−118.39	0.4570	0.3258
500	−10.85	0.6639	0.5525	−28.[illegible]	0.61[illegible]	[illegible]	−46.40	0.5671	0.4796	−65.02	0.5148	0.4385	−84.23	0.4589	0.3939	−105.06	0.3985	0.3411	−129.04	0.3412	0.2749
600	−13.50	0.5466	0.5256	−31.80	0.505[illegible]	[illegible]	−50.70	0.4624	0.4503	−70.15	0.4164	0.4073	−90.38	0.3669	0.3603	−112.81	0.3117	0.3036	−141.93	0.2518	0.2217
800	−[illegible].95	0.4005	0.4812	−39.05	0.367[illegible]	[illegible]	−59.42	0.3317	0.4005	−80.85	0.2933	0.3538	−103.47	0.2501	0.3002	−133.11	0.1922	0.2262	−200.48	0.1088	0.0267
1000	−[illegible].25	0.3137	0.4441	−46.57	0.285[illegible]	[illegible]	−68.60	0.2540	0.3579	−92.21	0.2188	0.3058	−121.66	0.1714	0.2355	−163.64	0.1178	0.1321	−232.79	0.0635	−0.0655
1200	−32.80	0.2560	0.4124	−54.10	0.2305	[illegible]	−78.25	0.2022	0.3187	−105.87	0.1693	0.2587	−139.41	0.1329	0.1771	−186.98	0.0935	0.0599	−239.60	0.0505	−0.0907
[illegible]	−38.85	0.2149	0.3845	61.55	0.1923	0.[illegible]381	−87.80	0.1674	0.2838	−117.61	0.1394	0.2191	−152.50	0.1081	0.1350	[illegible]	0.0776	0.0222	−242.66	0.0490	−0.1075

P	−140° F. H	−140° F. V	−140° F. S	−170° F. H	−170° F. V	−170° F. S	−200° F. H	−200° F. V	−200° F. S	−230° F. H	−230° F. V	−230° F. S
0	−101.44	.....	....	−116.33	.....	....	−131.1[illegible]	.....	....	−146.03	.....	....
14.696	−102.59	14.386	0.7523	−117.76	12.95[illegible]	[illegible]	−132.91	13.455	0.6475	−148.45	9.891	0.5851
[illegible]	−103.40	8.401	0.6846	−118.71	7.59[illegible]	[illegible]	−134.05	6.581	0.5787	−150.05	5.587	0.5135
[illegible]	−105.42	4.115	0.5948	−121.08	3.630	[illegible]	−136.97	3.141	0.4858			
[illegible]	−107.50	2.681	0.5406	−123.50	2.35[illegible]	[illegible]	−139.89	2.021	0.4271			
100	−109.55	1.970	0.5005	−125.95	1.72[illegible]	[illegible]	−142.89	1.481	0.3844			
[illegible]	[illegible]	1.264	0.4418	−131.05	1.112[illegible]	[illegible]						
[illegible]	[illegible]	0.9242	0.3953	−136.51	0.81[illegible]	[illegible]						
[illegible]	[illegible]	0.5789	0.3213									
[illegible]	[illegible]	0.3989	0.2510									

[a] P = pressure, lb./sq. in. abs.; H = enthalpy, B.t.u./lb.; V = specific volume, cu. ft./lb.; S = entropy, B.t.u./(lb.)(° R.)

in Equation 1 are from $i = 1$ to $i = 9$. The values for the vibrational heat capacity as a function of θ_i/T are given by Wenner (10).

Enthalpies of methane at zero pressure were calculated by integrating graphically the differential relation between C_{P_0} and T, and arbitrarily setting the enthalpy equal to zero at a datum state corresponding to zero pressure and 60° F. To obtain enthalpy values at various pressures and temperatures, isothermal enthalpy changes for pressure intervals of 10 kg./sq. cm. given by Eucken and Berger (3) were utilized. Enthalpies of saturated gas and saturated liquid methane were taken from Wiebe and Brevoort (11) and converted to the basis of the given reference point. Vapor pressures were obtained from data presented by Eucken and Berger (3). The critical constants were determined with the assistance of the law of rectilinear diameters as applied to plots of H vs. T and H vs. P. These plots were smoothed simultaneously by reference to the vapor pressure curve. It is believed that the uncertainty in the enthalpy values should not be greater than 0.5 B.t.u./lb.

From a plot of enthalpy vs. pressure at constant temperature, values of $-(\partial H/\partial P)_T$ were read, and $(\partial Z/\partial T)_P$ was calculated using the following expression, which may be obtained by combining the definition of compressibility factor with a suitable thermodynamic equation of state (6):

$$-\left(\frac{P}{bT^2}\right)\left(\frac{\partial H}{\partial P}\right)_T = a\left(\frac{\partial Z}{\partial T}\right)_P \qquad (2)$$

A plot of $(\partial Z/\partial T)_P$ against temperature was utilized for integration to give isobaric changes in the compressibility factor, Z.

Compressibility factors at 70° F. in the pressure range from 0 to 1500 pounds per square inch were obtained from the values of Sage, Budenholzer, and Lacey (7). Using calculated values of ΔZ, the compressibility factors for temperatures from 70° to −80° F. and pressures from 0 to 1400 pounds per square inch were determined. It was not believed desirable to extend compressibility factor calculations below a temperature of −80° F. because of the uncertainty in $(\partial H/\partial P)_T$ resulting from the rapid variation of H with respect to P at the higher pressures.

Specific volumes of methane for temperatures down to −80° F. were calculated from the compressibility factors. Specific volumes of the gas at saturation were obtained by combining saturated liquid densities (5), vapor pressures (3), and smoothed values of the latent heat of vaporization (11) in the Clapeyron equation. To bridge the gap in specific volume values from −80° F. to saturation, a plot of P against T at constant even values of V was prepared from an isothermal plot of log P vs. log V. By nearly linear interpolation of the even-volume P vs. T plot between −80° F. and saturation, the remainder of the specific volumes for the given pressure range were obtained. Sufficient care was taken in graphical integration and interpolation that uncertainty in specific volume at any point should not be greater than 0.5% of the value.

Entropies in the temperature region from 70° to −80° F. were determined from a relationship involving the isobaric residual volume-temperature derivative and the specific heat. The isobaric residual volume-temperature derivative was obtained from the equation:

$$a\left(\frac{\partial V}{\partial T}\right)_P = \frac{1}{T}\left[\left(\frac{\partial H}{\partial P}\right)_T + aV\right] \qquad (3)$$

The equation for change in entropy can be written in the following form:

$$dS = \frac{C_P dT}{T} - a\left(\frac{\partial V}{\partial T}\right)_P dP - \frac{abdP}{P} \qquad (4)$$

TABLE II. THERMODYNAMIC PROPERTIES OF SATURATED-GAS AND SATURATED-LIQUID METHANE

Temp., ° F.	P	Saturated Gas H	V	S	Saturated Liquid H	V	S
−230	43.42	−152.9	3.076	0.4378	−361.0	0.040	−0.4720
−220	62.58	−150.0	2.158	0.4095	−354.0	0.041	−0.4435
−210	86.94	−147.3	1.613	0.3831	−346.8	0.042	−0.4162
−200	117.33	−145.1	1.243	0.3591	−339.2	0.043	−0.3885
−190	154.21	−143.4	0.979	0.3372	−331.3	0.045	−0.3602
−180	198.61	−142.4	0.784	0.3149	−323.2	0.046	−0.3315
−170	249.23	−142.3	0.634	0.2922	−314.4	0.048	−0.3024
−160	308.18	−142.9	0.513	0.2683	−305.0	0.050	−0.2726
−150	375.84	−145.1	0.413	0.2420	−294.4	0.052	−0.2396
−140	453.11	−149.2	0.327	0.2130	−281.5	0.055	−0.2011
−130	541.38	−156.3	0.252	0.1765	−265.0	0.061	−0.1530
−120	638.70	−173.6	0.175	0.1140	−239.7	0.072	−0.0805
−116.5	673.0	−205.4	0.116	0.0186	(critical values)		

Since values of C_P at zero pressure had been calculated, the change in entropy was obtained by integration from 60° F. and 1 atmosphere to the desired state at T and P:

$$S - S_{519.69} = \int_{519.69}^{T} \frac{C_P dT}{T} + a\left[\int_{14.696}^{0} \left(\frac{\partial V}{\partial T}\right)_P dP + \int_{0}^{P} \left(\frac{\partial V}{\partial T}\right)_P dP - b \ln \frac{P}{14.696}\right] \quad (5)$$

$[P = 0]$ $[T = 519.69]$ $[T = T]$

The datum value of S was taken as 1 at 60° F. and 1 atmosphere.

At pressures below 500 pounds per square inch and temperatures below −80° F., entropies were obtained by utilizing values of ΔS at constant pressure, calculated from the relation:

$$\Delta S = \int_{T_1}^{T_2} \frac{1}{T}\left(\frac{\partial H}{\partial T}\right)_P dT \quad [P = \text{constant}] \quad (6)$$

Since the variation of enthalpy with temperature was essentially linear in the region considered, the uncertainty in the entropy calculations was minimized.

Below −80° F. and above 500 pounds per square inch a plot of $(\partial P/\partial T)_V$ against V at constant temperature was used for graphical integration to obtain values of ΔS. Values of entropy at dew point were obtained by application of the following equation:

$$\left(\frac{dS}{dT}\right)_d = \frac{1}{T}\left[\left(\frac{dH}{dT}\right)_d - aV\left(\frac{dP}{dT}\right)''\right] \quad (7)$$

The saturation dome was completed by use of the relationship:

$$\Delta S_{vapor} = \frac{\Delta H_{vapor}}{T} \quad (8)$$

In calculating heat capacities at zero pressure, a value of 1.4386 cm.° K. was used for hc/k, the molecular weight of methane was taken as 16.042, and the value 0.66898 was used for the specific gas constant b.

RESULTS

Table I lists calculated thermodynamic data for methane in the single-phase region. Table II gives the thermodynamic properties of saturated gas and saturated liquid, as well as critical constants. Figure 1 is a temperature-entropy diagram of methane in the low-temperature region. The diagram shows lines of constant pressure, enthalpy, volume, and quality.

It was possible in some instances to compare the calculated thermodynamic properties of methane with those of other investigators. In this way an additional measure of the uncertainty in the data was obtained. Calculated values of C_{P_0} are in close agreement with those presented in the literature.

In the superheated region, comparison with enthalpy values obtained by Sage, Lacey, and co-workers (*1*, *7*, *8*) from Joule-Thomson studies and P-V-T measurements, and values calculated by Edmister (*2*) from P-V-T data indicate a maximum uncertainty of 1 B.t.u./lb. in the enthalpy values.

Comparison of the superheated vapor volumetric data with those of Edmister (*2*) showed good agreement, but no volumetric data near the critical point were available for comparison. Entropies in the superheated gas region agree with those calculated by Edmister (*2*) to within 0.01 B.t.u./(lb.)(° R.).

Using temperature and volume as independent variables, a comparison of data was made with the diagram presented by Keesom and Houthoff (*4*). The comparison between the two sets of data was inconvenienced by the absence of tabulated thermodynamic properties in the publication by Keesom and Houthoff (*4*). It was found that the pressures differ by about 3%. Average deviations in enthalpies of about 4 B.t.u./lb. and in entropies of 0.01 B.t.u./(lb.)(° R.) were observed. Three typical points of comparison in the superheated region are given in Table III.

TABLE III. COMPARISON OF VALUES

Temp., ° F.	Sp. Vol., Cu. Ft./Lb.	Pressure, Lb./Sq. In. Authors	Keesom & Houthoff
10	0.5671	500	540
−110	0.4570	400	416
−170	3.630	50	53.4

ACKNOWLEDGMENT

The assistance of Louise M. Reaney in preparing Figure 1 is gratefully acknowledged.

NOMENCLATURE

a = conversion factor = 0.185184, (B.t.u.)/(lb./sq. in.) (cu. ft.)
b = specific gas constant, (lb./sq. in.) (cu. ft./lb.)/° R.
c = velocity of light
C_P = heat capacity at constant pressure, B.t.u./(lb.)(° R.)
C_{P_0} = heat capacity at zero pressure, B.t.u./(lb.)(° R.)
C_V = heat capacity at constant volume; Btu./(lb.)(° R.)
e = base of natural logarithms
H = enthalpy, B.t.u./lb.
h = Planck's constant
i = integer
k = Boltzmann's constant
n_g = weight fraction of a system in gas phase
P = pressure, lb./sq. in. absolute
S = entropy, B.t.u./(lb.)(° R.)
T = thermodynamic temperature, ° R. = ° F. + 459.69
V = specific volume, cu. ft./lb.
V = residual specific volume ($bT/P - V$), cu. ft./lb.
Z = compressibility factor
θ_i = "characteristic temperature", ° R.
Subscript d = a system which is at dew point (saturated gas)
Superscript $''$ = a system in which two phases are present

LITERATURE CITED

(1) Budenholzer, Sage, and Lacey, IND. ENG. CHEM., 31, 1288 (1939).
(2) Edmister, *Ibid.*, 28, 1112 (1936).
(3) Eucken and Berger, *Z. ges. Kälte-Ind.*, 9, 145 (1934).
(4) Keesom and Houthoff, *Commun. Phys. Lab. Univ. Leiden Suppl.* 65 (Sept., 1928–April, 1928).
(5) Keyes, Taylor, and Smith, *J. Math. Phys.*, 1, 271 (1922).
(6) Lewis and Randall, "Thermodynamics and Free Energy of Chemical Substances", p. 124, New York, McGraw-Hill Book Co., 1931.
(7) Sage, Budenholzer, and Lacey, IND. ENG. CHEM., 32, 1169 (1940).
(8) Sage and Lacey, *Ibid.*, 31, 1497 (1939).
(9) Vold, *J. Am. Chem. Soc.*, 57, 1192 (1935).
(10) Wiebe, "Thermochemical Calculations", New York, McGraw-Hill Book Co., 1941.
(11) Wiebe and Brevoort, *J. Am. Chem. Soc.*, 52, 622 (1930).

PRINTED IN U. S. A.

PROPOSITIONS

Propositions Submitted by William H. Corcoran

Ph.D. Oral Examination, May 25, 1948, 1:00 P.M., Crellin Conference Room
Committee: Professor Sage (Chairman), Professors Badger, Lacey, Liepmann, Lindvall

---

Chemical Engineering

1. The efficiencies of absorption towers may be increased by addition of non-volatile wetting agents to the absorbing fluids.

2. Heat transfer from a channel wall to a fluid stream may be accurately determined from a precise measurement of the temperature field at the wall. This measurement together with detailed temperature and velocity data provides a more satisfactory means than gross methods for establishing accurate values of heat transfer coefficients.

3. The eddy conductivity for heat, ϵ_c, is a constant across the central core of a fluid flowing turbulently in a closed conduit. This is different from the evaluation by Boelter[1] who gives $\epsilon_c = k^2y^2(1 - y/r_o)du/dy$ for isothermal heat transfer in a circular pipe. In his analysis y is the distance from the pipe wall, r_o is the radius, du/dy is the velocity gradient, and k is a constant. Thus at the center of the pipe where $y = r_o$, ϵ_c becomes zero as indicated by his equation.

[1] Boelter, Martinelli, and Jonassen: Trans. A.S.M.E. 63, 447 (1941)

4. In the presentation of multicomponent thermodynamics, it is suggested that the use of the external and internal points of view be explicit rather than implicit. By specifically dividing the discussion into these two parts it is possible to obtain a more clear picture of their combination in mathematical manipulations to present various useful engineering relations.

5. Hougen and Watson[1] present the equation

$$-\frac{dp_D}{dZ} = \frac{2f_D G^2 a_v}{\rho g_c F_D^{1.7}}$$

for the pressure drop in flow through granular beds having a random dense arrangement. Their nomenclature is given as:

p_D = pressure in a bed in dense arrangement expressed in force (mass units) per unit area
Z = length of packed bed
f_D = friction factor for dense arrangement as a function of the modified Reynolds number $N_{Rep} = G/a_v\mu$
g_c = standard gravitational constant = 32.2 ft/(sec.)^2
G = mass velocity per unit of total cross-sectional area of the bed
a_v = surface area of particles per unit volume of bed
F_D = fraction of void space in the bed in dense arrangement $= (1 - \rho_B/\rho_p)$
ρ = density of fluid
ρ_p = average density of solid particles
ρ_B = apparent bulk density of the granular bed

5. (continued)

Actually p_D should be represented as the force in the force-length-time system. If it is to be given as the force in mass units, then g_c should be eliminated from the equation.

[1] Hougen and Watson: Chemical Process Principles, III, Kinetics and Catalysis; John Wiley and Sons, 1017 (1947)

Mechanical Engineering

6. Refrigeration units should be rated on the basis of compressor horsepower rather than on capacity in standard commercial tons.

7. A suggested design for mounting propellant charges in spin-stabilized rocket motors or Jato units is given as follows:

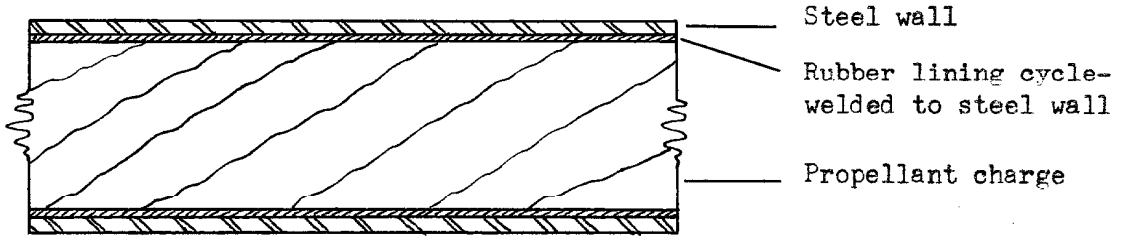

8. In the manufacture of commercial heat exchangers, the tubes are usually fastened in the headers by means of crimps applied with mechanically actuated rolls. Difficulties are encountered because variations in wall thickness cause variations in the strengths of the crimps. It is suggested that the mechanical crimping be replaced by a hydraulic method. The proposed equipment is schematically shown as follows:

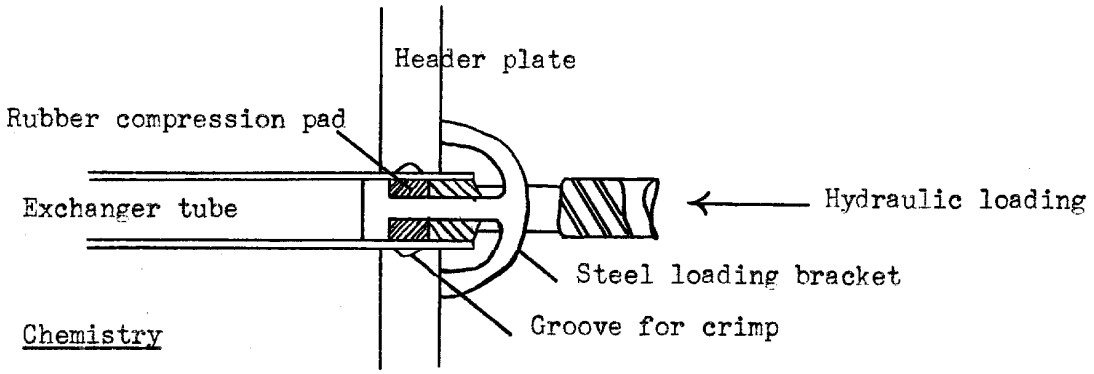

Chemistry

9. A process for treating both low and high grade ores in the preparation of commercial chromium is proposed. It involves the production of chromyl chloride, CrO_2Cl_2, and its distillation from the ore mixture. Collection in water would yield chromic and hydrochloric acids, and the solution would be electrolyzed to obtain the chromium metal. The procedure eliminates expensive high temperature hydrogenation and chlorination steps.

10. Chromium oxide, Cr_2O_3 is soluble in pure chromium. Hydrogen reduction at high temperature is required to remove the impurity. To eliminate this difficult step it is believed that a study of the liquid system Cr - Cr_2O_3 - M, where M is an added constituent, may lead to the

10. (continued)

possibility of the formation of two phases. One phase would be Cr with only a small percent Cr_2O_3. The other would be M - Cr_2O_3 or possibly just M_xO_y resulting from the oxide reduction. It is possible that the Cr - Cr_2O_3 - Si system would give the desired situation.

11. Experiments by Bridgman[1] and Smith[2] on thermal conductivities of liquids could have been slightly improved by computing values of k at a zero temperature difference rather than not correcting data obtained with a temperature difference of 0.6° C. Also energy measurements could have been made more accurate by using potentiometric methods rather than direct measurement of current with a milliammeter. In all, the data could have an improvement in accuracy of about 0.5 percent.

[1] Bridgman, P. W.: Proc. Am. Acad. Arts & Sciences 59, 141 (1923)

[2] Smith, J. F. D.: Ind. Eng. Chem., 22, 1246 (1930)

Pedagogy

12. The treatment of exact differential equations in thermodynamics to obtain certain partial quantities may be expanded to yield more information from one equation. The use of second derivatives is eliminated and less reliance upon additional exact equations results. For example we may treat the equation

$$dE = TdS - PdV$$

to give

$$\left(\frac{\partial S}{\partial P}\right)_T = -\left(\frac{\partial V}{\partial T}\right)_P$$

and in addition

$$\left(\frac{\partial S}{\partial V}\right)_T = \left(\frac{\partial P}{\partial T}\right)_V$$

13. In understanding the philosophy of the force-length-time and the mass-length-time systems, it is necessary that definitions of physical quantities such as density be kept clearly in mind. With the definitions fixed, it is then necessary to think in terms of one system and not move between the systems. Therefore for teaching the use of the systems it is suggested that the procedure using a constant K in the equation $F = Kma$ be eliminated. The constant would be replaced by a better knowledge of the concepts involved together with the application of the equation $w = mg$ which relates weight and mass within a given system.

14. The term fugacity is insufficiently explanatory and should be replaced by the phrase "gas phase activity".

15. For greatest return to the student, problem courses in engineering and science should be arranged so that all outside work is independent and accordingly weighted.